The small G-protein MglA connects the motility machinery to the bacterial actin cytoskeleton

Dissertation

zur Erlangung des Doktorgrades
der Naturwissenschaften
(Dr. rer. nat.)

dem
Fachbereich Biologie
der Philipps-Universität Marburg
vorgelegt von

Edina Hot

aus Bijelo Polje, Montenegro

Marburg / Lahn 2013

Die Untersuchungen zur vorliegenden Arbeit wurden von Oktober 2008 bis Oktober 2013 am Max-Planck-Institut für terrestrische Mikrobiologie, Marburg, und Centre National de la Recherce Scientific (CNRS), LCB, Marseille unter der Leitung von Prof. Dr. Lotte Søgaard-Andersen und Dr. Tâm Mignot durchgeführt.

Vom Fachbereich Biologie der Philipps-Universität Marburg als Dissertation angenommen am 11.11.2013

Erstgutachter: Prof. Dr. Lotte Søgaard-Andersen

Zweitgutachter: Prof. Dr.Michael Bölker

Tag der mündlichen Prüfung: 20.11.2013

Die während der Promotion erzielten Ergebnisse sind zum Teil in folgender Orginalpublikationen veröffentlicht:

Herzog A, Voss B, Keilberg D, **Hot E**, Søgaard-Andersen L, Garbe C, Kostina E. A strategy for identifying fluorescence intensity profiles of single rod-shaped cells. J Bioinform Comput Biol. 2013 Apr;11(2):1250024.

M. Miertzschke, C. Koerner, I.R. Vetter, D. Keilberg, **E. Hot**, S. Leonardy, L. Sogaard-Andersen, A. Wittinghofer. Structural analysis of the Ras-like G protein MglA and its cognate GAP MglB and implications for bacterial polarity. EMBO J. 2011 Aug 16;30(20):4185-97.

Die Ergebnisse dieser Arbeit, wie auch anderer Arbeiten auf demselben Gebiet, wurden während der Dissertation in folgendem Review diskutiert:

I. Bulyha, **E. Hot,** S. Huntley, L. Sogaard-Andersen GTPases in Bacterial Cell Polarity and Signalling. Current Opinion in Microbiology, 2011 Dec;14(6):726-33.

Table of contents

Abstract

Motility of *Myxococcus xanthus* cells is powered by two distinct engines: S-motility allows grouped cells movement and is driven by type IV pili (T4P) at the leading cell pole that use ATP for their function and pull the cell forward upon their retraction. Single cell movement is called gliding or A-motility and its AglQ/R/S engine is powered by proton-motive force and is incorporated at focal adhesion complexes in the cell. The control of motility and its direction is accomplished by cells rapidly switching their leading into lagging cell pole (cellular reversal), a process regulated by the small Ras-like G-protein MglA and its cognate GTPase activating protein (GAP) MglB.

Using fluorescence microscopy it was previously shown that MglA localizes at the leading cell pole and MglB at the lagging cell pole and both proteins dynamically switch polarity during cellular reversal. Further, recent experiments showed that an A-motility protein AglZ, and A-motility engine AglQ/R/S localize at clusters distributed along the cell body that stay fixed relative to the substratum as the cell moves forming focal adhesion complexes (FACs). Based on the *in vivo* experiments it has been proposed that gliding motility machinery assembles at the leading cell pole and that it is guided by the cytoskeletal element to the lagging cell pole, where it disassembles.

In this work we investigated the function of MglA during gliding motility. First, we demonstrate that MglA in its active state forms a focal adhesion cluster, which co-localizes with AglZ and AglQ, thus showing that active MglA is a component of the FACs. We show that MglA is essential for incorporation of AlgQ in the FACs, and that MglA GTPase cycle regulates the number of AglQ clusters. Further, we provide evidence that the GTPase negative MglA variant MglA^{Q82A} leads to regularly reversing cells after movement of only one cell length, and that MglA GTPase cycle regulates the disassembly of the FACs at the lagging cell pole. Fluorescent YFP-MglA^{Q82A} forms a

focal adhesion cluster which appears to regularly oscillate between the poles, and causes the cell to move in a pendulum-like manner. Unlike wildtype MglA, MglA^{Q82A} is insensitive to the GAP activity of MglB, and upon reaching the lagging cell pole where MglB localizes, it causes a cellular reversal by starting to oscillate in the opposite direction. The co-localizing YFP-MglA^{Q82A}/AglZ-mCherry and YFP-MglA^{Q82A}/AglQ-mCherry FAC also appear to continuously oscillate between the poles suggesting that the gliding motility machinery coupled to active MglA needs to be disassembled at the lagging cell pole by MglB GAP, and in this way allow uni-directional motility for distances longer than one cell length.

Furthermore, in this work we demonstrate that active wt MglA and MglA^{Q82L} variant interact directly with filament forming MreB actin homolog. Additionally, our results show that the formation and localization of FACs depend on intact MreB, thus indicating that MreB acts as a scaffold for the assembly of gliding motility machinery. The addition of antibiotics which inhibit peptidoglycan (PG) synthesis and reduce the dynamics of MreB in other bacteria did not inhibit single cell motility and did not cause mislocalization of MglA and AglQ. This strongly suggests that the major proposed function of MreB as a scaffold for PG elongation machinery is not coupled to its essential role during gliding motility in *M. xanthus*. Thus, we demonstrate that MreB is required for MglA, AglZ and AglQ localization at FACs during gliding, and this function of MreB is separable from its major proposed function in PG synthesis.

Zusammenfassung (German)

Myxococcus xanthus Zellen nutzen zur Fortbewegung zwei verschiedene Bewegungsmaschinerien. Die S-Bewegungsmaschinerie ermöglicht die Fortbewegung in Zellgruppen und wird durch Typ-IV-Pili (T4P) angetrieben. T4P werden am vorderen Pol ausgebildet und benötigen ATP für ihre Funktion, bei der die Zelle durch die Retraktion der T4P nach vorne gezogen wird. Die Fortbewegung von einzelnen Zellen wird gleitende Bewegung oder A-Bewegung genannt. Der antreibende Motor, bestehend aus den Proteinen AglQ/R/S, wird durch den Protonengradienten angetrieben und wird in fokalen Adhäsionskomplexen in der Zelle eingebunden. Fortbewegung und Bewegungsrichtung werden dadurch kontrolliert, dass *M. xanthus* Zellen in regelmäßigen Abständen ihre Bewegungsrichtung wechseln. Bei diesem Richtungswechsel wird der vordere Zellpol zum Hinteren und umgekehrt. Diese Richtungswechsel werden von dem kleinen Ras-ähnlichen G-Protein MglA und dessen GTPase-aktivierenden Protein (GAP) MglB reguliert.

Fluoreszenzmikroskopische Untersuchungen haben gezeigt, dass MglA am vorderen und MglB am hinteren Zellpol lokalisieren und beide Proteine wechseln den Zellpol während eines Zellrichtungswechsels. Des Weiteren konnte gezeigt werden, dass das zum A-Bewegungssystem gehörige Protein AglZ und der Motorkomplex AglQ/R/S in Clustern organisiert sind, welche sich entlang der Zelle ausbilden und relativ zum Untergrund fixiert bleiben, während sich die Zelle fortbewegt. Anhand der *in vivo* Experimente wurde vermutet, dass diese fokalen Adhäsionskomplexe sich am vorderen Zellpol ausbilden und entlang einer Cytoskelett-Struktur zum hinteren Zellpol geführt werden, wo sie dann disassembliert werden.

In dieser Arbeit haben wir die Funktion von MglA im Kontext des A-Bewegungssystems untersucht. Zunächst konnten wir demonstrieren, dass MglA in seiner aktiven Form, fokale Adhäsionscluster bildet, welche mit AglZ und AglQ ko-

lokalisieren. Dies lässt vermuten, dass aktives MglA ein Bestandteil der fokalen Adhäsionskomplexe ist. Wir konnten zeigen, dass MglA für die Eingliederung von AglQ in die fokalen Adhäsionskomplexe essentiell ist und der MglA GTPase Zyklus die Anzahl der AglQ Cluster bestimmt. Des Weiteren konnten wir feststellen, dass die Inaktivierung der GTPase-Aktivität durch die Mutation Q82A in MglA dazu führt, dass die Zellen regelmäßig die Bewegungsrichtung ändern, wobei sie lediglich eine Zelllänge zurücklegen, was vermuten lässt, dass die GTPase-Aktivität von MglA die Disassemblierung der fokalen Adhäsionskomplexe am hinteren Zellpol reguliert. Das Fusionsprotein YFP-MglA^{Q82A} lokalisiert in einem fokalen Adhäsionskomplex, welcher regelmäßig zwischen beiden Zellpolen oszilliert, was dazu führt, dass sich die Zelle wie ein Pendel hin und her bewegt. Im Gegensatz zu dem Wildtyp Protein MglA, kann das Protein MglA^{Q82A} nicht von MglB aktiviert werden. Erreicht MglA^{Q82A} den hinteren Zellpol an dem MglB sitzt, so wird ein Zellrichtungswechsel ausgelöst, indem MglA^{Q82A} wieder in die entgegengesetzte Richtung oszilliert. Die Ko-Lokalisierung der Proteine YFP-MglA^{Q82A}/AglZ-mCherry und YFP-MglA^{Q82A}/AglQ-mCherry zeigte, dass diese ebenfalls kontinuierlich zwischen beiden Zellpolen oszillieren. Daher vermuten wir, dass die Bewegungsmaschinerie mittels fokaler Adhäsionskomplexe an MglA gekoppelt ist und am hinteren Pol durch MglB GAP disassembliert werden muss, um die Bewegung in eine Richtung zu ermöglichen.

Darüber hinaus konnten wir demonstrieren, dass MglA, als auch MglA^{Q82A} direkt mit dem Filament-bildenden, Actin-homologen Protein MreB interagieren. Wir konnten zeigen, dass die Ausbildung und Lokalisierung der fokalen Adhäsionskomplexe von MreB abhängig sind, was bedeutet, dass MreB vermutlich als eine Art Gerüst für das A-Bewegungssystem dient. Die Zugabe von Antibiotika, welche die Peptidoglycan-Synthese inhibieren und das dynamische Verhalten von MreB in anderen Bakterien reduzieren, hat weder die gleitende Bewegung von einzelnen Zellen inhibiert, noch die Mislokalisierung von MglA oder AglQ zur Folge gehabt. Daraus schließen wir, dass die Funktion von MreB als Gerüst während der Peptidoglycansynthese unabhängig von dessen Funktion in der Fortbewegung in M. xanthus ist. Folglich konnten wir in dieser Arbeit zeigen, dass MreB für die Organisation von MglA, AglQ und AglZ in fokalen Adhäsionskomplexen während der gleitenden Bewegung benötigt wird und, dass diese Funktion von MreB unabhänig von dessen Funktion in der Peptidoglycansynthese ist.

Abbreviations

FAC(s)	Focal adhesion complex(es)
PG	Peptidoglycan
IM	Inner membrane
OM	Outer membrane
CW	Cell wall
bp	Base pairs
BSA	Bovine serum albumin
Cm	Chloramphenicol
CTT	Casitone Tris medium
ECM	Extracellular matrix
GDP/GTP	Guanosine di- /Guanosine triphosphate
ADP/ATP	Adenosine di- /Adenosine triphosphate
DTT	Dithiothreitol
Rpm	Rounds per minute
IPTG	Isopropyl β-D-1-thiogalaktopyranoside
Km	Kanamycin
min	Minutes
s	seconds
SDS-PAGE	Sodium dodecyl sulfate polyacrilamide gel electrophoresis
T4P	Type IV pili
YFP	Yellow fluorescent protein
mCherry	Red fluorescent protein derived from mDsRed
OD	Optical density
PMSF	Phenylmethylsulfonylfluoride
Sf-GFP	super-folding GFP
WT	Wildtype

1 Introduction

Most organisms move from one place to another in search for food and shelter, and to protect themselves from enemies. Eukaryotes can move by swimming in liquid environments and by crawling and gliding across solid surfaces (Friedl and Gilmour, 2009). Prokaryotes can move by swimming in liquid and swarming in semi-solid environments. On solid surfaces prokaryotes move by twitching using type 4 pili, and by gliding without any appendages on solid surfaces (Jarrell and McBride, 2008).

1.1 Directional cellular motility

Directional cell motility is central to many physiological and pathological processes in metazoans, including embryogenesis, development of tissues, wound healing, immune response and tumor metastasis (Rorth, 2009). There are currently two modes of motility across a surface described for eukaryotic cells: crawling and gliding.

In the following sections, I concentrate on crawling and gliding motility in eukaryotic cells and then contrast that with parallel mechanisms in bacteria.

1.1.1 Surface-associated crawling in eukaryotic cells

In many metazoan cells, one way to accomplish directed net movement is by crawling – also known as ameboid locomotion. Crawling motility requires protrusion of the membrane at the leading cell edge, adhesion to the substratum and its retraction at the rear edge (Lauffenburger and Horwitz, 1996; Pollard and Borisy, 2003; Rafelski and Theriot, 2004). To move forward, the front edge of the cell adheres to the substratum via interactions with extra-cellular matrix, and the rear of the cell detaches from the substratum and retracts (Bershadsky and Kozlov, 2011; Elson *et al.*, 1999; Lee *et al.*, 1993; Opas, 1995; Wehrle-Haller, 2012). As a consequence, crawling involves continuous change in cell shape and the formation of leading edge structures including filopodia, lamellipodia, stress fibers and arcs (Block *et al.*, 2008; Danuser, 2009; Guillou *et al.*, 2008; Mattila and Lappalainen, 2008; Mejillano *et al.*, 2004; Ponti *et al.*, 2004). These morphological changes are controlled by molecular machinery complexes, of which the most important will be discussed in the following paragraphs.

Directed movement occurs when environmental cues activate a complex network of signal transduction pathways including actin cytoskeleton, small GTPases, myosin II motor, and kinases. Actin represents one of the most abundant proteins in the cytoplasm of eukaryotic cells, and it is involved in cell division, scaffolding of myosin related proteins in muscle cells, and cellular motility. Actin co-exists in monomeric and

polymeric states, and its filaments / polymers can be joined together to form a three dimensional network or actin cytoskeleton (Pollard *et al.*, 1990). Actin polymers incorporated into the cytoskeleton do not only provide mechanical support, but they exhibit highly dynamic behavior in response to external and internal stimuli, thus actin plays a central role in the establishment and maintenance of cell shape during growth and division, and cell adhesion and motility (Heng and Koh, 2010; Mogilner and Keren, 2009; Pollard and Cooper, 2009).

Crawling motility is driven by dynamic reorganizations of actin cytoskeleton (Pollard and Cooper, 2009; Rafelski and Theriot, 2004; Ridley and Hall, 1992a). Filaments of the actin cytoskeleton provide the backbone of leading edge protrusions, and the force for membrane deformation is provided by actin polymerization at the plasma membrane, (Figure 1) (Cooper and Schafer, 2000; Insall and Machesky, 2009; Pollard and Borisy, 2003; Pollard and Cooper, 2009).

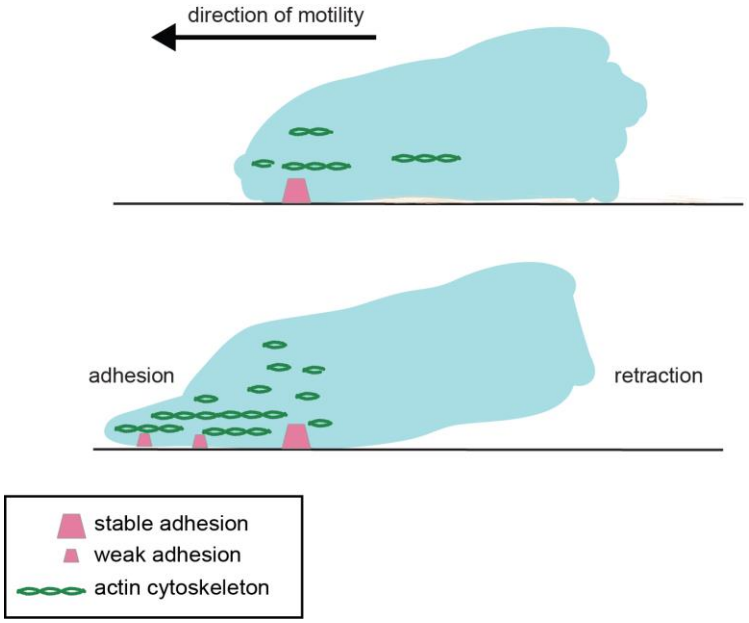

Figure 1. Mechanism of crawling in eukaryotic cells. At the front edge membrane protrusions allow attachment to the substratum and formation of new adhesion sites, which mature as the cell moves through them. At the rear end the cell detaches from the substrate due to adhesions weakening and disconnection from the substrate.

The interactions of the cell membrane at the ventral side of the cell with the extra-cellular matrix (ECM) on the substratum are called focal contacts or focal adhesions, (Figure 1) (Petit and Thiery, 2000). The second type of adhesion is (focal)

adhesion complex, found at the tip of the protruding membrane structures and smaller in size than focal adhesion (Abercrombie *et al.*, 1971).

The function of actin and formation of focal adhesion complexes in motility is regulated by small G-proteins (GTPases), most prominent of which are in the Rho subfamily - Cdc42, RhoA and Rac (Charest and Firtel, 2007; Raftopoulou and Hall, 2004). Rho GTPases are small Ras-like proteins, which act as molecular switches that can be activated by a variety of extra-cellular signals. Small G-proteins cycle between the GTP-bound, active state in which they activate the downstream effectors, and GDP-bound, inactive state, Figure 2 (Vetter and Wittinghofer, 2001).

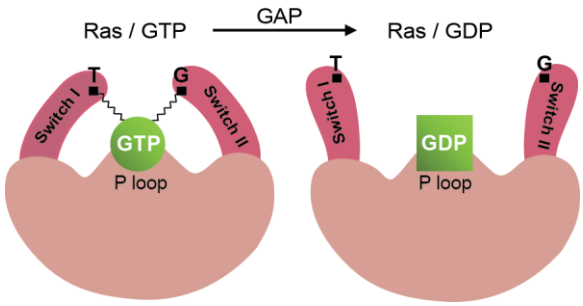

Figure 2. Canonical GTPase activation cycle of small Ras G-proteins by GAPs. Structural changes occur in the dynamic switch I and II regions, which contain the conserved threionie and glycine for γ-phosphate binding of GTP.

The activity and localization of small GTPases involved in motility constitute a hierarchical cascade in which first Cdc42 initiates the formation of focal adhesions by stimulating actin polymerization at specific sites of the cell edge (Insall and Machesky, 2009; Le Clainche and Carlier, 2008; Nobes and Hall, 1995; Wehrle-Haller, 2012). Then, activated Rac acts with Cdc42 to promote the extension of filopodia, lamellipodia or stress fibers in the direction of migration at the leading edge, where additionally new signaling molecules needed for clustering, adhesion and chemotaxis are recruited (Nobes and Hall, 1995; Sander and Collard, 1999).

The actin cytoskeleton provides the driving force for motility by acting through focal adhesions that link the cell to the extra-cellular matrix (ECM) at the leading edge (Hu *et al.*, 2007). Focal adhesions form first as adhesive contacts as the leading edge protrudes and interacts with the ECM through integrin-mediated contacts, initiated by actin polymerization, which in turn is regulated by Cdc42 and Rac (Ridley and Hall, 1992b; Sander *et al.*, 1999). The initial (nascent) adhesions to the substratum (ECM or other cells) are at first small, less than 0.25 μm in diameter, and they are prone to quick

disassembly unless they are stimulated to undergo maturation (Choi *et al.*, 2008). Adhesions grow in response to motor-driven mechanical forces, which drive the cell body forward, and the maturation of nascent adhesions leads to formation of focal complexes (first observed in the constitutively active Rac expressing cells), which are about 0.5 μm in diameter and can last up to 5 min during motility. Finally, the fully mature adhesions are referred to as focal adhesions – and they evolve slowly over time into large complexes ranging from 1 to 5 μm in size, and last up to 20 min before they disassemble (Balaban *et al.*, 2001; Zaidel-Bar *et al.*, 2007).

Breaking of the adhesions occurs at the rear of the cell where they are disassembled and allow cell detachment from the substratum (Gupton and Waterman-Storer, 2006; Laukaitis *et al.*, 2001; Webb *et al.*, 2004). Focal adhesion disassembly is stimulated by RhoA activation and requires the motor protein myosin (Le Clainche and Carlier, 2008; Zigmond, 2004). Myosin proteins represent a class of intra-cellular motors whose superfamily includes more than 13 different classes classified into different groups. Classifications are based on the myosin head domain sequence which drives its activity; following is the neck domain of variable sequence and different function, which is turn followed by a C-terminal tail domain which can dramatically vary between different myosin classes and determines protein's specific activity (Krendel and Mooseker, 2005). Myosin globular head (motor) domain can bind and hydrolyze ATP and convert chemical energy into force and motion (Krendel and Mooseker, 2005; Vicente-Manzanares *et al.*, 2009). It is thus proposed that the cell can retract its rear and disassemble the focal adhesions using the contractile force provided by bundles of myosin II that slide over the actin filaments, leading to disruption of molecular interactions and weakening of the integrin-ECM linkage (Le Clainche and Carlier, 2008; Sun *et al.*, 2010; Vicente-Manzanares *et al.*, 2009).

1.1.2 Polarization of cells moving by crawling

As a form of directed cellular movement over surfaces, crawling requires that cells distinguish the front and back by spatial asymmetry through physical separation of the signaling processes at the front and back of the cell, and that the cells can respond dynamically to the environmental cues. It is widely accepted that during motility the front – back polarity is achieved through chemoattractants (extra-cellular signaling) inducing migratory and polarized behavior in the following way: at the leading cell edge specific protein kinases perceive signals and further transduce them downstream to

activate signaling cascades in which actin polymerization is nucleated at the front of the cell. This generates the zones of protrusion, and the cell symmetry is broken by myosin II which re-organizes actin filaments into non-protrusive bundles at the cell rear (Abercrombie *et al.*, 1970; Small *et al.*, 1978; Verkhovsky *et al.*, 1999; Vicente-Manzanares *et al.*, 2008; Yam *et al.*, 2007).

Actin is not the only protein in the cells whose polarization is essential for spatial asymmetry in the cells. In addition to actin polarization in the cells, the microtubule cytoskeleton is also polarized in migrating cells, and the polymerization at their plus ends at the leading cell edge is also necessary for cellular protrusion (Verkhovsky *et al.*, 1999; Yam *et al.*, 2007). Microtubules play three roles in polarization of cells during motility; first, they primarily serve as tracks for directed intra-cellular transport to the leading edge. Second, microtubules directly promote cellular protrusion at the leading edge, and third, they regulate the local formation of adhesions and contractions (Wittmann and Waterman-Storer, 2001).

Crucial for all these aspects of crawling motility is the activity and localization of small Rho GTPases which regulate protein kinases, and organize actin, microtubules, and myosin II, to generatethe asymmetries in motile cells (Abercrombie *et al.*, 1970; Chrzanowska Wodnicka and Burridge, 1996; Nobes and Hall, 1995; Raftopoulou and Hall, 2004; Ridley and Hall, 1992a, b; Ridley *et al.*, 2003; Sander and Collard, 1999; Vicente-Manzanares *et al.*, 2008; Vicente-Manzanares *et al.*, 2009; Yam *et al.*, 2007; Zigmond, 2004).

1.1.3 Surface-associated gliding in eukaryotic cells

While some cells move by crawling, others use gliding as a primary mode of moving across surfaces. Gliding motility is employed by numerous eukaryotic cell types. In eukaryotes, gliding depends on actin assembly / disassembly, but it is different than actin-based motility during crawling as membrane protrusions and structures like lamellipodia, filopodia and stress fibers do not form (King, 1988). Species such as *Labyrinhula* colonial protozoan plant pathogen, flagellegated green alga *Chlamydomonas*, and diatom species *Navicula* exhibit substrate-dependent gliding motility (Bigelow *et al.*, 2005; Drum and Hopkins, 1966; King *et al.*, 1986). However, I will focus on the well-investigated gliding of the coccidian Apicomplexa parasites as a model of eukaryotic gliding motility. Protozoan parasites *Plasmodium* and *Toxoplasma* from the phylum Apicomplexa are obligate intra-cellular parasites that use gliding

motility to infect a host and to actively move across biological barriers to find new sites of infection (Kappe *et al.*, 1999).

The gliding mechanism employed by Apicomplexan parasites depends on three fundamental elements. First, gliding depends on a slime trail consisting of surface proteins and lipids, which is deposited as the cells glide forward; second, gliding depends on an actin-myosin motor, and third, a protein complex consisting of more than 12 components ("glideosome") is essential for gliding (Baum *et al.*, 2006; Morrissette and Sibley, 2002; Russell and Sinden, 1981; Soldati and Meissner, 2004; Stewart and Vanderberg, 1988, 1991).

Initial studies describing the molecular model for Apicomplexan motility showed that latex beads attached to the surface of the cell are translocated toward the posterior end of the cell at similar rates as the gliding cells (King, 1981, 1988; Russell and Sinden, 1981). Together, these results demonstrated a cell surface-substrate association through adhesion molecules, a motor complex in the cell cortex, and trans-membrane linkers connecting the surface adhesion molecules to the motors and cell cytoplasm. Like gliding motility itself, the translocation of the cell-surface attached beads is inhibited by using cytochalasin – an actin disrupting compound (Dobrowolski and Sibley, 1996; King, 1988; Russell and Sinden, 1981). Furthermore, the of jasplakinolide, which stabilizes polymerized (F-) actin, reversibly inhibits the secretion of the slime trail and blocks motility in a dose-dependent manner (Mizuno *et al.*, 2002; Shaw and Tilney, 1999; Wetzel *et al.*, 2003). This suggested that gliding motility depends on the abundance of actin filaments, and their polymerization is essential for gliding motility. Although drug injection experiments show that the actin cytoskeleton is essential for gliding motility, biochemical analyses of actin *in vitro*, or its localization in the cells has proved difficult to study and needs further characterization.

Gliding motility of Apicomplexans relies on myosin, in whose absence cells are non-motile (Dobrowolski *et al.*, 1997; Heintzelman and Schwartzman, 1999; Soldati and Meissner, 2004). Moreover, Apicomplexan myosin is closely associated with the cell membrane, and binds actin in an ATP-dependent manner (Heintzelman and Schwartzman, 1999; Herm-Gotz *et al.*, 2002; Hettmann *et al.*, 2000). Finally, the inhibition of myosin heavy chain ATPase by the injection of butanedione monoxime to the cells led to an arrest in gliding motility (Dobrowolski *et al.*, 1997; Lew *et al.*, 2002; Pinder *et al.*, 1998). These results therefore suggest that an active myosin motor linked to actin is required for gliding.

In order for actin and myosin to create the forces necessary for motility, one of them has to be anchored in the cell, whereas the mobile partner has to interact with the cytoplasmic membrane components to, in turn, link the motor to the substrate (King, 1988; Opitz and Soldati, 2002). Recent work suggests that it is most likely myosin which is associated with the inner membrane complex (IMC) of the gliding machinery components, thus suggesting that actin is directly or indirectly associated with the cell membrane-substratum adhesive molecules (Bergman *et al.*, 2003). The cell adhesion molecules responsible for these interactions include the thrombospondin-related anonymous protein (TRAP) and TRAP-like MIC2 proteins which are transported from the anterior to the rear cell pole and whose dynamics depends on actin polymerization (Carruthers *et al.*, 2000; Jewett and Sibley, 2003; Robson *et al.*, 1995; Robson *et al.*, 1988; Yuda *et al.*, 1999). Additionally, the cytoplasmic tail of the TRAP-like proteins is essential for gliding, thus indicating that this protein is associated with the motor system driving motility; furthermore, the gliding-associated protein (GAP) 45 of the inner membrane complex is essential for myosin anchoring to the IMC (Gaskins *et al.*, 2004; Kappe *et al.*, 1999).

Exactly how all the components of the glideosome are linked is still to be elucidated, but it has been shown that a proteolytic event which breaks the interaction between the adhesion and the substratum leads to a continuous movement forward (Charest and Firtel, 2007; Sibley, 2004).

1.2 Cellular motility in bacteria

As in eukaryotes, bacteria can move on solid and semi-solid surfaces by swarming, twitching, and gliding. Swarming allows groups of bacteria to move over semi-solid surfaces using peritrichous or lateral flagella; twitching motility allows bacteria to move over solid surfaces using type-4-pili (T4P) structures found on cell exterior, and gliding allows motility of cells over solid surfaces without the use of any cellular appendages.

1.2.1 Surface-associated motility in bacterial cells

Swarming motility allows movement of groups of bacteria across a semi-solid surface, powered by flagella distributed randomly on the cell surface (Harshey, 2003; Jarrell and McBride, 2008). Peritrichious flagella bundle together when rotated to increase flagellar stiffness and enable more efficient swarming, Figure 3A (e.g. in *Escherichia coli*). Flagella are also used for swarming in *Proteus mirabilis, Vibrio*

parahaemolyticus, *Rhodosprillum centenum* and *Aeromonas* spp, Figure 3A (Harshey, 2003; Jarrell and McBride, 2008; Kim and McCarter, 2000). Swarming on agar surfaces is displayed by numerous bacterial species although many bacteria (*Salmonella enterica* and *Yersinia entercolitica* among others) require the presence of specific nutrients or lower agar concentrations in order to swarm (Young *et al.*, 1999).

Some bacteria move over surfaces by twitching motility using T4P (Figure 3B). Twitching motility is driven by pilus extension, its attachment to the surface or nearby cells, and retraction (Pelicic, 2008). T4P are long (10 µm or longer) and flexible structures which extend from the cell body (Craig *et al.*, 2006; Pelicic, 2008). The pilus fiber is composed of polymers of pilin protein PilA and minor pilins, and its extension is powered by ATP hydrolysis by the PilB extension ATPase. The retraction of the pilus is powered by the PilT ATPase (Burrows, 2005; Craig *et al.*, 2006; Mattick, 2002; Satyshur *et al.*, 2007). Bacteria which produce T4P are phylogenetically diverse, including *Myxococcus xanthus*, *Neisseria gonorrhoeae*, *Pseudomonas aerugoinosa*, and *Nostoc punctiforme* (Mattick, 2002; Pelicic, 2008).

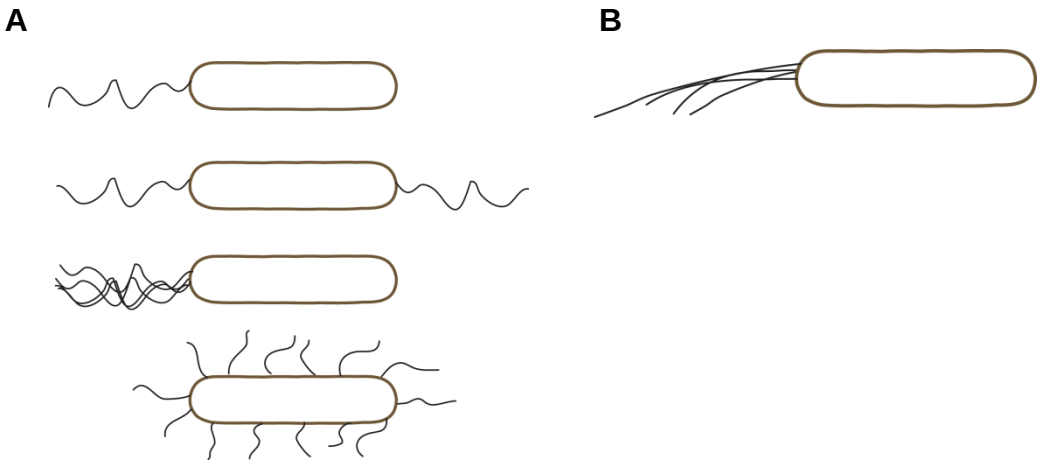

Figure 3. Bacterial surface organelles used in motility. (A) Flagella arrangements in different bacterial species (described in the text); from top down: monotrichous, amphitrichous, lophotrichous and peritrichous flagella. (B) Type-4-pili (T4P) extending from the bacterial cell pole.

Some bacteria can actively move over hard surfaces without the use of flagella or pili, by gliding in the direction of the long axis of the cell. This type of motility is called gliding, and it is displayed by some members of *Mycoplasma*, *Flavobacterium* and Myxobacteria species (Harshey, 2003;Jarrell and McBride, 2008). This type of bacterial motility is less well characterized than others.

Mycoplasma mobile cells are asymmetric, and their gliding in the "head" direction depend on the proteins found in the "neck region" which is essential for gliding (Hasselbring and Krause, 2007; Seto *et al.*, 2005). Gliding of *M. mobile* depends on ATP, but the exact mechanism is still under investigation (Ohtani and Miyata, 2007;Uenoyama and Miyata, 2005). On the other hand, gliding by *Mycoplasma pneumoniae* is less understood, but recent data suggest that the cytoskeleton-like structure causes an attachment organelle containing multi-protein complex with motor to extend and contract and in this way enable movement (Henderson and Jensen, 2006).

Gliding motility of *Flavobacterium* spp is characterized by rapid movement and occasional reversals of the direction of movement (McBride, 2004). In *Flavobacterium johnsoniae* it has been shown that the proton motive force powers gliding, even though the gliding motility motor has not yet been identified (Duxbury *et al.*, 1980; Dzink-Fox *et al.*, 1997). Genetic analyses have shown that many genes required for *Flavobacterium* gliding encode for trans-membrane, periplasmic and cytoplasmic proteins suggesting that some of these might be a part of the motor complex powering gliding (McBride and Braun, 2004; McBride *et al.*, 2003; Nakane *et al.*, 2013; Pate and Chang, 1979). An interesting new finding is that the cell surface protein SprB is required for gliding, as inactivation of SprB by antibody binding inhibits cell motility (Nelson *et al.*, 2008). Furthermore, recent data suggest a role of SprB in surface attachment / adhesion, which is activated by a yet unidentified motor powering gliding (Nakane *et al.*, 2013; Sato *et al.*, 2010).

1.3 Introducing *Myxococcus xanthus*

M. xanthus is a Gram-negative rod shaped bacterium characterized by a complex lifestyle. In the presence of nutrients, the bacteria can spread from the colony center. In the absence of nutrients, *M. xanthus* initiates a stringent response which induces the expression of developmental genes, and causes the cells to enter a metabolically inactive state (Singer and Kaiser, 1995). This developmental process begins first by aggregation of cells, proceeds through the stages of fruiting body development to form dormant spores (Kaiser and Welch, 2004). Motility is required for extended colony growth, and for fruiting body formation in the absence of nutrients (Kroos *et al.*, 1988).

1.3.1 *M. xanthus* uses two distinct motility systems

M. xanthus cells can move on surfaces as groups of cells using T4P driven S-(social) motility, and as single isolated cells by A-(Adventurous) or gliding motility. Early genetic work showed that T4P motility is genetically separable from gliding motility, suggesting that two distinct machineries drive T4P and gliding motility (Hodgkin and Kaiser, 1979). Interestingly and as described in detail in the following chapters, at least two regulatory proteins characterized so far are needed for regulation of both motility systems.

T4P motility depends on polar retractile T4P, whose assembly and disassembly depends on 10-15 conserved T4P proteins (Bulyha *et al.*, 2009; Clausen *et al.*, 2009; Kaiser, 1979; Sun *et al.*, 2000). This type of motility depends on cell-cell contact, extra-cellular matrix (ECM) and lipopolysaccharide O-antigen (Arnold and Shimkets, 1988; Bowden and Kaplan, 1998).

Gliding motility allows single cells to move on hard agar, in the absence of any visible organelles (Wolgemuth *et al.*, 2002a). I will discuss the previously identified components necessary for gliding of single cells in *M. xanthus* in the following sections of this introduction, and will shortly address my new findings on gliding motility.

1.4 Gliding motility in *M. xanthus*

Gliding motility in *M. xanthus* allows cell movement in the direction of its long axis, with occasional stopping and reversal of the direction of gliding. Several proteins have been shown to be required for gliding motility, such as the motor, actin-like cytoskeleton protein MreB, multiple sets of components required for gliding, extra-cellular slime and at least three regulatory proteins.

1.4.1 Motor powering gliding motility

In the past, several models have been proposed to explain gliding motility and all of them require a motor protein to generate mechanical force. There are currently three motors known to provide the energy required for mechanical force for different processes in the membranes of bacterial cells: MotA-MotB, ExbB-ExbD, and TolQ-TolR protein complexes (Figure 4). These sets of proteins are important for harvesting the energy from the proton flux and converting it to a mechanical output to regulate different membrane processes (Gerding *et al.*, 2007; Minamino *et al.*, 2008; Postle and Kadner, 2003; Zhang *et al.*, 2009).

As the motor which powers gliding motility was not known for many years, a large collection of gliding motility mutants was analyzed for mutations in genes that have previously been shown to convert chemical energy into mechanical output in other bacteria. The motor which powers the rotation of bacterial flagella is composed of the MotA-B stator complex which forms a proton channel in the cytoplasmic membrane, and is fixed to the peptidoglycan by MotB; MotA component interacts with the FliG rotor protein to generate torque (Figure 4, from Sogaard-Andersen, 2011) (Minamino *et al.*, 2008). ExbB-D proteins form a protein channel in the cytoplasmic membrane, and they provide the energy for transport across the outer membrane by interacting with TonB; this interaction causes a conformational change in TonB, which in turn changes the conformation of the TonB-dependent receptors in the outer membrane, Figure 4 (Postle and Kadner, 2003). TolQ-R form a proton channel in the cytoplasmic membrane which is essential for membrane integrity through interactions with TolA and Pal (peptidoglycan associated lipoprotein) in the outer membrane (Figure 4) (Gerding *et al.*, 2007; Zhang *et al.*, 2009).

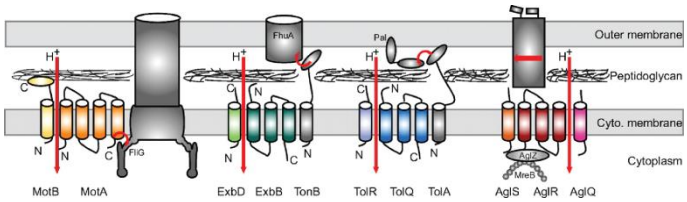

Figure 4.The three distinct force generating bacterial cell envelope complexes. MotA-B, ExbB-D, TolQ-R-S and AglQ-R-S channels allow proton passage (indicated by red arrows) which fules the motors involved in different cellular processes. Figure reproduced from Sogaard-Andersen, 2011.

Based on this knowledge, gliding motility mutants obtained by transposon mutagenesis suggested a few promising candidates for identification of the molecular motor which powers gliding (Youderian *et al.*, 2003). Insertion and deletion mutations of *aglX*, *aglV*, *aglR* and *aglS* genes rendered cells non-motile by gliding motility. AglX and AglV proteins are homologous to TolQ-R proteins from the Tol-Pal system, and their non-motile phenotypes were predicted to be caused by an effect on the outer membrane integrity or cell division, which when perturbed causes secondary defects in gliding motility (Nan *et al.*, 2011; Sun *et al.*, 2011). Additionally, AglX mutant has a strong T4P phenotype, resulting in an S-motility defect (Youderian *et al.*, 2003).

On the other hand, protein AglR was found to be homologous to TolQ/ExbB/MotA and AglS is homologous to TolR/ExbD/MotB proteins; *aglR/S* genes

are encoded in one locus with *aglQ*, whose gene product is also a protein homologous to TolR/ExbD/MotB, as is AglR (Nan *et al.*, 2011; Sun *et al.*, 2011). Deletions of individual genes in the *aglQ/R/S* showed that all three genes are essential for gliding motility. Furthermore, AglQ/R/S proteins were found to interact in pull-down assays, and bioinformatic analyses show that all three proteins contain key residues essential for building a proton channel in the cytoplasmic membrane, thus predicting that functional proton channels formed by the AglR-Q and AglR-S complexes (Sun *et al.*, 2011). Because these proteins are homologous to MotA-B complexes, which are known to drive flagella rotation by proton motive force (PMF) and which can be inhibited by a general PMF-inhibitor drug CCCP (Berg and Anderson, 1973; Blair and Berg, 1990), Moving *M. xanthus* cells were exposed to CCCP. After CCCP addition, gliding motility was abolished within minutes, suggesting that the PMF powers the gliding motility engine (Nan *et al.*, 2011; Sun *et al.*, 2011). As PMF can arise from gradients in chemical potential (pH difference across the membranes), or electrical potential (voltage difference across membranes), detailed analyses using nigericin (specific inhibitor of pH gradient) and valinomycin (specific inhibitor of membrane potential) revealed that *M. xanthus* gliding is powered specifically by the pH gradient created by the PMF (Sun *et al.*, 2011). Furthermore, a point mutation of the conserved aspartic acid residue required for proton binding in AglQ completely abolished gliding motility, confirming that the AglQ component of the AglQ/R/S complex is directly responsible for harnessing the energy required for the motor function in gliding (Sun *et al.*, 2011).
These data strongly suggested that the AglQ/R/S protein complex is functionally the motor, which drives gliding motility in *M. xanthus*.

1.4.2 AglZ is required for gliding and localizes to FACs

Early work showed that a protein containing an N-terminal pseudo-receiver and C-terminal coiled-coil domain (with high similarity to the myosin II C-terminal coiled coil domain), AglZ, is essential for gliding but dispensable for T4P motility (Yang *et al.*, 2004). When over-expressed, the AglZ C-terminal coiled coil domain formed regularly repeated band-like structures along the cell length in *E. coli*, and electron microscopy revealed that this domain formed short filamentous structures *in vitro*, suggesting that AglZ forms filamentous structures of certain order in *M. xanthus* (Yang *et al.*, 2004). In *M. xanthus*, AglZ-YFP displayed an interesting dynamic localization, forming multiple clusters in the cell, which translocated from the leading to the lagging

cell pole during gliding (Mignot *et al.*, 2007b). In fact, analyses of AglZ localization revealed that the protein formed a cluster at the leading cell pole and multiple clusters distributed along the cell length which appeared stationary with respect to the substratum even as the cell moved forward. These data suggested that AglZ could form or be a part of motility complexes in the cell which act similarly to eukaryotic focal adhesions. AglZ focal adhesion complexes (FACs) stayed fixed on the substratum until they reached the lagging/back pole, where they disappeared (Mignot *et al.*, 2007b). Interestingly, AglZ interacts with a small G-protein MglA, which is an essential regulator of both motility systems, as demonstrated in a yeast two-hybrid approach and in an *in vitro* pull-down experiment using purified proteins (Mauriello *et al.*, 2010b; Yang *et al.*, 2004). Furthermore, AglZ C-terminal coiled coil interacted with purified MreB in an *in vitro* pull-down experiment (Mauriello *et al.*, 2010b). Moreover, AglZ was also shown to interact in an *in vivo* co-immunoprecipitation experiment with a component of the Frz chemosensory system – FrzCD, which controls the direction of cellular motility by regulating reversals of motile *M. xanthus* cells (Mauriello *et al.*, 2009; Nan *et al.*, 2010). In addition, gliding motility components GltD/AgmU, GltE/AglT, GltJ/AgmX and GltI/AgmK were used as bait in pull-down assays they were found to interact with AglZ (Nan *et al.*, 2010).

To analyze whether AglZ protein localizes in force-producing complexes, Sun and colleagues showed that immobilizing cells on a surface led to a continuous uni-directional transport of AglZ-YFP clusters, suggesting the machinery which powers gliding is continuously moving and not attached to the substrate due to artificial immobilizing of the cell (Sun *et al.*, 2011). Importantly, when polystyrene beads were applied to the surface of the immobilized cells, they co-localized with AglZ-YFP and were transported along the exterior of the cell, indicating that there exists an active system that powers gliding. The localization of AglZ-YFP (and the polystyrene beads on cell surface) was dramatically perturbed in the presence of MreB cytoskeleton perturbing drug, A22 (Sun *et al.*, 2011). Additionally, in recent work on gliding motility, where the cells were elongated by the cell division inhibitor cephalexin, AglZ-YFP clusters localized to the front half of the cells, and the number of clusters was directly proportional to the drag force necessary to drive motility of the cell, further indicating that the sites of AglZ localization are where the force for motility is produced (Sliusarenko *et al.*, 2007). Furthermore, PMF inhibition of the gliding motor by

nigericin was shown to disrupt the localization of AglZ-YFP focal adhesion clusters (Sun *et al.*, 2011).

Together, these data support a model where gliding motility in *M. xanthus* is powered by complexes of regularly spaced AglZ to FACs, which act together with a motor and other components of the machinery to allow surface-associated movement without any extra-cellular organelles.

1.4.3 AglQ, GltD/AgmU and GltF span the cell envelope and localize to FACs

It was recently shown that genes which co-evolved with the gliding motor encoding *aglQRS* genes, are scattered in three different regions of *M. xanthus* genome (Figure 5) (Luciano *et al.*, 2011). Based on phylogenomics it was proposed that the minimal motility machinery is constituted by the AglQ/R/S motor encoded by the M (motor) region with at least 11 additional proteins encoded by genes in two distinct genetic regions called G1 and G2 (Figure 5). Proteins GltA-K in the G1 and G2 regions are predicted to form a complex which spans the cell envelope, as they contain domains which would localize them to the cytoplasm, inner and outer membrane. Cellular fractionation analyses showed that GltD/AgmU, GltE/AglT, GltG/PglI and GltF are found in the inner membrane fraction, whereas GltH is the only protein so far found in the outer membrane (Luciano *et al.*, 2011; Nan *et al.*, 2010).

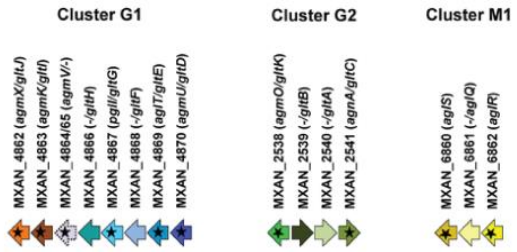

Figure 5. Genes found in the G1, G2 and M genetic clusters code for proteins which are proposed to constitute the minimal machinery required for gliding. G1 and G2 gene cluster members co-evolved with *aglQ/R/S* (M cluster) genes encoding the gliding motility motor. Figure adopted from Luciano *et al*., 2011.

Analyses of fluorescently tagged AglQ motor subunit demonstrated that its localization matches that of AglZ: AglQ-mCherry localizes to multiple FACs in the cell which disappear at the lagging cell pole (Figure 6). In addition, Sun and colleagues report that the subcellular fluorescent localization of the motor subunit AglQ with abolished protein binding ($AglQ^{D28N}$-mCherry) showed that the protein forms multiple paralyzed clusters within a cell, which do not display any dynamics, indicating that the

motility machinery can be formed, but it is not functional in the blocked motor (Sun *et al.*, 2011). Examination of fluorescently tagged GltD/AgmU revealed that the protein localizes to FACs and to a cluster at the leading cell pole, similarly to AglZ, (Figure 6). An additional component of the minimal motility machinery – GltF tagged to a fluorescent reporter was also shown to localize at the leading cell pole and to FACs in the cell (Figure 6) (Luciano *et al.*, 2011).

The findings that machinery components GltA, K and H are predicted to localize in the outer membrane, and that several outer membrane lipoproteins are essential for gliding, favor a model in which the proton channel powers force generation through transient contacts with the outer membrane adhesions, depicted in Figure 6.

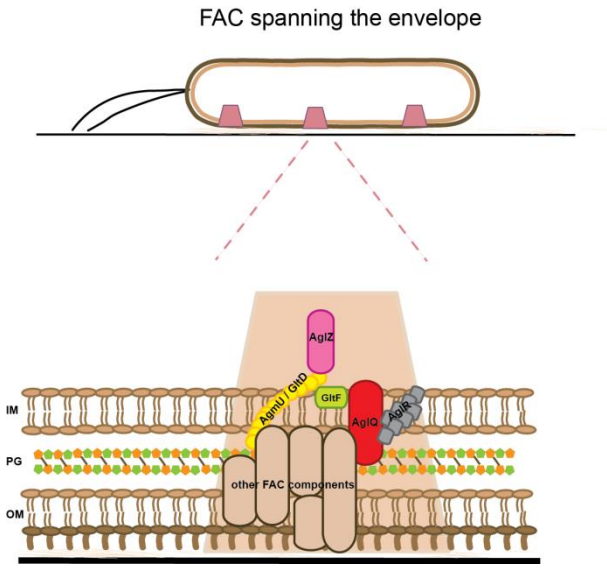

Figure 6. Model showing subcellular localization of the gliding motility components. AglQ and AglR motor subunits interact together localize to FACs. Further, fractionation analyses suggest that the above shown AglQ, AglZ, GltG/PglI, GltD/AgmU, GltC, GltA, GltB, GltK/AgmO and GltH localize to indicated cell envelope compartments. Additionally, GltD/ AgmU, GltF, and AglZ have been localized to FACs by fluorescent tags. It is predicted that large protein complex required for gliding consist of the proteins shown in the model. Other components of the FACs could include so far unidentified lytic enzymes which break the peptidoglycan (Vollmer *et al*., 2008), and surface associated proteins which attach the cell to the substratum.

Additionally, co-tracking of polystyrene beads on the cell surface with the cytoplasmic AglZ supports that the motility machinery spans the cell envelope as the beads are transported with the machinery complex despite the presence of the membranes.

Taken together, the evidence AglQ, AglZ, GltD/AgmU and GltF are components necessary for gliding which localize to FAC which get disassembled at the lagging cell pole, strongly suggested a motility mechanism where the activation of the motility

machinery occurs at the leading cell pole, and the power for gliding is exerted at FAC sites which span the envelope and are deactivated at the lagging cell pole (Figure 6).

1.4.4 Motility complexes move in a helical loop in the cell envelope

Although the FAC model parallels known movement machinery in eukaryotes, there are data supporting an alternative interpretation in *M. xanthus*. Experiments using deconvolution and photobleaching studies suggest that GltD/AgmU tracks along a helical loop which spans the entire cell, and this movement is dependent on PMF and intact MreB (Nan *et al.*, 2011; Nan *et al.*, 2010). Recent work using photo-activatable mCherry tagged to AglR motor subunit shows that it localizes to sites which resemble FACs, but within which single molecules of AglR move laterally within the membrane in a helical pattern (similarly to GltD/AgmU) (Nan *et al.*, 2013). Based on this evidence, a second model to explain the gliding motility machinery has been suggested (Figure 7). In this model, the components of the machinery do not span the cellular membranes and PG of the Gram-negative cell wall, but instead a helical rotor generates force for gliding in the following way: motor complexes together with force generating and transducing components for gliding create "low drag cargo" which moves within the inner surface of the membrane in helical trajectories along a cell-spanning loop; they slow upon reaching the gliding surface which leads to an accumulation of the complexes at those sites, creating "high drag cargo", which in turn leads to a local deformation of the membrane, and this slowing down of the complexes at sites appear as FACs (Figure 7). *M. xanthus* cells are suggested not to rotate significantly during gliding as the dynamics of AglR/AgmU and other FAC components is observed in both directions in immobilized cells (Koch and Hoiczyk, 2013; Nan *et al.*, 2013).

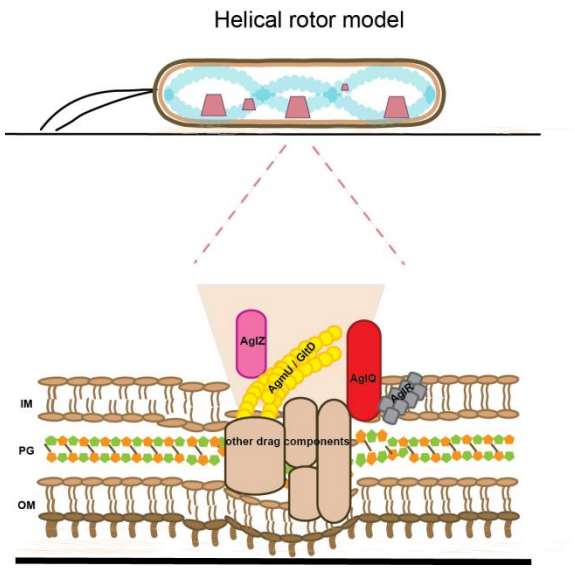

Figure 7. Helical rotor model. Motility protein complex functions inside the envelope by translocating along a helical track which spans the whole cell; multiple small motility complexes (small pink trapezoids) represent "low" drag cargo which jam onto each other leading to formation of "high" drag cargo (large pink trapezoids) and local deformations of the membrane when the complexes are in contact with the substrate.

1.4.5 Slime in gliding motility

Another component implicated for gliding in *M. xanthus* is extra-cellular slime. Slime (mucus) trails deposited by the cells at colony edges were first reported to be the favoured paths of motility for other cells in a study by Burchard, 1982 (Burchard, 1982). This finding led to a model where the engine which powers gliding motility by secreting the slime from the lagging cell pole provides enough force to directly propel the cell forward. The slime secretion was hypothesized to occur through nozzles (pores) found in the cell envelopes by electron microscopy, which were specifically enriched at the cell pole (Wolgemuth *et al.,* 2002b). Even though *M. xanthus* cells may recognize adhesive molecules deposited by other cells, this model of propulsion driven by secretion from the lagging pole is not in accordance with findings that artificially elongated cells were not affected in gliding motility, and that the motility machinery components are distributed along the cell body (Sliusarenko *et al.*, 2007; Sun *et al.*, 1999). More importantly, the components which constitute the nozzle structures have thus far not been identified.

A recent finding using wet-surface enhanced ellipsometry microscopy technique (Wet-SEEC) by Ducret and colleagues shows that the slime is deposited underneath the cell body, and it does not mediate propulsion of the cell from the lagging cell pole (Ducret *et al.*, 2012). Additionally, the slime was not continuously deposited underneath the cell, rather, its thickness varied from 0 to 5 nm, and widths from 200 to 900 nm. This study further demonstrated that the slime mediates cellular adhesion and enhances gliding motility by being in direct contact with motility complexes at the sites of the focal adhesions on the cell surface, where slime patches were specifically deposited at the sites where AglZ-YFP and AglQ-mCherry proteins co-localized at the FAC sites (Ducret *et al.*, 2012). It has been proposed that in this way slime most likely facilitates motility-driven attachment to the substratum by enhancing the attachment of the cell-surface components of the FACs to the substratum.

1.4.6 Bacterial cytoskeletal elements

In eukaryotes, cytoskeletal proteins have long been known as essential players in cellular organization, as described in section 1.1. The three canonical eukaryotic cytoskeletal proteins are actin, tubulin and intermediate filaments (Heng and Koh, 2010; Pollard and Cooper, 2009). Like eukaryotic cells, bacteria also contain cytoskeletal elements essential for cellular organization and maintenance of cell shape. The first

described bacterial cytoskeleton was FtsZ - a tubulin homolog (Bi *et al.*, 1991), followed by actin homolog MreB (Jones *et al.*, 2001), intermediate filament homolog crescentin and a novel class of filament - bactofilins (Ausmees *et al.*, 2003; Kuhn *et al.*, 2010). Bacteiral actins are structurally similar to F-actin, and they form filaments *in vitro* and *in vivo* (Jones *et al.*, 2001; van den Ent *et al.*, 2001). The superfamily of bacterial actin homologs includes MreB, FtsA, MamK, ParM, AlfA, Alp6/7/8, PilM subfamilies (Derman *et al.*, 2009). MreB homologs have been implicated in many cellular processes requiring spatial organization, including cell growth, morphogenesis, polarity, division, chromosome segregation and organelle positioning (Carballido-Lopez, 2006).

1.4.7 Bacterial actin cytoskeleton homolog MreB

MreB is the most widely conserved and best characterized bacterial actin-like protein found in most rod shaped bacteria. Biochemical analyses showed that MreB monomers can self-assemble laterally into bundles, often without requiring ATP or GTP *in vitro* (Carballido-Lopez, 2006). Assembly of *T. maritima* MreB depends on the temperature and concentration of different ions, but unlike actin, MreB can use both ATP and GTP as a substrate (Esue *et al.*, 2006b; van den Ent *et al.*, 2001). *B. subtilis* MreB polymerization does not depend on nucleotides, but it requires divalent ions and low pH (Mayer and Amann, 2009). Further work showed that, unlike for actin, MreB polymerization is rapid and does not require a nucleation step (Popp *et al.*, 2010). Additionally, MreB can catalyze ATP (and GTP for some MreBs) hydrolysis at a similar rate like F-actin (Esue *et al.*, 2006b). MreB depletion or disruption of polymerization by the drug A22 leads to formation of round cells in *B. subtilis*, *E. coli*, *C. crescentus, M. xanthus* and *P. aeruginosa* (Shaevitz and Gitai, 2010).

One role of the MreB cytoskeleton in cell shape is to apply the physical force that maintains cellular width; this is corroborated by the fact that micromanipulation of cells using optical traps is dependent on intact MreB (Wang *et al*., 2010). Also, addition of A22 drug which disrupts MreB polymerization, immediately reduces the stiffness of *E. coli*, a process which is reversible after A22 is washed out (Wang *et al.*, 2010). Studies in *B. subtilis*, *E. coli*, and *C. crescentus* have shown that one way in which MreB influences the cell wall is by directing the insertion of new PG cell wall material (Carballido-Lopez, 2006). The PG is a large glycopeptide composed of long strands of repeating N-acetylmuramic acid and N-acetylglucosamine subunits crosslinked by

peptide bridges and assembled by penicillin binding proteins (PBPs) and giving the bacterial cell rigidity and shape (Vollmer *et al.*, 2008).

MreB has an N-terminal membrane-binding amphipatic helix, which promotes its direct binding to the cytoplasmic membrane (Salje *et al.*, 2011). Additionally, MreB interacts directly with several cell wall-associated proteins such as MreC, MreD, PBP2, RodA, RodZ and MurG, thereby directly linking MreB to the cell-wall biosynthesis machinery, Figure 8 (Carballido-Lopez, 2006; Shaevitz and Gitai, 2010). The current model for how MreB maintains the rod-shape in bacteria during their growth, elongation and division is that there are two spatially distinct, and mutually exclusive pathways for PG synthesis: one for cellular elongation along the long axis, and the other for cell division (septum formation) (Dye *et al.*, 2005; Kruse *et al.*, 2003; Lleo *et al.*, 1990; Young, 2003).

The most recent findings on MreB's key role in PG synthesis are substantiated by the data that MreB forms short patches, which act as cytoplasmic scaffolds for the envelope-spanning PG machinery, summarized in a model in Figure 8. Moreover, these MreB short patches are highly dynamic and move circumferentially around the cell width (Dominguez-Escobar *et al.*, 2011; Garner *et al.*, 2011; Swulius and Jensen, 2012; van Teeffelen *et al.*, 2011). Importantly, in the studies by Dominguez-Esobar *et al*, Garner *et al* and van Teeffelen *et al*, it was also demonstrated that the dynamic movements of MreB are driven by PG synthesis, and that addition of antibiotics, which specifically inhibit PG synthesis stop MreB movement, as do the mutants of the molecular components involved in cell-wall elongation.

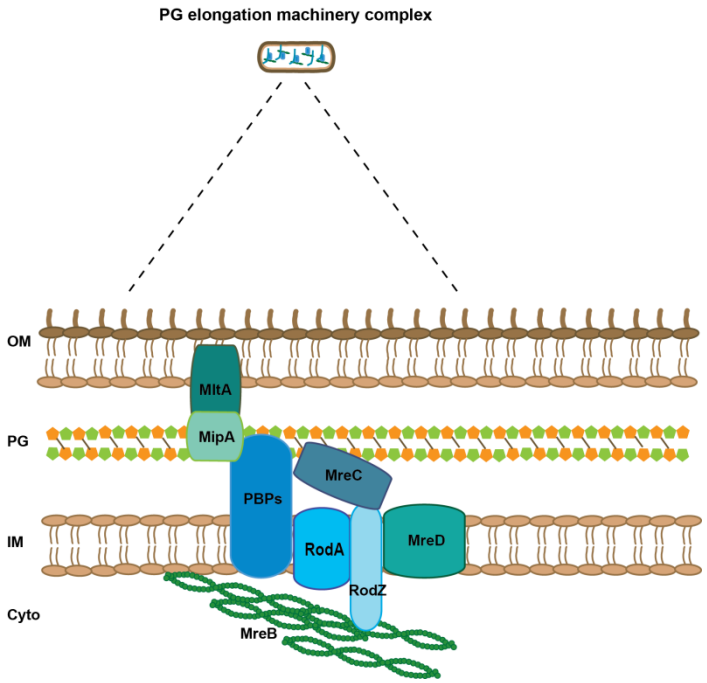

Figure8. A model depicting the role of MreB in peptidoglycan (PG) biosynthesis / cell wall in bacterial cells. MreB (in the cytoplasm) forms short patches (in green) all over the cell and determines the cell shape together with cell wall elongation machinery by acting as a cytoplasmic scaffold for the components of the machinery which span the membranes (in different shades of blue / green).

These three studies have shown that the addition of phosphomycin, mecillinam, ramoplanin, vancomycin and ampicilin blocks MreB dynamics in a specific manner, as the addition of antibiotics which target other cellular processes, such as kanamycin, rifampicin and chloramphenicol, do not inhibit MreB dynamics (Dominguez-Escobar *et al.*, 2011; Garner *et al.*, 2011; van Teeffelen *et al.*, 2011).

Since actin is known to be essential for surface-associated motility in eukaryotes, and MreB has been implicated in formation of AglZ FACs, the question of the exact function of MreB in *M. xanthus* gliding remained opened. Other functions of MreB have been implied mostly in polarity of bacterial cells. For example, localization of multiple polar markers in *C. crescentus* (PopZ, DivJ, CckA, PleC) depends on MreB (Bowman *et al.*, 2008; Gitai *et al.*, 2004). Localization of chemotaxis proteins in *E. coli* (Tar, CheY), and localization of T4P components and T4P driven motility in *P. aeruginosa* (PilT) depend on MreB (Cowles and Gitai, 2010; Shih *et al.*, 2005). Correct localization of MreB to the hyphal septa in *S. coellicolor* is required for sporulation, and in *M. xanthus* MreB is required for rod-sphere morphogenesis during sporulation, as well as for cell outgrowth and elongation of germinating spores in presence of nutrients (Mazza *et al.*, 2006; Muller *et al.*, 2012). Furthermore, in *M. xanthus* the localization of AglZ to FACs, which is essential for gliding, depends on MreB (Mauriello *et al.*, 2010b). Additional studies implicate a role of MreB in chromosome segregation and dynamics in *E. coli*, *B. subtilis* and *C. crescentus* (Formstone and Errington, 2005; Soufo and Graumann, 2003); furthermore, other studies firmly demonstrate the importance of MreB in chromosome segregation in *V. cholerae* and *H. pylori* (Srivastava *et al.*, 2007; Waidner *et al.*, 2009).

The role of MreB in PG synthesis in *M. xanthus* is not known, and apart from its importance in AglZ localization in FACs during gliding, it still remains to be elucidated whether MreB polymers generate force necessary for gliding, and if a motor protein tracks on them. Despite these hints, the role of MreB in gliding motility has not been elucidated so far, but in the Results sections 2. 3 and 2.4, I will present the data on the function of MreB during gliding in *M. xanthus*.

1.5 Spatial regulation of motility

The motor, FACs, chemosensory system, regulatory proteins and MreB are some of the components necessary for directed motility by gliding in *M. xanthus*. In the

next section, the signaling pathways regulating the motility, polarity and reversals will be discussed.

1.5.1 Spatial regulation of motility and stimulation of reversals by Frz chemosensory system

Directed cellular motility towards chemoattractants or away from chemorepellents is a phenomenon displayed by many different cell types. For example, human neutrophils and *Dictyostelium* amoebae are chemotactic towards cyclic AMP and migrate in response to its elevated levels (Kimmel and Parent, 2003). Bacterial cells also orient swimming in response to spatio-temporal chemical gradients, and this is regulated by chemosensory pathways consisting of signal perceiving and transducing components, which in turn regulate cellular behaviour in response to specific signals.

M. xanthus cells reverse their direction of gliding irregularly, on average every 10-25 minutes. Reversals are induced by Frz chemosensory system which, consists of cytoplasmic signal perceiving MCP FrzCD, two CheW homologs FrzA and FrzB, FrzE with a CheA histidine kinase domain and CheY receiver domain, FrzF - a methyl transferase, FrzG - a methylesterase, and FrzZ composed of two CheY receiver domains (Figure 9A) (Blackhart and Zusman, 1985).

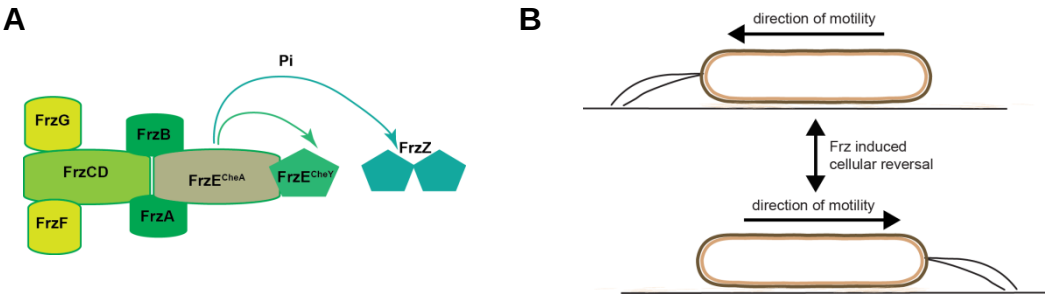

Figure 9. Cellular reversals are controlled by the Frz chemosensory pathway (A) Frz chemosensory system components and phosphor transfer in the presence of a signal. (B) Cellular reversal in *M. xanthus* is important for motility. Cells switch the poles, and the T4P structures are found at the new leading cell pole. Upon a cellular reversal cells start moving in the opposite direction.

The input signals which regulate the activity of the Frz system are not identified to date, but the current hypothesis is that they are sensed by FrzCD or FrzF (Bustamante *et al.*, 2004; Scott *et al.*, 2008). The output of the Frz system is generated by phosphorylation of FrzE on a conserved histidine residue in its kinase domain. In the absence of a signal, FrzE phosphorylated kinase domain transfers the phosphate group to its own receiver domain (Figure 9A, $FrzE^{CheA}$ phosphotransfers to $FrzE^{CheY}$) (Inclan *et al.*, 2008). In the

presence of a stimulating signal, FrzE autophosphorylates and transfers the phosphoryl group to FrzZ, which in turn stimulates cellular reversals (Figure 9A, B). Cellular reversals are stimulated by the Frz system, and dynamic switching of the poles is regulated by small G-protein MglA and its cognate GAP MglB (Leonardy *et al.*, 2010; Zhang *et al.*, 2010). Further, the Frz system interferes with MglA-B polarity through the RomR response regulator (Figure 9B) (Keilberg *et al.*, 2012; Zhang *et al.*, 2012). RomR contains site for possible phosphorylation by the upstream Frz system, and mutants which mimic the phosphorylation "on" and "off" states of RomR exhibit hyper- and hypo-reversing phenotype respectively, similar to the frz phosphorylation state mimicking "on" and "off" variants (Inclan *et al.*, 2008; Inclan *et al.*, 2007; Leonardy *et al.*, 2010). Furthermore, RomR localizes in a large cluster at the lagging cell pole, where it interacts with MglB GAP; also, RomR localizes in a small cluster at the leading cell pole where it forms a complex with MglA-GTP at the leading cell pole (pull-down experiments confirm the direct interactions of RomR with MglA and MglB wildtype proteins) (Keilberg *et al.*, 2012; Leonardy *et al.*, 2010; Zhang *et al.*, 2010). The exact interactions of FrzZ-FrzE and RomR-MglA-B have yet to be clarified, but based on the motility and reversals epistasis experiments it is suggested that RomR functions as a positive regulator of MglA-GTP by targeting it to the poles and possibly acting as a GEF, and that RomR inhibits MglB and in this way activates MglA indirectly by formation of the large cluster at the lagging cell pole. This is corroborated by the findings that RomR is essential for wildtype MglA polar localization, and furthermore, that continuously active $MglA^{Q82A}$ fluorescently tagged protein does not bind the poles in the absence of RomR (Zhang *et al.*, 2012, Keilberg *et al.*, 2012). Taken together, these results link the MglA-B/RomR polarity module to the Frz chemosensory system which induces cellular reversals and acts on MglA-MglB via RomR.

1.5.2 Regulation of different cellular processes in bacteria by GTP-binding proteins

As mentioned in section 1.5.1, MglA protein is essential for motility, and it acts downstream of the Frz chemosensory system to activate cellular reversals in *M. xanthus* (Figure 9). MglA defines a bacterial subclass of Ras-like small G-proteins (GTPases) (Brown, 2005; Caldon and March, 2003).

Ras-like small G-proteins consist of a single G domain (containing the P loop, switch I and switch II regions) of approximately 20 kDa in mass, made up of a six-stranded β-sheet and 5 α-helices on both sides of the sheet (Vetter and Wittinghofer,

2001). The G-domain contains the key residues for conformational changes, GTP binding and hydrolysis, depicted in Figure 10. Small G-proteins are molecular switches that cycle between the inactive, GDP, and active, GTP bound, states (Vetter and Wittinghofer, 2001). Eukaryotic small G-proteins are well studied, and their cycling between the GTP- and GDP-bound states *in vivo* is controlled by regulatory guanine nucleotide exchange factors (GEFs) which increase the dissociation of GDP and thus lead to an active G-protein, and GTPase activating proteins (GAPs) which activate the GTPase cleavage reaction and render the protein inactive (Spoerner *et al.*, 2001).

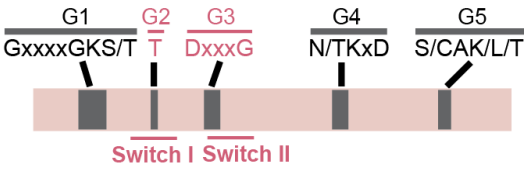

Figure 10. General features of the G domain. Conserved motifs (G1-G5) including the most important and conserved residues in each of the following regions: the phosphate binding P-loop (G1), switch I and switch II regions (G2 and G3, in pink text) change conformation during GTP binding, and G4 and G5 are responsible for contact with the guanine ring.

In eukaryotes, it has been established that the structure of the P-loop in the G-domain remains unchanged upon GTP binding, and the conformational changes are limited to switch I and switch II regions (Spoerner *et al.*, 2001; Wennerberg *et al.*, 2005). Switch I and II regions of the small G-proteins are dynamic, and they change confirmation depending on the nucleotide- and effector proteins-bound, in this way bringing the required residues active site. Previous works have shown that a threonine or a serine residue at position 17 in H-Ras coordinates the cofactor Mg^{2+} in both GDP- and GTP-bound states, and a conserved threonine at position 35 in H-Ras is essential for cofactor positioning after GTP hydrolysis (Figures 2, 10) (Vetter and Wittinghofer, 2001). Third invariant residue involved in Mg^{2+} binding is glycine at position 60 in H-Ras, which is crucial for the conformational change after GTP hydrolysis (Figures 2, 10). Furthermore, a conserved glutamine (at position 61 in Ras) is essential for GTP hydrolysis (Vetter and Wittinghofer, 2001).

In addition to MglA in *M. xanthus*, many bacterial species posses small Ras-like G-proteins made up of stand alone G-domains, and large G-proteins that also contain

additional domains, which are involved in cell polarity, signal transduction and cell division (Bulyha *et al.*, 2011; Caldon and March, 2003; Dong *et al.*, 2007). The large GTPase FlhF regulates the number and localization of flagella in *P. putida*, *P. aeruginosa*, *C. jejuni*, *V. cholera* and *V. alginolyticus* (Ataide et al., 2011; Balaban et al., 2009; Bange et al., 2007; Correa et al., 2005; Green et al., 2009; Kusumoto et al., 2008; Murray and Kazmierczak, 2006; Pandza et al., 2000). Bacterial dynamin-like large GTPase (BDLP) in *N. punctiforme* localizes to septation sites and plays a role in determining cellular morphology; further, DynA, a dynamin-like protein in *B. subtilis*, also localizes to septation sites, and promote membrane fusion *in vitro* (Burmann et al., 2011; Low and Lowe, 2006; Praefcke and McMahon, 2004). Small Ras-like CvnD9 protein in *S. coelicolor* is involved in signal transduction pathway, which regulate the onset of antibiotic production and morphological differentiation (Komatsu *et al.*, 2006). Recently, it has been shown that a small G-protein SofG regulates the recruitment of T4P proteins PilB and PilT to the poles in *M. xanthus*, together with a cytoskeletal element BacP (Bulyha *et al.*, 2013). In the absence of SofG, or in SofG GTPase negative mutant background, social motility by T4P is inhibited, and PilB and PilT cannot reach the poles where they drive the assembly and disassembly of T4P structures, respectively.

1.5.3 MglA small Ras like G-protein controls motility direction and cell polarity

MglA is the best characterized bacterial Ras-like G-protein, and is absolutely essential for both motility types in *M. xanthus* (Hartzell and Kaiser, 1991a). Recent studies revealed that MglA in the GDP-bound state has a similar structure like other small Ras-like GTPases, and that upon GTP-binding, MglA undergoes an unusual conformational change which involves a "screw"- type forward movement of the β2-strand, Figure 11 (Miertzschke *et al.*, 2011). This movement causes repositioning of the two essential catalytic residues, arginine 53 and glutamine 82 into the active site (Figure 11). Using an approach in which MglA variants locked in GDP- or GTP-bound conformations were analyzed *in vivo* and *in vitro*, it was shown that MglA acts as a nucleotide-dependent molecular switch. MglA-GDP represents the inactive form and is not able to stimulate cellular motility, whereas MglA-GTP is the active form which stimulates cellular motility and reversals (Leonardy *et al.*, 2010; Miertzschke *et al.*, 2011; Patryn *et al.*, 2010; Zhang *et al.*, 2010).

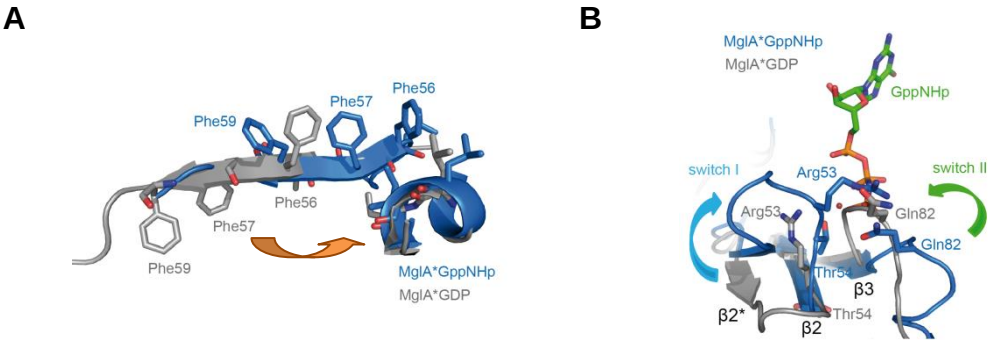

Figure11. Conformational changes in GTP-GDP transition (A) The β2-screw back-to-front (towards the nucleotide) movement of MglA on the GDP (grey) to GppNHp (blue) transition, reregistering Phe56, Phe57 and Phe59 besides other residues. (B) Structural change of switch I and switch II on the MglA·GDP (grey) to MglA·GppNHp (light green) transition highlighting Gln82. Figure modified from (Miertzschke *et al.*, 2011).

Fluorescently labeled wildtype MglA localizes to the leading cell pole, and upon cellular reversal MglA switches to the new leading cell pole (Leonardy *et al.*, 2010; Miertzschke *et al.*, 2011; Patryn *et al.*, 2010; Zhang *et al.*, 2010; Zhang *et al.*, 2012). The regulatory mechanism of MglA polarity at the leading cell pole has been shown to depend on MglB GAP and RomR response regulator. MglB functions as the cognate GAP of MglA by acting as a dimer to stimulate MglA GTPase activity by stabilizing switch I and II regions (Miertzschke *et al.*, 2011). MglB localizes to the lagging cell pole and excludes MglA from that pole by activating the transition to MglA-GDP. The localization of MglA at the leading cell pole depends on RomR, a response regulator which is also required for both motility systems (Keilberg *et al.*, 2012; Zhang *et al.*, 2012). Furthermore, fluorescently tagged MglA GTPase negative mutants (MglA variants locked in GTP-bound state) are able to localize to both cell poles, and are insensitive to MglB GAP activity (Zhang *et al.*, 2010; Miertzschke *et al.*, 2011).

Regulation of motility by MglA-MglB allows spatial control of both motility systems in *M. xanthus*, and enables dynamic polarity of the cell. The T4P-driven social motility is active at the leading cell pole containing T4P, and some of the proteins essential for T4P function are dynamic and re-locate to the new leading (PilB and FrzS) or new lagging cell pole (PilT), dependent on MglA, and in this way allowing T4P disassembly at the old leading cell pole and assembly at the new leading cell pole (Bulyha *et al.*, 2013; Bulyha *et al.*, 2009; Mignot *et al.*, 2007a). The importance of MglA GTPase cycle for activation of gliding machinery at the leading cell pole, and

disassembly at the lagging cell pole was suggested by the localization studies using AglZ, which is essential for gliding motility only. Cell polarization is known to be established by members of the small G-proteins in eukaryotic cells, and although the motility machinery is not conserved between eukaryotes and *M. xanthus*, the principles are rather similar.

In the following sections of my thesis work, I will describe the results on the function of MglA small G-protein and MreB actin-like cytoskeleton in *M. xanthus* gliding motility. We show that the function of MglA in gliding motility is to link the gliding motility machinery (AglZ and AlgQ motor subunit) to the MreB actin homolog protein. Further, we show that MglA in its active, GTP-bound state interacts directly with MreB to enable gliding, and formation and localization of FACs on the MreB cytoskeleton scaffold. In addition, we present evidence that MglA GTPase cycle is required for correct disassembly of the gliding motility machinery at the lagging cell pole. Furthermore, the data on cell wall elongation inhibition by specific antibiotics support the hypothesis that the previously proposed major function of MreB as scaffold for cell wall synthesizing machinery in other bacteria, is completely separable from its function in gliding of *M. xanthus*.

Some of the important questions remaining to be answered are considered in the last section of the Discussion chapter in this work.

2 Results

2.1 Regulation of motility by small Ras G-protein MglA and its GAP MglB

MglA is a well-characterized bacterial small G-protein, which is essential for both motility systems important for fruiting body formation during the developmental process in *M. xanthus*. The function of MglA in motility and cell polarity has been revealed in great detail, using crystallography, genetic, biochemistry, and cellular biology approaches (Hartzell and Kaiser, 1991a; Leonardy *et al.*, 2010; Mauriello *et al.*, 2010b; Miertzschke *et al.*, 2011; Patryn *et al.*, 2010; Zhang *et al.*, 2010; Zhang *et al.*, 2012). It was first reported that the MglA protein is important for motility two decades ago in a study by Hartzell and Kaiser (Hartzell and Kaiser, 1991a). Later, work from multiple laboratories showed that in addition to being essential for motility, MglA is crucial for correct polar localization and dynamics of motility proteins, thus representing a key regulator of cellular polarity in *M. xanthus* (Bulyha *et al.*, 2009; Leonardy *et al.*, 2010; Mauriello *et al.*, 2010b; Miertzschke *et al.*, 2011; Zhang *et al.*, 2010; Zhang *et al.*, 2012). The function of MglA as a master regulator of motility and polarity is carried out with its interaction partners, of which the most studied is MglB – a protein encoded in an operon with *mglA* (Hartzell and Kaiser, 1991b). Based on MglA sequence similarity to small Ras GTPases, earlier works showed that MglA nucleotide-bound state in the cell is essential for motility and cellular reversals (Leonardy *et al.*, 2010; Patryn *et al.*, 2010; Zhang *et al.*, 2010). A lack of MglA leads to completely non-motile and non-reversing cells. MglA$^{T26/27N}$ mutation (corresponding to S17N in Ras which locks the protein in the non-active state) led to a phenotype in motility and reversals identical to the cells lacking *mglA.* Typically, in small Ras/Rab/Ran/Arf/Arl G-proteins GTPase activation is based on correct positioning of the nucleophilic water by a crucial glutamine in the small G-protein, and by GAPs providing an arginine residue in the active site to neutralize the charges in the active site during GTP hydrolysis, Figure 5 (Scheffzek and Ahmadian, 2005). MglB sequence contains a Roadbloack/LC7 domain of unknown function, but no sequence similarities to eukaryotic GAP proteins were found. Loss of MglB causes hyper-reversing phenotypes, resembling those of MglA point mutants that lock the protein in the constitutively active, GTP-bound form. Cells lacking MglB or harboring MglA^{G21V} and MglA^{Q82L} point mutations corresponding to human GTP-locked active Ras G12V and Q60L variants, respectively), showed reduced overall motility and hyper-reversed with very

regular intervals of 5 to 7 minutes, compared to irregularly reversing wildtype (every 15 min, on average). With this in mind, it was shown that MglB is a cognate GAP protein of MglA, and to understand this further we used a crystallography approach. In the crystallography analyses MglA and MglB originating from *T. thermophilus* were used, due to inability to purify *M. xanthus* proteins in a soluble form. *T. thermophilus* MglA and MglB proteins have 62/81% and 28/25% sequence identity/similarity to their *M. xanthus* homologs, respectively, and they are able to partially complement the Δ*mglAB* deletion in *M. xanthus* (Miertzschke *et al.*, 2011). The crystals obtained for MglA and MglB separately confirmed that MglA is a small G-protein with similar structure and fold to small Ras/Ran/Arf. Additionally, crystals for the MglA-B complex were obtained; however, in that co-crystal five MglB residues were mutated in order to prevent previously observed self-polymerization of wildtype MglB (Q14A, R15A, R124A, Q127A and R131A, or $MglB^{A5}$). The MglA-B^{A5} co-crystals were obtained for MglA in the state which mimics the transition state of GTP hydrolysis ($MglA{\cdot}GDP{\cdot}AlF4^{-}$ $MglB^{A5}$), and in these crystals one MglA monomer was bound to two MglB monomers, making this an unusual stoichiometry for a small GTPase and GAP protein (Figure 12). The 1:2 MglA-B complex was confirmed by active site titration experiments and further supported by analytical size exclusion chromatography.

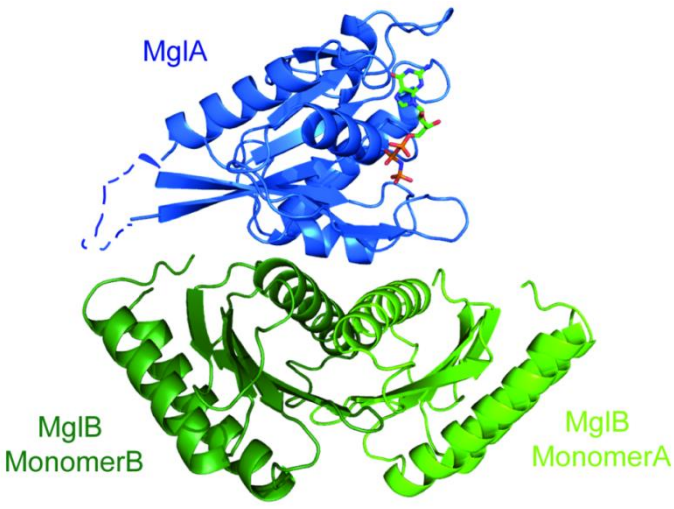

Figure 12. MglA and MglB proteins from *T. thermophilus* form a 1:2 complex. MglA monomer in blue interacts with MglB β-sheets in the two monomers (in green). Figure from (Miertzschke *et al.*, 2011).

Information from the structural analyses provided detailed insights into the function of MglA and MglB. The unusual MglA to MglB 1:2 ratio, and the fact that MglB provided no arginine or asparagine residues that could aid GTP hydrolysis at the MglA active site, led to the identification of a previously unidentified GAP mechanism. The crystal structure analyses showed that like in other small G-proteins, when MglA binds the GTP analogue (GppNHP) it undergoes a major structural change in the switch I and II regions. The most dramatic change is the back-to-front ("screw") movement of β2 in the β-sheet (Figure 11A), which leads to the positioning of arginine 53 and glutamine 82 residues in switch I and switch II region, respectively, (Figure 11B) towards the nucleotide. The glutamine at position 82 (position 62 in H-Ras) is the essential residue for GTPase activation and its replacement by alanine leads to a protein which cannot be deactivated by MglB. Upon binding MglB, the phenylalanine 57 and 59 residues in MglA are in contact with MglB, and the conserved threonine 54 residue is positioned to establish the canonical interaction between threonine and γ-phosphate of the GTP. Most importantly, the arginine residue at position 53 in MglA is positioned into the active site, thereby allowing GTPase activation and using MglB dimer as a structural stabilizer for MglA (Figure 12). Thus, the arginine that's usually provided by the GAP is not present in MglB, but is intrinsically present in MglA, making the mechanism of GTPase activation by MglB unique for so far characterized bacterial and eukaryotic small G-proteins. Detailed analyses of the MglA-B interaction and GTPase activity were carried out by substituting the crucial residues identified by bioinformatic analyses and confirmed by crystal structure in both proteins to alanine residues, followed by interaction studies and GTP hydrolysis assays. Individual substitutions in MglA of G21, R53 and Q82 to alanine all led to a loss of GAP-stimulated GTP hydrolysis, even though all protein variants were able to bind MglB similar to wildtype. Substitutions of A64 and A68 (corresponding to A68/72 residues which abolish MglA-MglB binding in *T. thermphilus* MglB) to arginine in MglB also caused hyper-reversing phenotypes. The GTPase activity of $MglA^{G21V}$ and $MglA^{R53A}$ was strongly reduced, whereas $MglA^{Q82A}$ had a completely abolished GTPase activity compared to wildtype, similar to the previously reported $MglA^{Q82L}$ variant (Zhang *et al.*, 2010).

To understand the importance of the MglA GTPase cycle, we constructed the GTPase negative substitutions that lock MglA in the constitutively active state *in vivo* based on the identified residues in the *T. thermophilus* homologs. We made use of the previously published *M. xanthus* $MglA^{G21V}$ variant that was published to complement the *mglA9*

non-motile phenotype (Leonardy *et al.*, 2010), and introduced it into a Δ*mglA* mutant, which could not be obtained in previous attempts to generate *mglA* deletion. Additionally, we constructed R53A and Q82A/L mutations in MglA, all of which were predicted to lock MglA in its active state.

The localization of MglA has been investigated in multiple studies by different research groups that revealed the polar localization of wildtype MglA and its dynamic re-localization to the new leading cell pole during cellular reversals (Leonardy *et al.*, 2010; Miertzschke *et al.*, 2011; Patryn *et al.*, 2010; Zhang *et al.*, 2010). Additionally, MglA was shown to localize in small adhesion complexes throughout the cell body, which were postulated to be important for gliding motility (Patryn *et al.*, 2010; Zhang *et al.*, 2010). For our analyses we used an N-terminal YFP tag because YFP-MglA successfully complemented Δ*mglA* (Table 1). The YFP-MglA^{G21V} mutant complemented the non-motile Δ*mglA* phenotype consistent with previous findings, resulting in hyper-reversing cells and reduced motility (Leonardy *et al.*, 2010). Additionally, YFP-MglA^{R53A} and YFP-MglA$^{Q82A/L}$ mutations led to hyper-reversing cells (Table 1). Thus, the *in vitro* analyses of *T. thermophilus* MglA protein identified the essential residues for GTPase activity of *M. xanthus* MglA. Furthermore, in the absence of MglB, MglA GTPase activity is abolished, thus leading to cells that phenocopy MglA mutants locked in the active state (hyper-reversing cells).

In contrast to Δ*mglA* mutants, cells lacking both *mglA* and *mglB* could not be fully complemented with YFP-MglA for their non-motile phenotype. Instead, Δ*mglAB* with a copy of YFP-MglA led to hyper-reversing phenotype as observed in the Δ*mglB* mutant, further supporting that MglB is the cognate GAP of MglA needed to regulate its nucleotide-bound state. The lack of MglB did not change the reversal phenotypes of cells containing YFP-MglA^{G21V}, YFP-MglA^{R53A} or YFP-MglA$^{Q82A/L}$ (Table 1).

Table1. Characterization of MglA variants *in vivo*

Genotype	Reversal period (min)	Cluster localization and dynamics			
mglB+A+	15.7				
Δ*mglBA*	Non-motile	Unipolar	Bipolar	Bipolar & fixed cluster	Fixed cluster only
Δ*mglA*	Non-motile			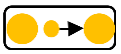	
Δ*mglA/yfp-mglA*	13.8 ± 3.2	84	16	-	-
Δ*mglA/yfp-mglA*^{G21V}	4.6 ± 0.3	11	-	-	89
Δ*mglA/yfp-mglA*^{R53A}	5.9 ± 0.8	-	30	70	-
Δ*mglA/yfp-mglA*^{Q82A}	6.9 ± 0.1	8	-	92	-
Δ*mglA/yfp-mglA*^{Q82L}	6.1 ± 0.3	-	10	90	-
Δ*mglBA/yfp-mglA*	7.7 ± 0.9	28	72	-	-
Δ*mglBA/yfp-mglA*^{G21V}	5.9 ± 0.3	7	-	0	93
Δ*mglBA/yfp-mglA*^{R53A}	6.5 ± 0.3	3	-	97	-
Δ*mglBA/yfp-mglA*^{Q82A}	7.1 ± 0.4	7	-	93	-
Δ*mglBA/yfp-mglA*^{Q82L}	6.8 ± 0.6	2	12	86	-

Table 1. Summary of *in vivo* characterizations of MglA mutants. Reversal periods in minutes, with standard deviations. Subcellular localization given as a percent of a total of 100 cells. The arrow in the localization diagrams indicates dynamic cluster of MglA variants.

Furthermore, to assay whether the GTPase activity was important for MglA localization *in vivo*, time-lapse microscopy was performed. Wildtype YFP-MglA localized to the leading cell pole and re-localized to the new leading cell pole during a cellular reversal (Figure 13A), as previously reported (Leonardy *et al.*, 2010; Patryn *et al.*, 2010; Zhang *et al.*, 2010). GTPase negative mutants YFP-MglA$^{Q82A/L}$ and YFP-

MglA^{R53A} localized to both cell poles, and also formed a large cluster that appeared to remain almost completely stationary/fixed during cell gliding. The arrival of this cluster at the lagging cell pole coincided with a cellular reversal (Figure 13C, 13D). The YFP-MglA^{G21V} mutant formed only one large cluster that appeared to stay fixed between the poles as the cell moved, shown in Figure 13B (similar to the one in YFP-MglA$^{Q82A/L}$ and YFP-MglA^{R53A}), but lacked polar clusters as previously described in the non-motile *mglA9* mutant background (Leonardy *et al.*, 2010). As expected, all of the GTPase negative mutants had similar phenotypes and localizations (Table 1). All three GTPase mutants formed a large cluster that appears to stay fixed relative to the substratum during cell movement, and the arrival of this cluster at the lagging cell pole coincided with a cellular reversal. The apparent dynamics of this cluster in all GTPase negative mutants, as viewed by the observer, is that the cluster oscillates between the cell poles, and once it reaches the lagging cell pole, it is not deactivated by MglB GAP, thus not disappearing but rather appearing to track back towards the new lagging cell pole, causing a cell to move one length length. Additionally, MglA$^{Q82A/L}$ and YFP-MglA^{R53A} were able to accumulate at the lagging cell pole, even in the presence of MglB, consistent with the GTPase assays by Miertzschke and colleagues, which show MglB interaction, but no GAP activation for these MglA mutant proteins.

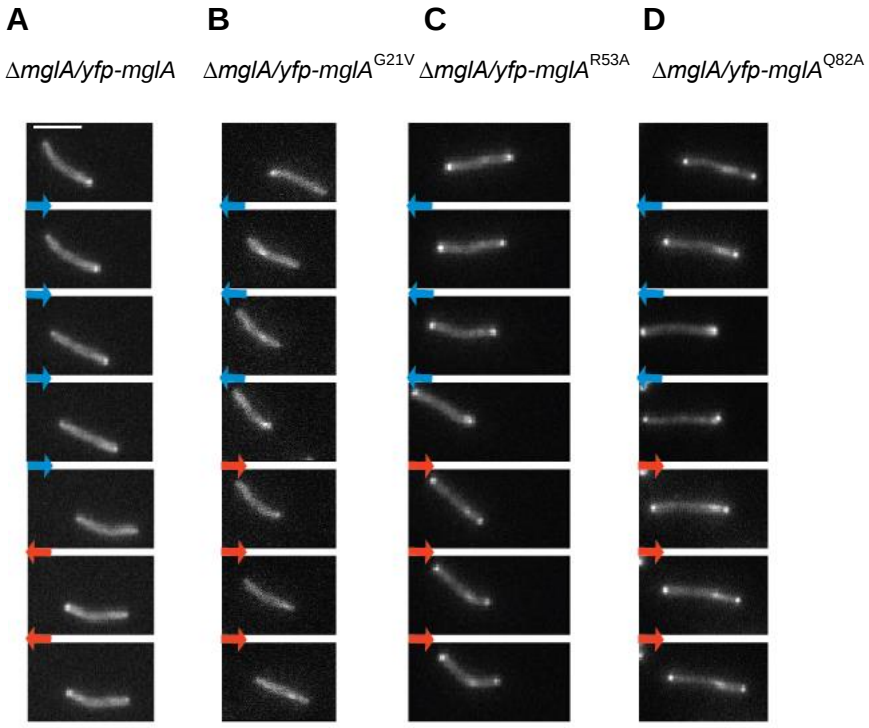

Figure 13. MglA GTPase activity is essential for its localization in the cell. (A) Localization of YFP-MglA in Δ*mglA*, (B) YFP-MglA^{G21V}, (C) YFP-MglA^{R53A}, (D) YFP-MglA^{Q82A}. Reversal of direction of movement indicated by arrows in red; Time lapse photos taken every 1 min.

In the Δ*mglAB* double mutant, YFP-MglA localized to both cell poles (Figure 14A) and YFP-MglA^{G21V}, YFP-MglA^{R53A} and YFP-MglA^{Q82A} (Figure 14B, C, D) all localized equivalent to a strain which contained MglB (Figure 14B, C, D). The finding that the phenotype of MglA GTPase negative mutants is epistatic to Δ*mglB* implies that MglA is the most downstream component in the signaling pathway regulating reversals. Furthermore, the fact that YFP-MglA in the absence of MglB does not restore the hyper-reversing phenotype to wildtype, and protein occupies both cell poles, supports the idea that the interaction between MglA and MglB and subsequent activation of GTPase hydrolysis by MglA is absolutely necessary for maintaining the polarity axis of the cell. Thus, MglA in its active form is kept at the leading cell pole and prevented from accumulating at the lagging cell pole where MglB exerts its GAP activity and converts it to MglA/GDP.

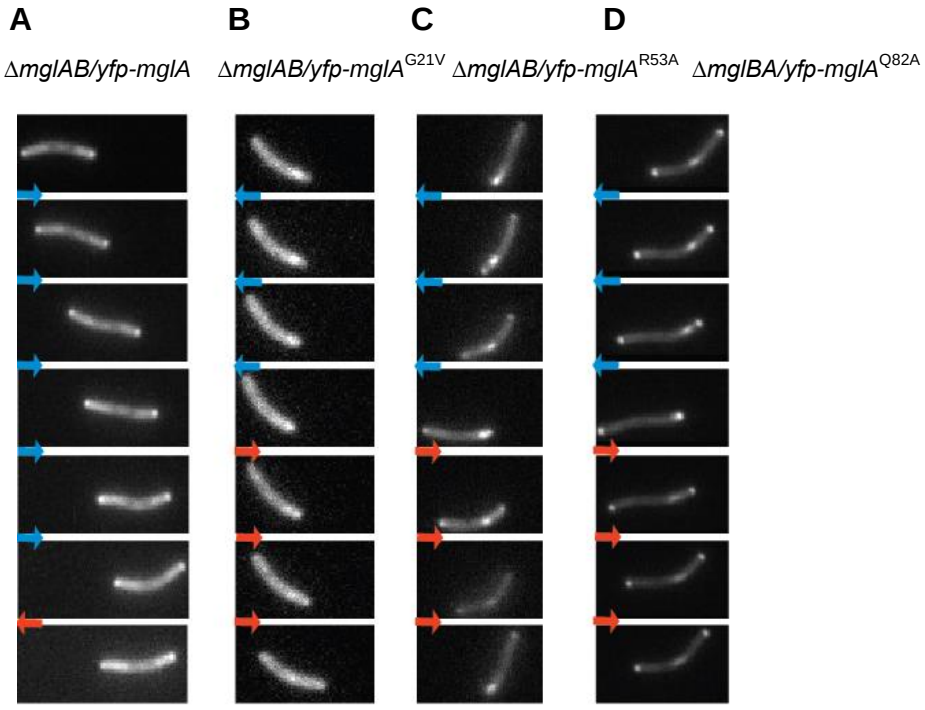

Figure 14. Localization of wildtype MglA depends on MglB. GTPase negative MglA mutants are insensitive to the absence of MglB. (A) Localization of YFP-MglA in Δ*mglAB* , (B) YFP-MglA^{G21V} in Δ*mglAB*, (C) YFP-MglA^{R53A} in Δ*mglAB*, (D) YFP-MglA^{Q82A} in Δ*mglAB*. Reversal and movement in the opposite direction is indicated by arrows in red; Time lapse photos taken every 1 min.

In summary, wildtype MglA protein showed a predominantly uni-polar localization at the leading cell pole. Perturbations in MglA GTP cycle led to cells which hyper-reversed at regular time intervals, which, importantly, coincided which a large non-polar cluster reaching the lagging cell pole. Cells harboring MglA GTPase negative

mutations continuously moved for a distance of one cell length, and the large MglA cluster appeared to remain fixed relative to the substratum during motility (and appears to oscillate between the poles relative to the cell body) causing the cell to reverse the direction of gliding once it reached the lagging cell pole. The results published by Miertzschke and colleagues describe a novel small G-protein-GAP activation mechanism, and these findings are supported by biochemical analyses and *in vivo* studies with different protein variants. MglA is the first characterized small G protein from Ras superfamily in bacteria, and it contains an intrinsic arginine "finger" essential for its GTPase activity, along with other previously described GTPase canonical residues. MglB is a first bacterial GAP described (Leonardy *et al.*, 2010; Mauriello *et al.*, 2010b; Zhang *et al.*, 2010), and we elucidated its mechanism of action on MglA using biochemistry and crystallography studies (Miertzschke *et al.*, 2011).

Current data suggest that MglA is essential for dynamic localization of motility proteins including FrzS, AglZ and PilT, and that locking MglA in its active ($MglA^{Q82L}$) or inactive ($MglA^{T26/27N}$) forms also affects the localizations of these proteins (Leonardy *et al.*, 2010; Zhang *et al.*, 2010). However, additional questions still remain such as: 1) How does MglA GTPase cycle regulate the gliding motility machinery? 2) What are the proteins which interact directly with MglA to enable gliding? and 3) What are the downstream effector proteins which interact with MglA in its active state to regulate gliding motility? To elucidate the function of MglA in motility, further studies of its direct interaction partners and functions are essential.

2.2 MglA GTPase cycle regulates FACs

Even though the role of MglA in motility has been studied extensively, only a few links between MglA and gliding motility have been made so far. To understand the function of MglA in gliding motility, we studied the link between MglA and the protein motility complexes that enable single cell gliding, but are dispensable for T4P-driven motility. Recent advances show that gliding motility machinery is composed of multi-protein complexes which are distributed along the cell body and appear to stay fixed relative to the substratum, thus resembling the eukaryotic-like FACs (Luciano *et al.*, 2011; Mauriello *et al.*, 2010b; Mignot *et al.*, 2005; Mignot *et al.*, 2007b; Nan *et al.*, 2011; Nan *et al.*, 2010; Nan *et al.*, 2013; Sun *et al.*, 2011).

Based on the previously reported interactions of MglA and AglZ, we hypothesized that active MglA might be localizing with AglZ FAC sites. Additionally,

the AglZ protein containing a pseudo response regulator N-terminal domain, and a C-terminal coiled-coild region was shown to interact with MreB cytoskeleton in an *in vitro* assay, and furthermore intact MreB was shown to be required for AglZ to localize to FACs (Mauriello *et al.*, 2009; Mauriello *et al.*, 2010b; Yang *et al.*, 2004). We then proceeded to analyze whether MreB is only required for positioning of AglZ to FACs, or if it also affect other components of FACs.

2.2.1 MglA localizes to FACs with AglZ

In the absence of MglA, or in the presence of MglA$^{T26/27N}$ inactive mutant, the localization of AglZ is diffuse (Leonardy *et al.*, 2010; Zhang *et al.*, 2012). In the presence of constitutively active MglA^{Q82L} mutant, AglZ forms one large cluster which stays fixed relative to the substratum as the cell moves (Zhang *et al.*, 2010). Second, AglZ and MglA interact in an *in vitro* pull-down experiment (Mauriello *et al.*, 2010b) and in a yeast-two hybrid approach (Yang *et al.*, 2004). Since the localization of the large non-polar YFP-MglA^{Q82A} cluster resembled a FAC which stayed fixed relative to the substratum as the cell moved (Figure 13D), it prompted us to use this GTPase negative mutant for further studies. First, we sought to investigate whether YFP-MglA^{Q82A} localizes to FACs by co-localization analyses with AglZ and AglQ. The AglZ-mCherry fusion integrated at the native site slightly affected gliding motility, but the protein localized similarly to the previously published fully functional AglZ-YFP. Thus, we proceeded with co-localization analyses, and found that AglZ-mCherry forms one large cluster that co-localizes with the YFP-MglA^{Q82A} large non-polar cluster, as the cell moved (Figure 15).

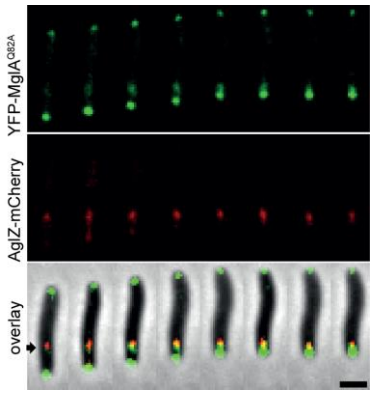

Figure 15. MglA^{Q82A} is found in the focal adhesion complex. YFP-MglA^{Q82A} co-localizes with AglZ-mCherry at one large focal adhesion cluster indicated by the black arrow (overlay in yellow). Time lapse every 1 minute, scale bar 1 µm.

To quantify the co-localization of AglZ with MglA^{Q82A} at FACs, we analyzed the strength of the correlation between YFP and mCherry signals between the poles in the strain co-expressing YFP-MglA^{Q82A}/AglZ-mCherry, and found that the Pearson coefficient *r* was 0.75, indicating a strong co-localization between AglZ and MglA^{Q82A} at positions between the cell poles.

To conclude, our co-localization of AglZ-mCherry with YFP-MglA^{Q82A} at FAC confirm that MglA is directly linked to the gliding motility machinery at FACs; further, the result that the formation of one prominent AglZ-mCherry cluster in MglA^{Q82A} background is consistent with the previous finding of AglZ forming one large FAC in a strain carrying MglA^{Q82L} variant (Zhang *et al*, 2010).

2.2.2 MglA localizes to FACs with AglQ

A recent breakthrough in *M. xanthus* gliding field was the discovery of the motor which powers gliding motility (Nan *et al.*, 2013; Sun *et al.*, 2011). The genes of the AglQ/R/S three-protein motor complex are encoded in an operon, and mutations in any of the genes abolish gliding motility without affecting T4P-driven motility.

These results prompted us to test whether active MglA^{Q82A} is also found together with AglQ motor subunit. Thus, we localized AglQ-mCherry in DK1622 wildtype (Figure 17A), and found that it forms multiple FACs, which is consistent with previously published results for DZ2 wildtype background (Sun *et al.*, 2011). When the lagging cell pole reached the AglQ-mCherry clusters, they disappeared, while new clusters were formed at the front of the cell. Interestingly, as seen with AglZ, in the presence of MglA^{Q82A}, AglQ-mCherry also formed one large FAC (Figure 17C). Furthermore, double-labeled strain containing AglQ-mCherry and YFP-MglA^{Q82A} revealed that the motor protein subunit co-localized with YFP-MglA^{Q82A} non-polar cluster (Figure 16A). The co-localizing cluster behaved similarly to what we previously observed for YFP-MglA^{Q82A} alone (Figure 13D); it retained a fixed position as the cell was moving and when the lagging cell pole reached the cluster, the cell immediately reversed its direction of gliding and the cluster did not disappear, but remained stationary as the new lagging cell pole approached it, thus appearing to the observer to oscillate towards new cell pole upon a reversal. Interestingly, the co-localizing FAC of AglQ-mCherry / YFP-MglA^{Q82A} did not disassemble at the lagging cell pole but stayed stationary with respect to the substratum as the cell reversed causing the cells to move in a pendulum-like motion, Figure 16A.

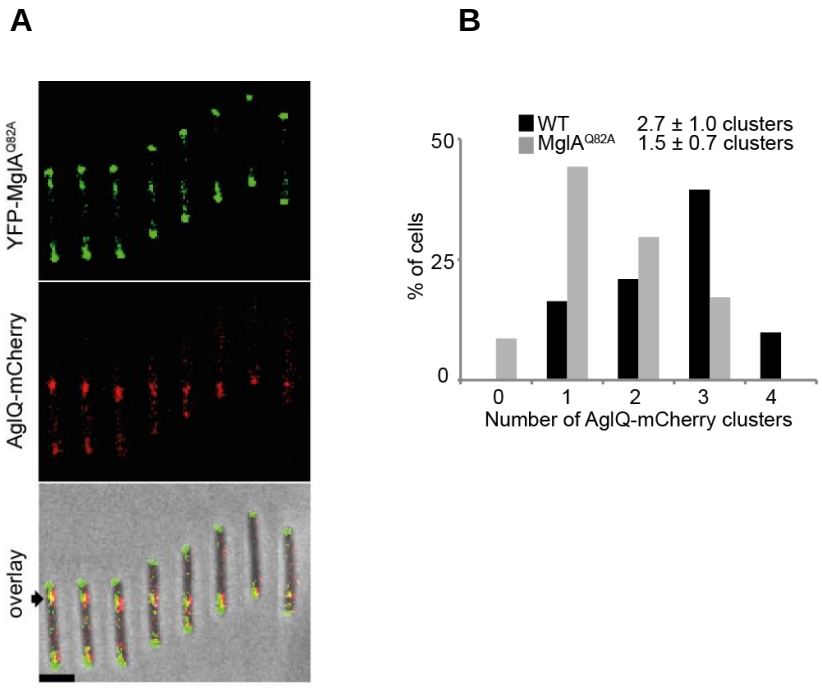

Figure 16. MglA^{Q82A} is a component of the focal adhesion complexes, and it regulates their formation. (A) YFP-MglA^{Q82A} co-localizes with AglQ-mCherry at one large focal adhesion cluster indicated by the black arrow (overlay in yellow). Time lapse every 1 minute, scale bar 2 µm. (B) The number of focal adhesion clusters of AglQ-mCherry in *yfp-mglA*$^{+}$ and *yfp-mglA*^{Q82A} backgrounds. Histogram representing the number of clusters found as a total percent of n=100 cells. Mean ±SD.

To quantify the co-localization of AglQ with MglA^{Q82A} at FACs, we analyzed the strength of the correlation between YFP and mCherry signals between the poles in the strain co-expressing YFP-MglA^{Q82A}/AglQ-mCherry. The Pearson coefficient *r* value was 0.81, indicating strong overlapping localizations of AglQ-mCherry and YFP-MglA^{Q82A} between the poles.

To conclude, our co-localization analyses of AglZ-mCherry or AglQ-mCherry and YFP-MglA^{Q82A} show that MglA in its active form is found in the FAC, suggesting that AglZ, AglQ and MglA are found at the same positions in FACs.

2.2.3 MglA GTPase cycle affects AglQ motor subunit

To test whether the incorporation of AglQ-mCherry to FACs depends on MglA, we analyzed AglQ-mCherry protein localization in a Δ*mglA* mutant. Contrary to the wildtype (Figure 17A), AglQ-mCherry was mostly diffuse in the cell envelope in the absence of MglA (Figure 17B). This result suggested that MglA regulates the

incorporation of AglQ into FACs (Figure 17B) as previously demonstrated for AglZ (Zhang *et al.*, 2010).

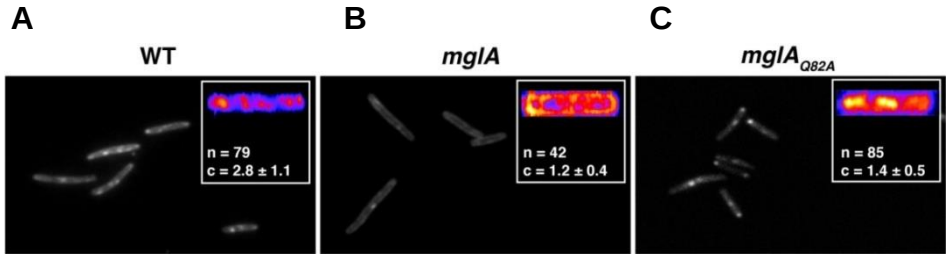

Figure 17. Localization of AglQ motor subunit depends on MglA. (A) AglQ-mCherry localizes to multiple focal adhesion clusters in the cell. The inset shows average cumulative localization of n cells; c = average number of prominent clusters ± SD. (B) AglQ-mCherry localizes diffuse in the absence of MglA. (C) AglQ-mCherry forms one prominent cluster in presence of MglA^{Q82A} variant.

Findings presented in this chapter strongly support the idea that MglA and its nucleotide-bound state regulate the disassembly and the number of FACs, respectively, and importantly, that the active form of MglA is a component of the FACs. However, questions underlying the formation of the YFP-MglA^{Q82A} cluster still remain.

2.2.4 Loss of AglQ affects YFP-MglA^{Q82A}

It was previously reported that the localization of AglZ-YFP in FACs is perturbed in the absence of AglQ (Sun *et al.*, 2011). Cells lacking *aglQ* displayed multiple non-polar clusters that resembled FACs but did not display the regular AglZ appearing at the front of the cell and disappearing at the back, as observed in wildtype cells during movement. Interestingly, AglQ was not required for dynamics of a polar AglZ-YFP cluster as this cluster re-located from pole-to-pole every few minutes, even though the cells were completely non-motile. These observations suggested that AglQ is not necessary for polar localization of AglZ-YFP, but it is important for dynamics of AglZ clusters in the FACs (Sun *et al.*, 2011). To investigate whether the localization of MglA at the poles or in the FAC depends on AglQ, we analyzed YFP-MglA^{Q82A} in a Δ*mglA*Δ*aglQ* mutant. The Δ*mglA*Δ*aglQ* cells are non-motile, and the expression of YFP-MglA^{Q82A} did not restore gliding motility. YFP-MglA^{Q82A} at both cell poles was not affected in Δ*aglQ* background (Figure 18). Interestingly, the internal cluster of YFP-MglA^{Q82A} was formed in many cells of Δ*aglQ* strain (Figure 18A, 18B), but it remained at one position at all times, suggesting that AglQ is required for proper FAC dynamics.

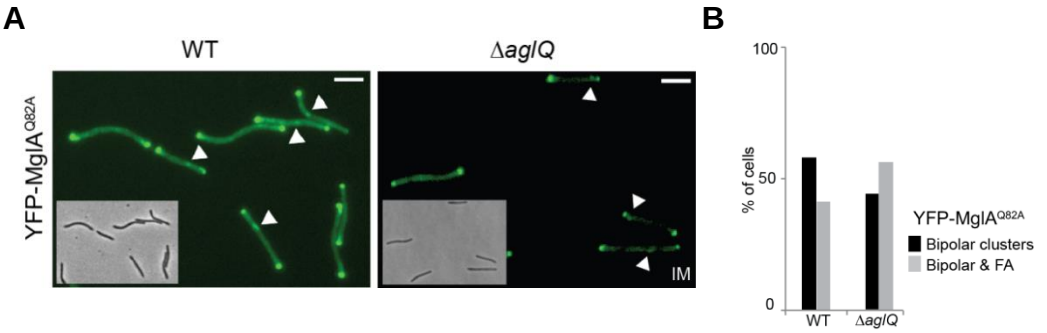

Figure 18. Absence of AglQ leads to impaired localization and dynamics of YFP-MglA^{Q82A} focal adhesion clusters. (A) Localization of YFP-MglA^{Q82A} in Δ*mglA/aglQ*$^{+}$ (on the left) and Δ*mglA/*Δ*aglQ* (on the right) background. White arrowheads indicating focal adhesion (FA) clusters of YFP-MglA^{Q82A}. Strain lacking *aglQ* displays defected and immobilized YFP-MglA^{Q82A} clusters indicated by white arrowheads. Insets showing phase contrast pictures (B) Histograms showing the localization of YFP-MglA^{Q82A} as a percent of total cells counted, at the poles (black bars) and in focal adhesion clusters (in grey bars) in Δ*mglA/aglQ*$^{+}$ and Δ*mglA/*Δ*aglQ*, n=100 cells per strain.

2.2.5 Inhibition of gliding motor by nigericin disperses YFP-MglA^{Q82A} from FAC

To determine whether a fully functional gliding motor is necessary for formation and localization of components found in FACs, we studied the effects of the antibiotic nigericin which inhibits PMF but does not affect the ATP pool levels in the cell (Sun et al., 2011). Nigericin at a concentration of 100 µM was shown to block gliding motility, disperse the localization of AglQ-mCherry FACs and block the rotation of AgmU-mCherry clusters moving in helical patterns in DZ2 strain background using agar pads buffered with nigericin (Nan et al., 2011; Sun et al., 2011). Thus, we tested the effects of nigericin on gliding of wildtype DK1622 strain, and found that it led to an arrest of motility within 1-2 minutes after its injection into a chitosan-coated flow chamber. Further, we tested the effect on nigericin on the localization of AglQ-mCherry or YFP-MglAQ82A in chitosan-coated flow chambers. Surprisingly, in contrast to previously reported data, injection of nigericin to AglQ-mCherry-expressing cells led to a complete immobilization of AglQ-mCherry FACs, Figure 19.

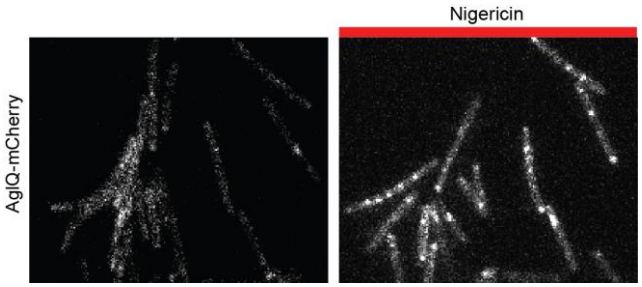

Figure 19. Addition of nigericin leads to an arrest in motility and formation of large paralyzed/immobile focal adhesions. Motile AglQ-mCherry cells before treatment (on the left) and after nigericin was added (on the right, red bar).

Addition of nigericin to cells led to a formation of large and prominent clusters of the AglQ-mCherry (Figure 19), but interestingly they were paralyzed in one position in the cell as long as nigericin was present in the chamber. As soon as nigericin was washed out, the cells started to move again, and AglQ-mCherry clusters resumed their dynamics.

Next, we tested whether nigericin affects the localization of YFP-MglA^{Q82A} and found that the polar clusters are not affected in presence of nigericin, but interestingly, the FAC between the poles disappeared when nigericin was present in the chamber (Figure 20A).

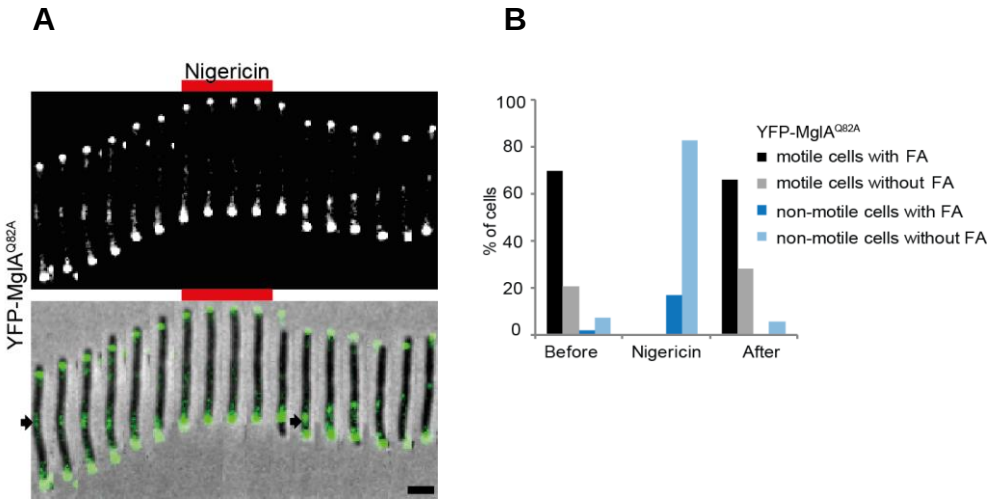

Figure 20. Nigericin disperses YFP-MglA^{Q82A} focal adhesion clusters (FAC). (A) Motile cell harboring YFP-MglA^{Q82A}; Red bar above the cell indicates nigericin presence in the chamber. Black arrow indicates the FAC. Lower row overlay of phase contrast and fluorescence images. Time lapse every 1 min. (B) Histograms showing quantification of YFP-MglA^{Q82A} focal adhesion clusters in pre-treated, nigericin-treated and post-treated cells, as a total percent of cells.

Upon addition of nigericin, cell motility was blocked and the disappearance of the YFP-MglA^{Q82A} FAC happened within 1-2 minutes after nigericin addition. Additionally, we observed that the cell motility was initiated and the FAC (marked by black arrow in Figure 20A) re-appeared 1-2 minutes after nigericin was washed out. This occurred in the majority of the cells (quantified in Figure 20B), and led us to conclude that blocking PMF and gliding engine leads to two different localizations of the proteins which localize to focal adhesions. Namely, AglQ-mCherry clusters were completely paralyzed in presence of nigericin (Figure 19); however, YFP-MglA^{Q82A} was not able to localize to the FACin presence of nigericin (Figure 20A).

To further understand the connection between YFP-MglA^{Q82A} and AglQ, but did not form any focal adhesion clusters in presence of nigericin, we examined YFP-MglA^{Q82A} localization and dynamics in presence of a gliding motor mutant AglQ^{D28N}.

2.2.6 Paralyzed motor affects the localization of YFP-MglA^{Q82A}

It was previously shown that AglQ gliding motor component contains an aspartate residue (D28) that is essential for its proton motive force driven function, and is in turn essential for gliding motility. Interestingly, the AglQ^{D28N} non-functional protein variant (paralyzed motor mutant) tagged to mCherry localized to fixed positions within the cell in multiple clusters (Sun *et al.*, 2011). To determine whether the paralyzed motor mutant influences the localization of MglA^{Q82A} to FACs, we tested the localization of YFP-MglA^{Q82A} in a strain where wildtype AglQ was replaced with AglQ^{D28N}. Strains carrying AglQ^{D28N} lacked gliding motility and displayed multiple YFP-MglA^{Q82A} clusters between the poles, resembling the focal adhesions (Figure 21A).

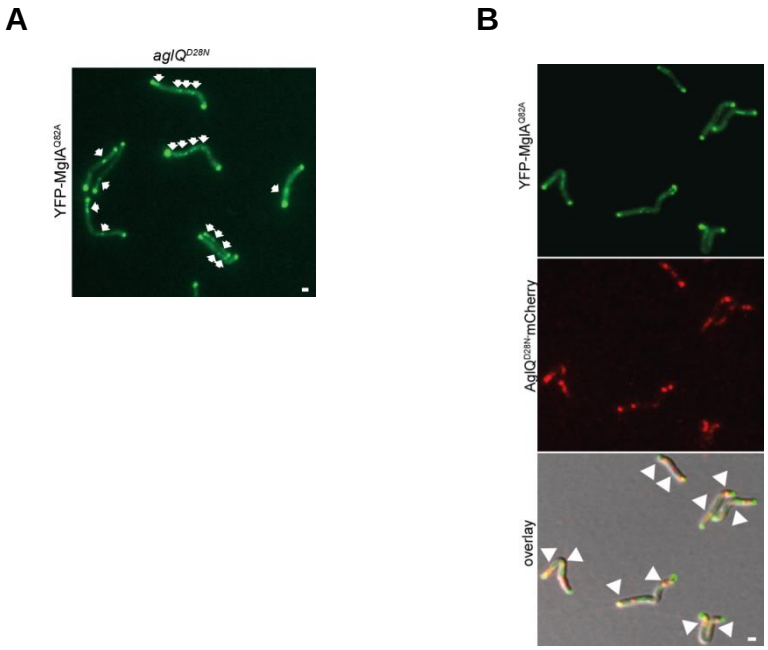

Figure 21. YFP-MglA^{Q82A} forms multiple clusters between the poles in paralyzed motor mutant. (A) Localization of YFP-MglA^{Q82A} in one focal adhesion cluster is inhibited in presence of AglQ^{D28N}. Multiple clusters forming between the poles marked with white arrowheads. (B) YFP-MglA^{Q82A} and AglQ^{D28N}-mCherry partially co-localize in the cell. Overlay photo in the third row shows yellow co-localization clusters between the poles, indicated by white arrowheads.

Localization of polar clusters of YFP-MglA^{Q82A} was not affected, but the multiple clusters between the poles reminded us of the previously published AglQ^{D28N}-mCherry localization (Figure 21A). This indicated that in the paralyzed motor mutant YFP-MglA^{Q82A} cannot form one FAC, but is rather forming multiple defective clusters

throughout the cell. One reason for this could be that there is a physical link between MglA and AglQ proteins, independent of the point mutant variants. Therefore, we sought to analyze the link between AglQ^{D28N}-mCherry and YFP-MglA^{Q82A} in a co-localization experiment. From the co-localization analyses we found that these two proteins co-localize at multiple positions within the cell only occasionally (Figure 21B). Therefore, this co-localization experiment uncovered that paralyzed AglQ^{D28N}-mCherry is not always co-localizing with YFP-MglA^{Q82A}, and that the formation of a single prominent FAC of YFP-MglA^{Q82A} between the cell poles depends on presence of the fully functional AglQ protein (Figures 20 and 21).

2.2.7 Lack of AglZ inhibits formation of MglA^{Q82A} in the FAC

To determine the effects of *aglZ* deletion on the FAC of MglA^{Q82A} we constructed Δ*mglA/*Δ*aglZ* double mutant and checked for motility and localization of YFP-MglA^{Q82A}. The absence of *aglZ* alone abolishes gliding motility, and the Δ*mglA/*Δ*aglZ* double mutant was also non-motile. Importantly, bringing YFP-MglA^{Q82A} in the double deletion strain lacking *aglZ* did not restore gliding, and led to localization of YFP-MglA^{Q82A} only at the cell poles, inhibiting FACs localizations (Figure 22A and B).

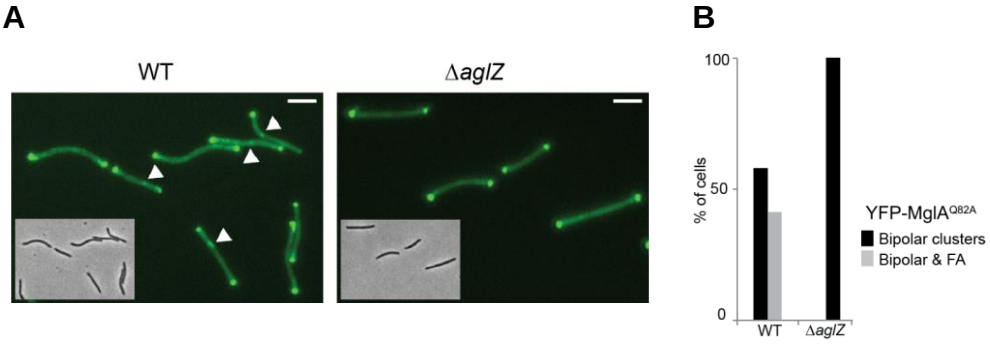

Figure 22. Loss of AglZ abolishes the formation of MglA^{Q82A} FAC. (A) Strain lacking aglZ displays only bi-polar localization of YFP-MglA^{Q82A} and no clusters between the poles. Inset phase contrast. (B) Histogram representing the distribution patterns of YFP-MglA^{Q82A} in wildtype and *aglZ* lacking strains at both cell poles (black bars) and with FACs (grey bars), n=100 cells.

These results implied that AglZ is absolutely required for the localization of MglA^{Q82A} to FACs. This could be due to AglZ being the component of the gliding machinery that interfaces between the machinery and MglA, thereby maintaining MglA in the FACs, as these two proteins have previously been shown to interact directly.

The reversal cycles of *M. xanthus* are controlled by the Frz chemosensory pathway (Figure 9). Earlier work in DZ2 strain background showed that a deletion of

the N-terminal part of FrzCD rescued the gliding motility phenotype of the Δ*aglZ* mutant (Mauriello *et al.*, 2009). Further work revealed that another suppression of the Frz system resulting from a *frzE* null phenotype due to a transposon insertion partially restored gliding motility of a Glt non-motile mutant (Luciano *et al.*, 2011). Based on this, we made use of the strain which lacks *aglZ* but has restored gliding motility due to a suppressor mutation in the Frz chemosensory system that bypasses the need of AglZ for gliding (Mauriello *et al.*, 2009).

To investigate whether we can bypass the need of AglZ for YFP-MglA^{Q82A} FAC formation, we first tested whether the Δ*aglZ* phenotype can be suppressed by introducing *frzE::*Tn5Ω226 mutation in DK1622 background. We found that motility in Δ*aglZ* strain was not recovered when combined with *frzE::*Tn5Ω226. We proceeded to test whether Δ*aglZ*Δ*mglA frzE::*Tn5Ω226 *yfp-mglA*$^{+}$ cells are motile, but were not able to confirm this as cells showed only slight displacement with time, but no major movement (data not shown). Furthermore, the fluorescently labelled cells of Δ*aglZ*Δ*mglA frzE::*Tn5Ω226 *yfp-mglA*^{Q82A} strain did not show restoration of YFP-MglA^{Q82A} in FACs, and additionally, we saw no significant restoration of gliding motility (Figure 23). These data suggested that AglZ is absolutely required for MglA^{Q82A} localization in the FAC.

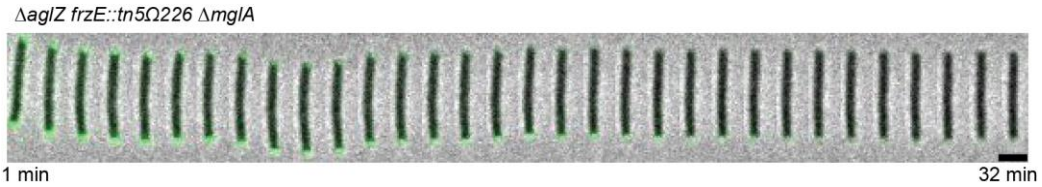

Figure 23. *frzE::*Tn5Ω226 mutation does not bypass the need of AglZ for gliding or MglA localization. (A) Time lapse movie of a cell harboring *yfp-mglA*^{Q82A} Δ*aglZ*Δ*mglA frzE::*Tn5Ω226 display MglA localization at both cell poles, but no focal adhesion clusters. Scale bar = 2 µm, time between frames 1 min.

The regulatory role of AglZ in gliding motility was proposed based on its ability to remove the negative effects on gliding. One of the possible reasons for the inability of Frz inactivation to surpass the need for AglZ in motility is the strain background differences used in this versus other studies and further investigations are needed to clarify the differences in the two wildtype backgrounds.

2.3 MreB is essential for motility and FACs

MreB is implicated in a variety of cellular processes such as cell shape morphogenesis, division and polarity. The central role of MreB in many bacterial

species is in spatial and temporal regulation of cell-wall growth (Figure 8) (Carballido-Lopez, 2006; Dominguez-Escobar *et al.*, 2011; Garner *et al.*, 2011; Shaevitz and Gitai, 2010; van Teeffelen *et al.*, 2011). In *M. xanthus*, MreB is essential for cell viability, and it has been shown to be required for gliding motility and spore formation (Mauriello *et al.*, 2010b; Muller *et al.*, 2012). MreB polymerization can be specifically inhibited by using a small antibiotic molecule A22 (Bean *et al.*, 2009), and addition of A22 to *M. xanthus* cells leads to a rapid arrest in motility, which can be reversed by washing away the inhibitor. Moreover, it was also reported that A22 disrupts the localization of AglZ-YFP to FACs in the DZ2 strain (Mauriello *et al.*, 2010b).

2.3.1 A22 affects cell shape and gliding motility

To analyze the effects of A22 on gliding motility and on the formation and stability of FACs, we performed experiments in presence of A22. First, we determined the minimal inhibitory concentration (MIC) of A22. At MIC of 10 µg/ml cells become more rounded and eventually lyse (Figure 24A, 24B). Also, 10 µg/ml (corresponding to MIC of A22) was notably the concentration of A22 which abolished single cell gliding (Figure 24C).

A

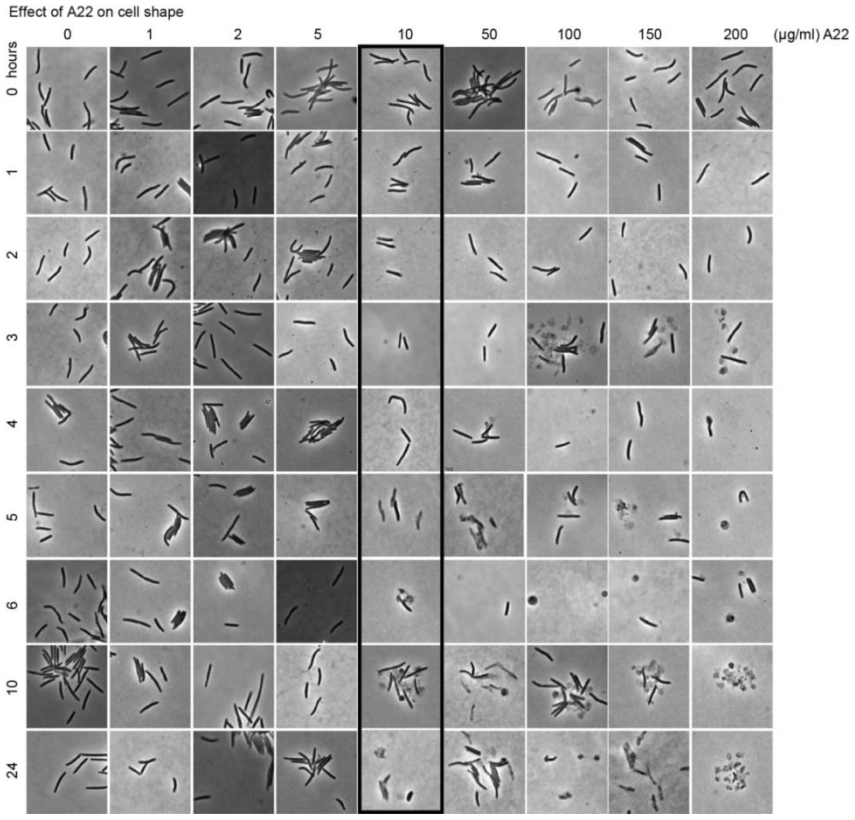

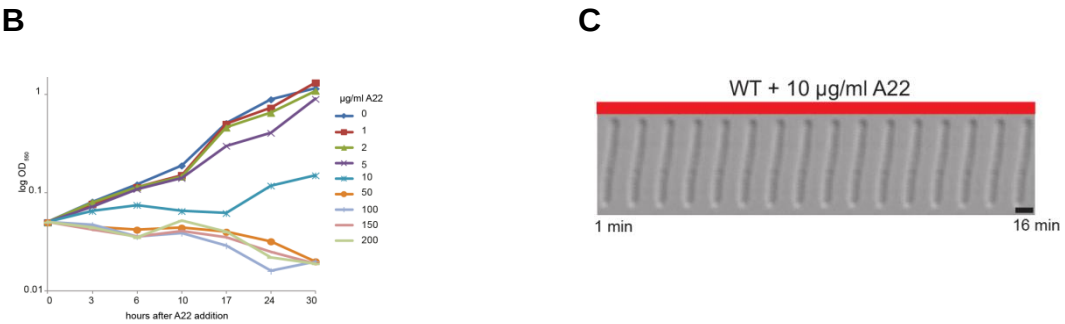

Figure 24. A22 causes growth inhibition and cell lysis in *M. xanthus.* (A) Determination of MIC of A22 on WT DK1622. Phase contrast images are displayed. The first time-point and concentration at which cells show evident shape changes with bulges are marked by black box. (B) Growth curves of WT DK1622 with different concentrations of A22. MIC of A22 is 10 µg/ml. (C) Gliding motility in WT DK1622 is blocked by 10 µg/ml A22.

MreB perturbation experiments in the chitosan-coated flow chamber led to a motility arrest after10 µg/ml A22 was manually injected; this method allows the scoring of the immediate effects of the injected compound. In agar based studies cells were mixed with A22 for a few minutes, then transferred onto an agar pad containing the same concentration of the drug, and analyzed microscopically after 10-20 min, for 15 min.

2.3.2 MreB perturbation affects the localization of MglA and AglQ in FACs

To elucidate the role of MreB in localization and preservation of FACs during gliding, we used the chitosan-coated flow chamber, for detection of the instantaneous effects of the injected drug. As previously shown, A22 blocked gliding of the cells 1-2 min post injection in a reversible manner: after washing A22 out of the chamber with TPM glucose containing buffer, cells resumed gliding after 1-2 min (Figure 25A, 25E). Importantly, while A22 was present in the flow chamber, YFP-MglA^{Q82A} polar localization was not perturbed, but the FAC was completely dispersed, Figure 25A, 24B. The control strain carrying A22-insensitive MreB^{V323A} variant did not stop gliding (Figure 25C, 25E), and did not show aberrant YFP-MglA^{Q82A} localization (Figure 25D).

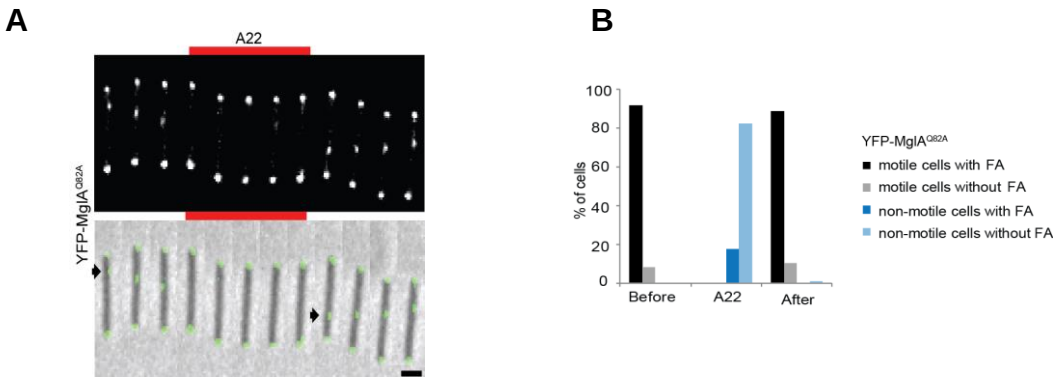

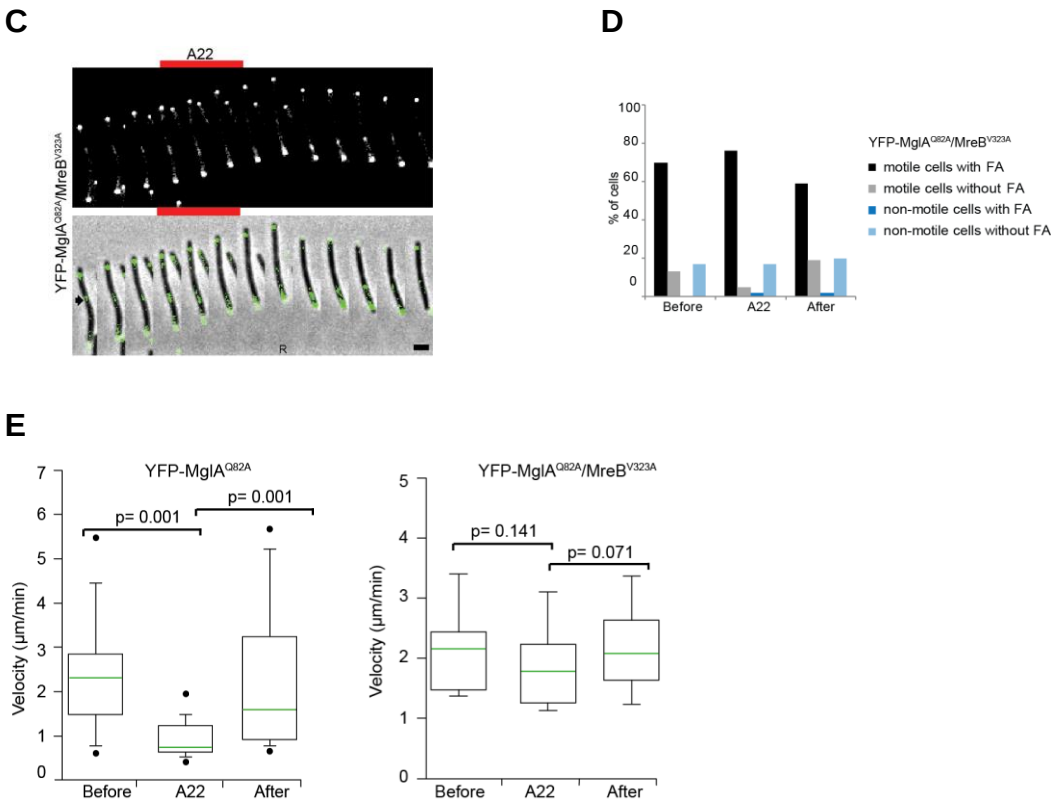

Figure 25. MreB is important for motility and focal adhesion cluster (FAC) formation. (A) YFP-MglA^{Q82A} mutants were imaged in 1 minute increments, and the addition of A22 (10 µg/ml) is indicated by red bar over the cells frames. Black arrows in the overlay indicate FACs. Scale bar = 2 µm. (B) Quantification of YFP-MglA^{Q82A} FACs and cell motility before, during and after A22 treatment, as a percent of cells. (C) YFP-MglA^{Q82A} and MreB^{V323A} double mutants were analyzed for their response to A22 as described in panel A. (D) Quantification of YFP-MglA^{Q82A} FACs and cell motility in a strain containing MreB^{V323A} before, during and after A22 treatment, as a percent of cells. (E) Boxplots showing the cell velocities in presence and absence of A22, of the YFP-MglA^{Q82A} strain on the left, and YFP-MglA^{Q82A}/MreB^{V323A} strain on the right. Green bars in boxes represent the average cell velocity for each condition. The *p*-values indicate statistically significant (values less than 0.05) or insignificant (values higher than 0.05) differences obtained using Student's *t*-test.

The observation that in the presence of A22 the gliding motility is inhibited and the localization of YFP-MglA^{Q82A} in the FACs is disrupted strongly implied that MreB is directly responsible for the localization of MglA^{Q82A} to FACs. To further analyze the importance of MreB for FACs, we tested the localization and dynamics of AglQ-mCherry in wildtype background, under the same flow chamber injection conditions of A22. AglQ-mCherry was rapidly dispersed from FACs in presence of A22 (Figure 26A, 26B), but motility and AglQ-mCherry localization was restored upon rinsing A22 from the chamber, shown in Figure 26A, similar to the previously published A22 effects on AglZ localization and dynamics.

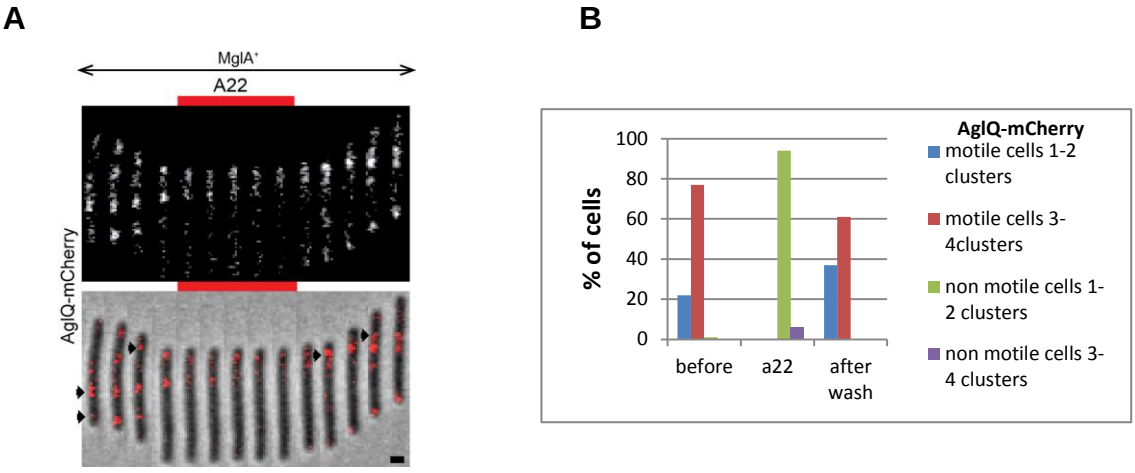

Figure 26. A22 disrupts the localization of AglQ-mCherry clusters. (A) Cells containing AglQ-mCherry were imaged at 1 min intervals. The red bar indicates time points when A22 was present, and black arrows mark focal adhesion clusters. Scale bar 1 µm. (B) Quantification of AglQ-mCherry clusters and cell motility present in the cell before, during and after A22 treatment, as a percent of cells.

To test whether AglQ-mCherry and YFP-MglA^{Q82A} co-localizing in a FAC disappear simultaneously in the presence of A22, we performed the A22 injection experiment on a double-labeled AglQ-mCherry/YFP-MglA^{Q82A} strain. Indeed, 1-2 min post A22 injections cells stopped gliding and AglQ and MglA^{Q82A} were dispersed from the FACs simultaneously, shown in Figure 27.

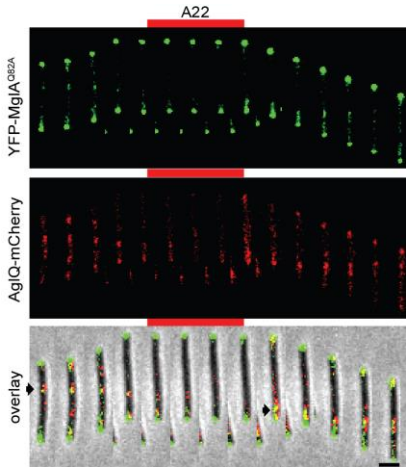

Figure 27. A22 disperses FACs of YFP-MglA^{Q82A} and AglQ-mCherry. The top panel shows YFP-MglA^{Q82A} localization, the middle panel shows AglQ-mCherry localization, and the bottom panel shows the overlay of the two. Red bar above indicates presence of A22 in the chamber. Time lapse every 1 min. Black arrows in the overlay indicate FACs.

A22 injection experiments led us to conclude that intact MreB is required for gliding motility and localization of AglQ and MglA in the FACs. Together with the previously published results on the MreB requirement for AglZ localization to FACs,

these findings strongly suggest that MreB is necessary for maintaining different components in the FACs. An additional important observation is that MglA in its active form also depends on intact MreB, which together with the *in vivo* co-IP result where MglA and MreB were found to interact (Supplementary figure 1), brings into question a possibility that the small GTPase MglA could be the component which regulates the recruitment of focal adhesions to the sites where MreB is in the cell, by directly interacting with MreB. Also, since MglA and AglZ are mutually dependent for localization to FACs (Figures 22 and 23, and Zhang *et al* 2012), and they interact directly, we reasoned that MreB perturbation could affect MglA localization to FACs directly or indirectly, through AglZ. Thus we analyzed direct interactions between MglA and MreB.

2.3.3 MreB from *M. xanthus* polymerizes *in vitro* and forms filaments

Polymerization and mechanical properties of MreB have been studied in depth for MreB originating from bacterium *Thermotoga maritima.* It has been shown that MreB can assemble and organize into different filamentous and sheet structures, depending on the nucleotide, cation and temperature used. In presence of ATP or GTP, MreB from *T. maritima* forms multilayered sheets composed of filaments, whereas in the presence of ADP and GDP it forms unstructured aggregates and long twisted structures. (Esue *et al.*, 2005; Esue *et al.*, 2006a; Popp *et al.*, 2010; van den Ent *et al.*, 2001). MreB from *B. subtilis* has been shown to polymerize into filaments in absence of any nucleotides, in a temperature dependent manner, but only polymerized into organized structures when mixed with ATP or GTP (Mayer and Amann, 2009). Recently, MreB from *E. coli* has been shown to form filaments and bundles only in presence of cations and ATP (Nurse and Marians, 2013). Despite the high structural similarity between actin and MreB, their assembly properties are distinct from each other, but a consistent feature is that both can polymerize in presence of ATP nucleotides and cations.

We first purified His-tagged *M. xanthus* MreB soluble (Figure 28), and then tested its preferred condition for polymerization using high-speed sedimentation assays.

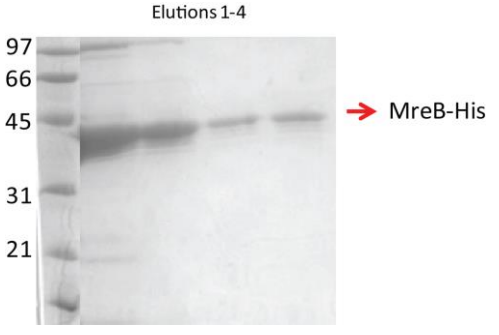

Figure 28. Purfied MreB-His protein. Elutions with increasing concentrations of imidazole shown, from right to left: 100mM, 150mM, 200mM, 250mM. MreB band marked by red arrow; Marker on the left.

MreB sedimentation assays were carried out four different conditions (Figure 29). Based on the eukaryotic actin polymerization G-buffer components, we used a buffer containing 40mM HEPES, 300mM KCl, 2mM $MgCl_2$, 1mM DTT, pH 7.7, without any nucleotides, or with 2mM final concentrations of ADP, ATP, GDP or GTP were used, and the reactions were carried out in a temperature and time controlled manner. After separating supernatant and pellet following high-speed centrifugation, we found that MreB-His_6 sediments in a temperature dependent manner at 37°C after 30 min (Figure 29). At 37°C after 10 min incubation in presence of ATP there was slightly more protein recovered in the pellet, whereas there were no significant differences noted between the different nucleotides present in the reaction after 30 min of incubation.

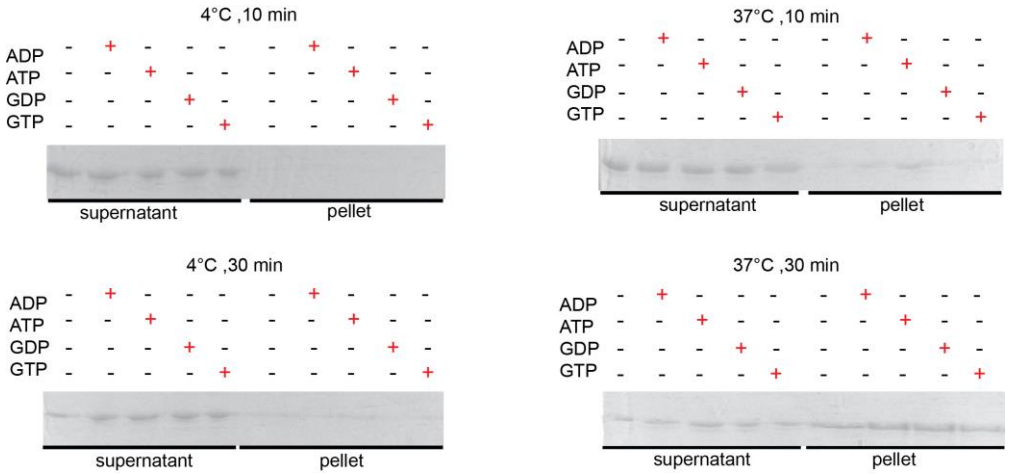

Figure 29. *M. xanthus* MreB-His_6 polymerizes *in vitro*. MreB-His_6 (5 µM) purified protein was incubated in presence of indicated nucleotides (final concentration 2 mM) at 4°C (left column) or 37° C (on the right column) for 10 min (upper row) or 30 min (bottom row), followed by high speed sedimentation (70000g, 15 min, 4°C). Equivalent volumes of supernatants and pellets were separated by SDS-PAGE and stained by Coomassie blue.

Thus, the optimal sedimentation of MreB was observed after 30 min incubation at 37°C. However, from the sedimentation assays it is not possible to firmly distinguish whether the protein is forming aggregates under certain conditions, or forming organized filaments, as previously published for actin and MreB.

To examine whether MreB-His_6 forms filaments *in vitro*, we used electron microscopy (EM) to examine the protein incubated with ADP or ATP nucleotides for 30 min, at 37°C. Using EM, we found no specific structures in presence of ADP with MreB-His_6 (Figure 30B). Interestingly, the protein incubated with ATP at 37°C, 30 min formed long and thick filaments which were often found bundled together (Figure 30A).

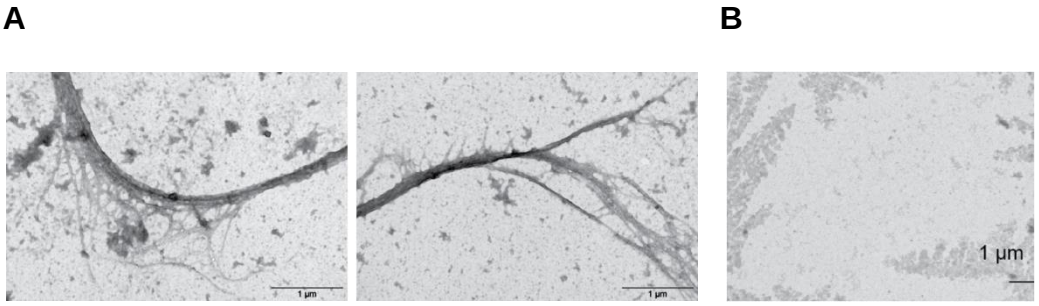

Figure 30. MreB forms filaments in vitro. (A) EM micrograph of purified MreB-His_6 after incubation at 37° C for 30 min in presence of 2 mM ATP, visible filaments and bundles. Scale bar: 1 µm. (B) No specific structures were detected when MreB-His_6 was incubated in polymerization buffer under similar conditions with ADP at 37°C or with ATP at 4°C for 30 min.

As structured MreB filaments were readily observed under our experimental conditions at 37°C and 2mM ATP, we continued using this polymerization condition for all further *in vitro* experiments with MreB-His_6.

2.3.4 MreB interacts directly with MglA-GTP

Injection experiments using A22 hinted that MglA localization depends on intact MreB. Furthermore, we also found that MreB was pulled-down with wildtype MglA, active $MglA^{G21V}$and $MglA^{Q82A}$ variants, but not with $MglA^{T26/27N}$ inactive form when we performed an immunoprecipitation experiment to search for MglA interaction partners (Supplementary Figure 1). This prompted us to analyze whether MglA and MreB interact directly in *in vitro* interaction experiments using purified *M. xanthus* proteins. We used purified MglA-His_6, $MglA^{Q82L}$-His_6 proteins from *E. coli* in soluble forms (Figure 31).

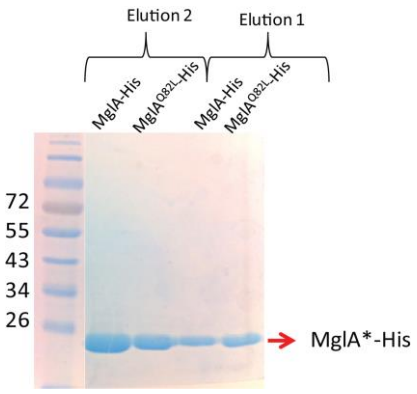

Figure 31. Purfied MglA-His and $MglA^{Q82L}$-His proteins. Elution1 performd in presence of 150mM imidazole, and Elution 2 in presence of 250mM imidazole. MglA* band marked by red arrow; Molecular weight marker on the left.

Of note, $MglA^{Q82L}$ variant has the same hyper-reversing phenotype and localization at both cell poles and to a FAC like $MglA^{Q82A}$ in *M. xanthus* and its biochemical

properties are similar to MglA^{Q82A} (Leonardy *et al.*, 2010; Miertzschke *et al.*, 2011; Zhang *et al.*, 2010). MreB-His$_6$ was polymerized in presence of ATP nucleotides at 37°C as described in the previous chapter. Purified MglA-His$_6$ and MglA^{Q82L}-His$_6$ were pre-loaded with GDP or GTP nucleotides for 30 min at 20 °C prior to being mixed with polymerized MreB-His$_6$. The samples then underwent high-speed centrifugation and the soluble and pellet fractions were analyzed by SDS PAGE gels. These experiments revealed that MglA-His$_6$ and MglA^{Q82L}-His$_6$ pre-bound to GTP were recovered in the pellet with MreB unlike the MglA variants pre-bound to GDP (Figure 32A). Additionally, we repeatedly found slight amounts MglA-GTP without MreB in the pellet fraction, indicating that the protein is either unstable in presence of GTP and thus aggregates on its own, or when bound to GTP MglA self-interaction is stronger thus leading to formation of larger and denser fraction.

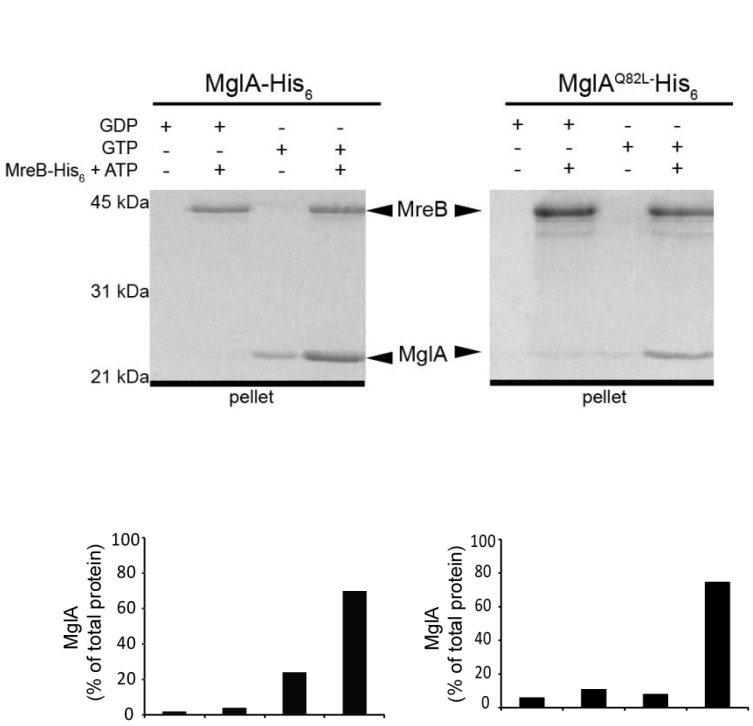

Figure 32. MreB interacts directly with MglA-GTP and MglA^{Q82L}-GTP. (A) MreB-His$_6$ (5µM) was incubated in presence of 2 mM ATP at 37°C, 1 h. Subsequently, the proteins were mixed with MglA variants as indicated, followed by high speed sedimentation. Equivalent volumes of supernatants and pellets were analyzed by SDS-PAGE, and gels were stained with Coomassie blue. Molecular weight markers are indicated. (B) Histograms show bound MglA as a percent (%) of total protein, columns correspond to the conditions shown above in panel A.

To check MreB non-specifically binds soluble proteins, we performed an *in vitro* pull-down using purified *E. coli* formate dehydrogenase FdhD-His$_6$, and this protein did not sediment with MreB-His$_6$ (Supplementary Figure 2). We also

investigated the effect of concentration on the MreB and MglA interaction by conducting an *in vitro* experiment where the concentration of wildtype MglA prebound to GTP was kept constant in the reaction, but different concentrations of previously polymerized MreB were added, followed by high speed centrifugation to separate the pellet and supernatant fractions (Figure 33A). When mixed with increasing concentrations of MreB, MglA-GTP was recovered in the pellet in an MreB concentration-dependent manner as shown on the gel in Figure 33A. The corresponding supernatants showed decreasing amounts of soluble MglA, and all the results were quantified in Figure 33B.

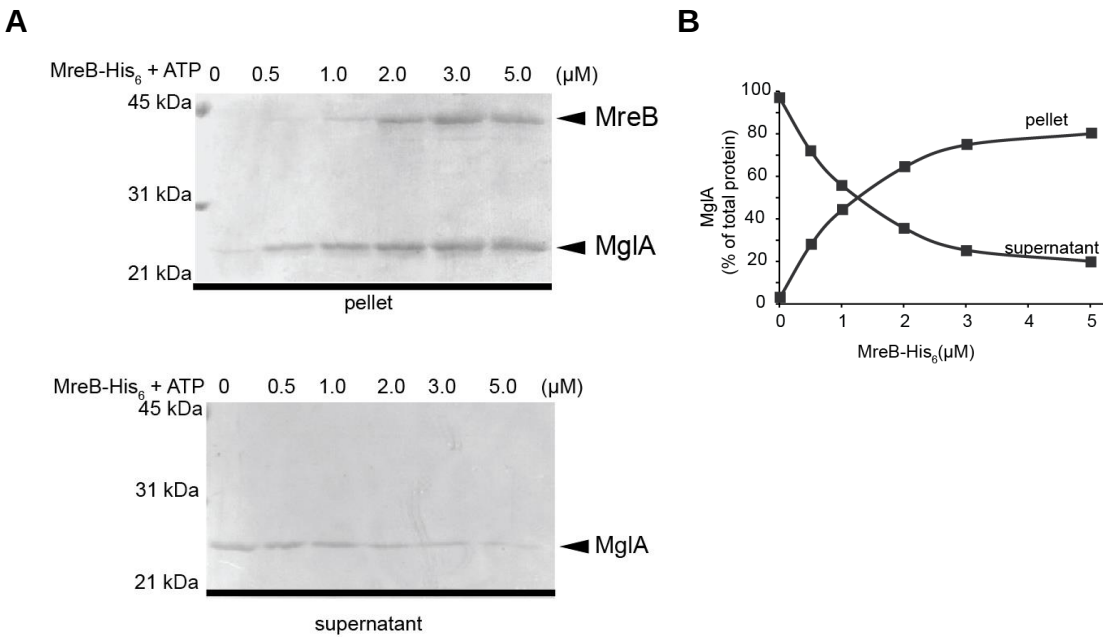

Figure 33. MreB-His_6 interacts with MglA-His_6 in a concentration-dependent manner. (A) MglA-His_6 (2 μM) was incubated for 30 min, 20° C with MreB-His_6 which was preincubated with ATP (2 mM ATP, 30min, 37° C) at the indicated concentrations, followed by high speed sedimentation as in (Figure 32). Equivalent volumes of pellets (top row) and supernatants (bottom row) were separated by SDS-PAGE and gels stained with Coomassie blue. (B) Diagram shows the amount of MglA in the supernatant and pellet fractions as a function of MreB-His_6 concentration.

In summary, the evidence for direct and dose-dependent interactions of MglA-GTP and MreB (Figures 32, 33 and Supplementary Figures 1 and 2) presented in this chapter is most likely a true reflection of the cellular events between these two proteins. Taken together the *in vitro* results with the *in vivo* A22 injection experiments, we demonstrated that MreB is involved in *M. xanthus* gliding motility by a direct and specific interaction with MglA-GTP, the active form of MglA.

2.4 The roles MreB in cell wall biosynthesis and gliding motility are independent

2.4.1 Mecillinam inhibits cell wall elongation, but does not affect gliding

Genetic, biochemical and cell biology studies strongly suggest that the major function of MreB in bacteria is scaffolding of the peptidoglycan (PG)-synthesizing machinery. MreB patches are thought to guide the synthesis of PG by interactions with a number of components from the PG elongation machinery (Figure 8). The dynamic localization of MreB observed around the circumference of the cell has been shown to be driven by PG synthesis, and antibiotics which inhibit PG synthesis block the MreB dynamics (Carballido-Lopez *et al.*, 2006; Dominguez-Escobar *et al.*, 2011; Figge *et al.*, 2004; Garner *et al.*, 2011; van Teeffelen *et al.*, 2011).

In Figure S3 we show the localization of MreB by immunofluorescence using MreB antibodies in wildtype DK1622, similar to the approach used by Mauriello and colleagues to study MreB in wildtype DZ2 *M. xanthus* (Mauriello *et al.*, 2010b). MreB forms multiple clusters along the cell length, similar to the previously published localizations of MreB short patches that are linked to the membranes in *E. coli*, *B. subtilis* and *C. crescentus* (Dominguez-Escobar *et al.*, 2011; Figge *et al.*, 2004; Garner *et al.*, 2011; van Teeffelen *et al.*, 2011).

To determine whether MreB function in *M. xanthus* gliding is linked to its function in PG synthesis, we focused on using antibiotics that have been shown to block PG biosynthesis and blocking the dynamics of MreB patches within minutes of addition.

Mecillinam is an antibiotic that blocks PG synthesis by specifically binding the elongation protein PBP2 (Spratt, 1975). We first performed detailed analyses of the effects of mecillinam on *M. xanthus*. The cells were grown in liquid and spotted on agar pads for microscopy analysis. Cell shape changes with visible bulges were evident at 24 hours post treatment at MIC of 10 µg/ml, and even earlier with higher concentrations of antibiotic, all ultimately leading to cell death (Figure 34).

A

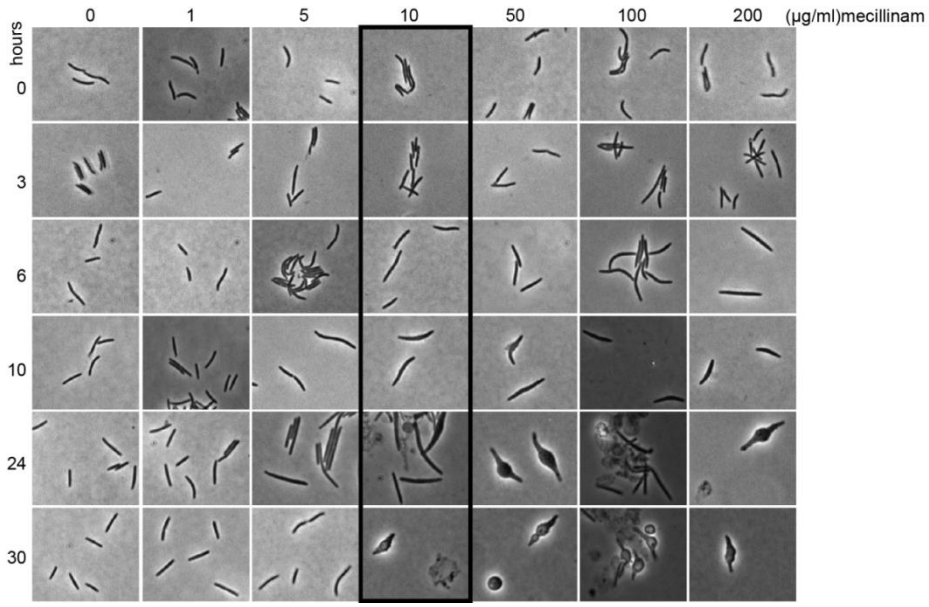

B

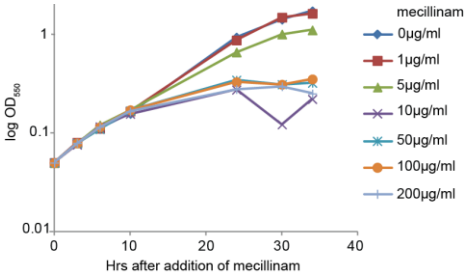

Figure 34. Mecillinam causes growth inhibition and cell lysis in *M. xanthus.* (A) Determination of minimal inhibitory concentration (MIC) of mecillinam on WT DK1622. The concentration at which cells show evident shape changes with bulges are marked in black box. (B) Growth curves of WT DK1622 with different concentrations of mecillinam.

To examine whether mecillinam (at MIC or higher concentration) has an effect on gliding motility, we mixed the cells with increasing concentrations of the drug and ensuring that the same concentration of the drug in the agar pad on which gliding is assayed, and checked for motility 10-15 min after spotting cells on the agar pad. These experiments demonstrated that mecillinam at concentrations ranging from 10-150 µg/ml does not have an effect on motility or a significant effect on cell velocity (Figure 35A). Furthermore, to test if the localization of YFP-MglA^{Q82A} or AglQ-mCherry to FACs depends on mecillinam, we treated cells harboring each fusion protein with 10 µg/ml of mecillinam and immediately transferred them onto the agar pad. Checking for localization in presence of mecillinam revealed that YFP-MglA^{Q82A} (Figure 35B) and

AglQ-mCherry (Figure 35C) localizations were not affected, and their dynamics were not affected either.

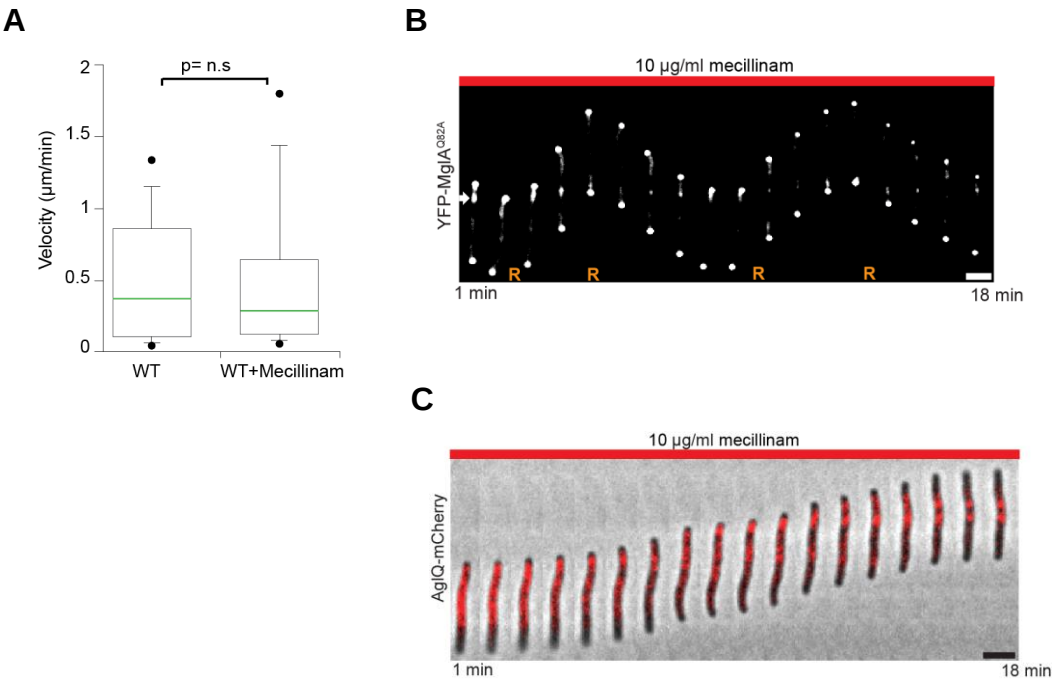

Figure 35. Gliding motility and FACs localization and dynamics are not affected in presence of mecllinam. (A) Gliding motility in WT DK1622 is not blocked with MIC of mecillinam. Solid green bars in boxes represent the average cell velocities for each condition. The *p*-values indicate statistically insignificant differences using Student's *t*-test ($p>0.05$). (B) YFP-MglA^{Q82A} localization in the presence of mecillinam. Time lapse every 1 min. Scale bar = 2 µm. R indicates a cellular reversal. (C) AglQ-mCherry localization in the presence of mecillinam. Time lapse every 1 min. Scale bar = 1 µm).

The fact that mecillinam has a cell wall elongation inhibitory effect on *M. xanthus*, but does affect gliding motility or localization and dynamics of YFP-MglA^{Q82A} or AglQ-mCherry even at concentrations significantly higher than MIC, strongly indicated that MreB has a function in gliding which is not directly linked to its major role in PG synthesis. To test this, we wanted to further check the localization and dynamics of MreB, in presence of A22, or in presence of PG synthesis inhibitory antibiotics such as mecillinam.

2.5 Preliminary results on PG synthesis inhibition

To further substantiate our finding that mecillinam affects cell growth (PG synthesis) but does not have an effect on gliding, we performed a set of experiments using antibiotics which target different cellular pathways (including PG synthesis) for their effects on cell growth and gliding motility. These analyses revealed that apart from mecillinam (affects PBP2), phosphomycin (affects MurA enzyme for PG precursors synthesis), cephalexin (affects PBP3) and cefsulodin (affects PBP1A/B) all affect cellular growth (Supplementary Figures 7, 8, 9), but do not have an effect on gliding motility (Figure 36).

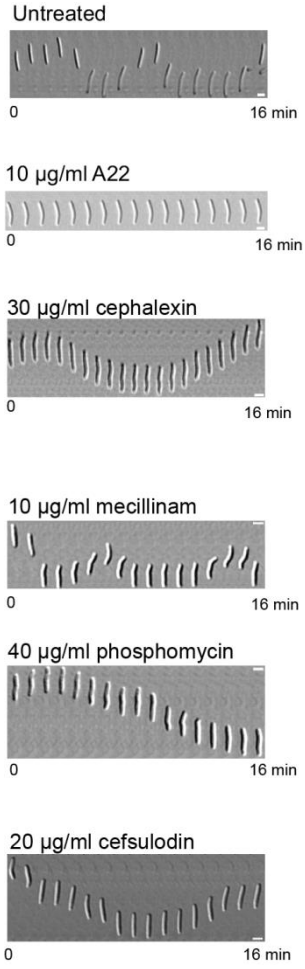

Figure 36. Gliding motility in presence of different antibiotics. All abtibiotics are added at minimal inhibitory concentrations. A22 blocks motility, and the PG-synthesis inhibiting antibiotics (cephalexin, mecillinam, phosphomycin, cefsulodin) do not affect motility.

Thus, our preliminary results on the effects of different antibiotics on PG synthesis in *M. xanthus* suggest that they do not affect gliding motility.

2.5.1 Pencillin Binding Protein 2 (PBP2) as a proxy for MreB in PG biosynthesis

We and multiple other laboratories failed to obtain a functional MreB fluorescent fusion. To track MreB *in vivo* during PG synthesis inhibition we focused on another protein directly involved in PG elongation during growth - PBP2 (mxan2647), Figure 37.

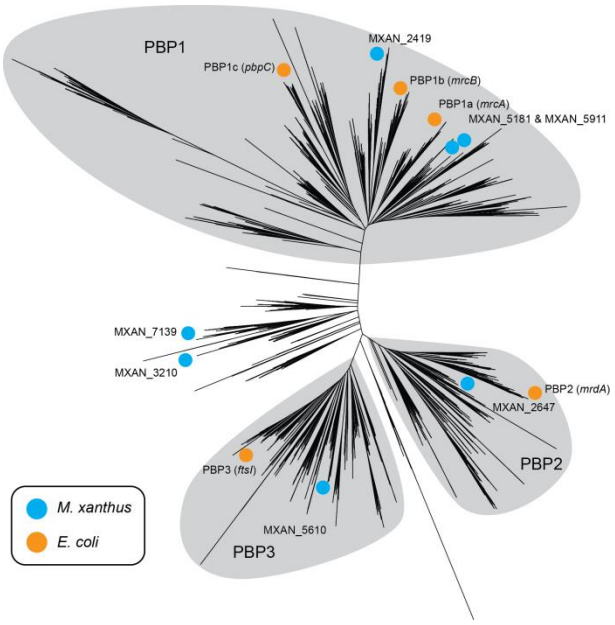

Figure 37. A phylogenetic tree of PBP sequences reveals distinct families. The approximate locations of all putative PBPs of *Myxococcus xanthus* DK 1622 are shown in addition to the characterized PBP1, PBP2 and PBP3 proteins of *Escherichia coli* str. K-12 substr. MG1655. Analyses performed by Dr. K. Wuichet, MPI Marburg.

A fusion protein PBP2-sfGFP expressed ectopically in the wildtype background displayed multiple clusters localized throughout the cell (Figure 38, untreated cells). As PBP2 is known to be specifically inhibited by mecillinam, we tested whether mecillinam MIC has an effect on the localization of PBP2-sfGFP (Figure 38, mecillinam treated cells), and found that the localization and number of clusters were not significantly affected in presence of the drug. Additionally, we analyzed if A22 MreB perturbing compound, phosphomycin, cephalexin and cefsuldin PG synthesis inhibiting antibiotics, affect the localization of PBP2-sfGFP, and found no major differences in the localization or the number of clusters in treated versus non-treated cells (Figure 38).

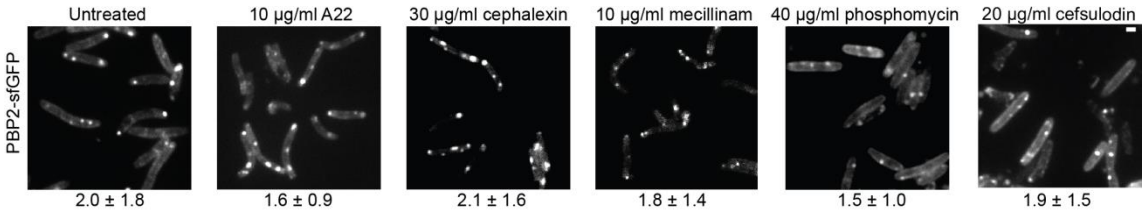

Figure 38. PBP2-sfGFP/PBP2^{+} localizes to multiple clusters in the cell. Localization of PBP2-sfGFP in the absence (first photo on the left) and presence of different drugs. Average number of clusters in untreated and treated cells are displayed with standard diviations.

Numerous previous studies have shown that the dynamics of MreB and PBP2 along tracks perpendicular to the cell axis can be inhibited by addition of mecillinam within a few minutes (Dominguez-Escobar *et al.*, 2011; Garner *et al.*, 2011; van Teeffelen *et al.*, 2011). To test whether PBP2-sfGFP in *M. xanthus* displays dynamic localization, we performed time-lapse analyses with photos taken every 30 seconds with the appropriate filter. Interestingly, in untreated wildtype cells expressing PBP2-sfGFP we observed both dynamic (25%) and non-dynamic (75%) clusters. We traced the movements of 20 dynamic clusters by joining the X and Y position coordinates through time, and analyzing the trajectory of the movement. Interestingly, we found that in wildtype cells, PBP2-sfGFP displays random "wandering" in the cell without a specific directionality (Figure 39A). Importantly, when we performed the same analyses for cells treated with mecillinam (at concentrations ranging from 10 µg/ml to 150 µg/ml) the cluster dynamics (usually observed in 25% of the total clusters) was almost completely abolished (Figures 39D). Furthermore we tested the additional PG synthesis inhibiting drugs, and found that phosphomycin and cefsulodin at MIC drastically reduce the PBP2-sfGFP dynamics (Figures 39E, 39F), whereas cephalexin has an intermediate reducing effect on the PBP2-sfGFP dynamics (Figure 39C). Time-lapse analyses of PBP2-sfGFP in presence of A22 at MIC suggest that the dynamics of PBP2-sfGFP is unaffected (Figure 39B).

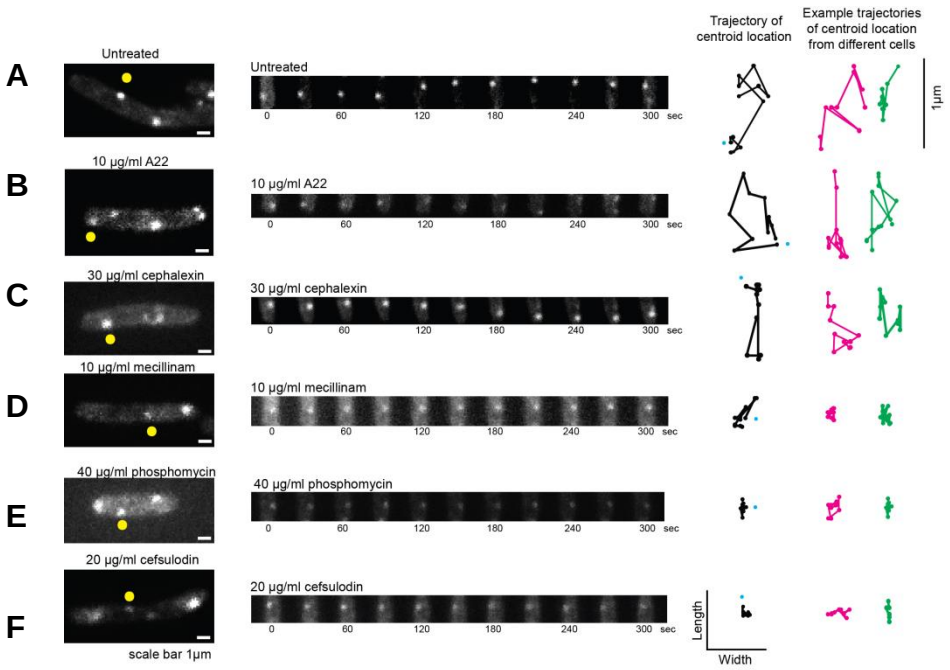

Figure 39. PBP2-sfGFP clusters dynamics over time. Representative examples of a PBP2-sfGFP clusters followed over time in the absence (A) and presence (B) of 10 µg/ml A22, (C) 30 µg/ml cephalexin, (D) 10 µg/ml mecillinam, (E) 40 µg/ml phosphomycin and (F) 20 µg/ml cefsulodin; images taken every 30 sec. Black lines, trajectories of centroid position in the cells shown on the left. Blue dot indicates the starting position of the centroid of the cluster. Pink and green additional trajectories of other clusters. Yellow dot on the image of the cell indicates the cluster followed over time.

In presence of A22 MreB polymerization cycle is perturbed, and the dynamics of PBP2-sfGFP seemed to be unaffected. It was previously reported that MreB dynamics in *E. coli* are unaffected by A22, but the antibiotic-mediated inhibition of cell wall synthesis blocks MreB movement (van Teeffelen *et al.*, 2011), and we observe similar effects of A22 on PBP2-sfGFP dynamics in our experiments.

To quantify PBP2-sfGFP dynamics in untreated and treated cells, we performed detailed analyses of clusters velocities over time, and the mean squared displacement (m.s.d) over time. The velocity analyses revealed that clusters in non-treated cells moved from 30 to 1000 nm/30 sec, whereas the velocity of mecillinam, phosphomycin and cefsulodin-treated clusters velocities were drastically reduced and restricted to a velocity range of 0 to 250 nm/30 sec (Figure 40A). Lastly, the analyses of the m.s.d (Figure 40B) indicated that PBP2-sfGFP clusters in untreated or cell treated with A22, moved at longer distances than the cells treated with mecillinam, phosphomycin or cefsulodin, further supporting that mecillinam specifically blocks the dynamics and cluster "wandering" of PBP2-sfGFP in *M. xanthus*.

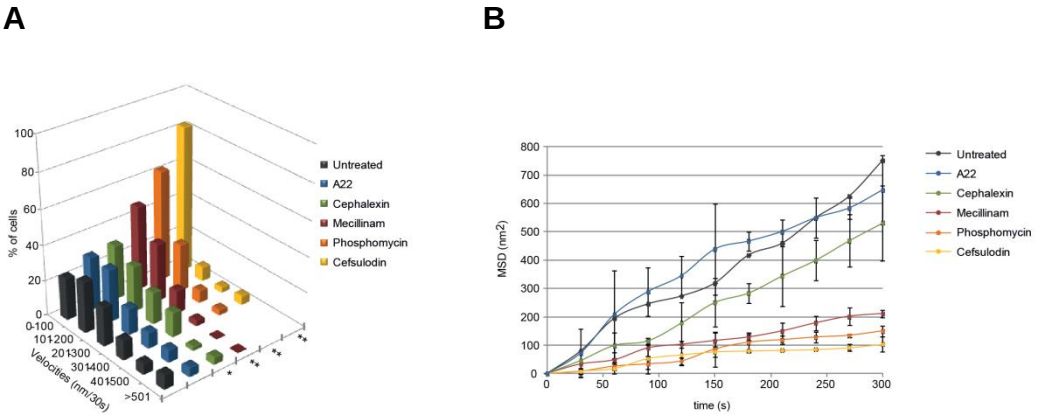

Figure 40. Mecillinam, phosphomycin and cefsulodin PG synthesis inhibiting drugs reduce PBP2-sfGFP cluster dynamics. Cells containing PBP2-sfGFP were imaged every 30 sec. Subsequently, centroids of PBP2-sfGFP clusters were tracked as described in Figure 40. For every time interval of 30 sec and the velocity were calculated for 10 clusters. The velocity distribution (A) and the mean-squared displacements (B) of the centroids for untreated (black), A22-treated (blue), cephalexin-treated (green), mecillinam-treated (red), phosphomycin-treated (orange) and cefsulodin-treated (yellow) cells are shown with error bars indicating standard deviations. Calculations of velocities and m.s.d. done by P. Lenz, Philipps University, Marburg, and the figure by A. Treuner-Lange.

Lastly, the analyses of the m.s.d (Figure 40B) indicated that PBP2-sfGFP clusters in untreated or cell treated with A22, moved at longer distances than the cells treated with mecillinam, phosphomycin or cefsulodin, further supporting that mecillinam specifically blocks the dynamics and cluster "wandering" of PBP2-sfGFP in M. xanthus.

In Figure 35 we have shown that in presence of mecillinam, cell gliding and FACs are not affected, thus strongly suggesting that the function of MreB as a scaffold for PG synthesis machinery is independent from its function in gliding motility. Also, our results on motility in presence of different PG-synthesis inhibiting antibiotics, show that gliding is not affected when PG is perturbed. Furthermore, our preliminary results on the localization and tracking of PBP2-sfGFP (as a proxy for MreB dynamics), suggests that dynamics of PBP2 is unaffected in presence of A22, but that most of the dynamic clusters become stationary in presence of mecillinam which is known to specifically bind PBP2 and reduce MreB dynamics in other organisms. Similar preliminary results on the effects of cephalexin, cefsulodin and phosphomycin (affecting different steps in PG synthesis) suggest that PBP2 dynamics is largely inhibited by cefsulodin and phosphomycin (Figures 39, 40).

To summarize, our data show that MreB continuous polymerization is required for gliding motility, and that interfering with PG synthesis does not have an effect on

gliding. Also, the initial results on tracking the dynamic of PBP2 clusters suggest that PBP2 (and subsequently MreB) can be inhibited by cell wall antibiotics mecillinam, phosphomycin and cefsulodin, without perturbing the gliding motility.

3 Discussion

Myxococcus cells temporally and spatially coordinate motility in order to swarm and predate in presence of nutrients or form multi-cellular fruiting bodies in the absence of nutrients. The capacity of these cells to move in a coordinated manner in groups, or as single cells, depends on two genetically distinct systems – T4P driven motility of cell groups, and single cell gliding driven by the AglQ/R/S engine of three protein complex (Bulyha *et al.*, 2009; Kaiser, 1979; Nan *et al.*, 2011; Sun *et al.*, 2011). The intrinsic and dynamic polarity of *M. xanthus* cells allows them to simultaneously use both motility systems and reverse the direction of movement by switching the leading and lagging cell poles. Previous studies have shown that MglA, a bacterial Ras-like small G-protein is absolutely required for motility in *M. xanthus* and its accumulation predominantly at the leading cell pole was thought to activate motility machineries at that pole (Hartzell and Kaiser, 1991a; Leonardy *et al.*, 2010; Miertzschke *et al.*, 2011; Zhang *et al.*, 2010). Recently, it was shown that MglA is restricted to the leading cell pole by the action of its cognate GTPase Activating Protein (GAP) MglB, which localizes predominantly at the lagging cell pole and prevents the accumulation of the active, GTP-bound form of MglA by its GAP activity. Re-location of MglA and MglB to opposite cell poles is triggered by the Frz chemosensory system, leading to a reversal in polarity and cell movement (Inclan *et al.*, 2008; Inclan *et al.*, 2007; Keilberg *et al.*, 2012; Leonardy *et al.*, 2010; Miertzschke *et al.*, 2011; Patryn *et al.*, 2010; Zhang *et al.*, 2010; Zhang *et al.*, 2012).

Despite extensive studies of MglA in the past years, its function in gliding remained poorly understood. In this work we addressed the function of the small G-protein MglA in gliding motility. We show for the first time that MglA is linked to gliding machinery complexes in the focal adhesions, and the bacterial actin homolog MreB. Additionally, we demonstrate that the nucleotide-bound state of MglA regulates the correct disassembly of the machinery components once they reach the MglB GAP at the lagging cell pole. Furthermore, we demonstrate a direct interaction between MglA and MreB, which is necessary to keep FACs coupled to MglA. In addition, our results on cell wall elongation inhibition by specific antibiotics support the hypothesis that the previously proposed major function of MreB as scaffold for cell wall synthesizing machinery in other bacteria such as *E. coli* and *B. subtilis* is separable from its role in the gliding motility in *M. xanthus*.

3.1 MglA function in gliding motility

3.1.1 MglA GTPase cycle regulates its localization in the cell

To address the mechanism by which MglA is required for gliding in *M. xanthus*, we used results of the structural and *in vitro* biochemical analyses of the *T. thermophilus* MglA homolog (Figure 12). We showed that MglA is a *bona fide* bacterial small Ras-like G-protein and that its cognate GAP is MglB (Miertzschke *et al.*, 2011). In this work it was also shown that MglA residues G21 and Q82, which are conserved in other small G-proteins, are absolutely essential for MglA GTPase activity *in vitro*, and when mutated to alanines, MglB cannot stimulate the GTPase activity of these MglA variants. Moreover, MglA contains an intrinsic arginine (R53) residue, usually provided by the GAP for other characterized Ras-like G-proteins, which is positioned in the active site during GTP hydrolysis. Mutations of this arginine to alanine led to a GTPase negative variant that was insensitive to the presence of MglB (Miertzschke *et al.*, 2011). To rationalize the physiological relevance of the MglA GTPase cycle, we used predictions for GTPase negative variants based on the crystal structures and biochemical assays of *T. thermophilus* proteins. Introducing corresponding substitutions into Δ*mglA* caused the cells to have abnormal reversals (with regular 5-7 min intervals) and protein localizations in the cell. Consistent with the earlier findings in *mglA9* non-motile background (Leonardy *et al.*, 2010), YFP-MglA expressing cells complemented the non-motile Δ*mglA* phenotype and caused the cells to reverse with highly irregular intervals, as observed in wildtype (Table 1). YFP-MglA localized to the leading cell pole between reversals and relocated to the new leading pole during a reversal (Figure 13A). In the absence of MglB, cells reversed in a regular manner that was 2- to 3-fold more frequent than wildtype cells. In these cells YFP-MglA localized in a bipolar pattern that did not change during reversals (Table 1, Figure 14A). This was a first indication that MglA is excluded from the lagging cell pole by MglB and only the active GTP-bound form of MglA localizes to cell poles. Similar to what has been reported for YFP-MglA^{G21V} and YFP-MglA^{Q82L} in *mglB*$^{+}$ cells (Leonardy *et al.*, 2010; Zhang *et al.*, 2010), YFP-MglA^{G21V}, YFP-MglA^{R53A} or YFP-MglA^{Q82A} caused a hyper-reversing phenotype, independent of the MglB presence (Table 1). These three GTPase negative mutants hyper-reversed in a highly regular fashion, exhibiting a pendulum-like movement with displacements equal to one cell length (Table 1). While regular hyper-reversals are similar for all the three GTPase

negative mutants, their localizations are slightly different. YFP-MglA^{G21V} forms a single cluster that appears to be dynamic between cell poles as the cell moves, and the arrival of the cluster at the lagging pole coincides with reversal of the gliding direction, Figure 13B. In contrast, YFP-MglA^{R53A} and YFP-MglA^{Q82A} localize in a bipolar pattern at the leading and lagging poles in addition to forming what appears as a dynamic cluster similar to that observed in the YFP-MglA^{G21V} mutant (Figure 13C, 13D). In cells lacking MglB, all three GTPase negative mutants localized similar to *mglB*$^{+}$ cells *in vivo*, consistent with their insensitivity to MglB observed *in vitro* (Figure 14B-D). The loss of diffuse signal observed with the GTPase-negative mutants compared to YFP-MglA suggests that only the active form of MglA forms clusters. A possible reason for different localization patterns in the three constitutively active MglA variants could be due to a stronger interaction of active MglA form with one or more effector proteins.

The observation that asymmetric unipolar binding of MglA depends on MglB suggests that MglB prevents the accumulation of MglA at the lagging cell pole via its GAP activity, allowing the accumulation of active MglA only at the leading cell pole. The localization of MglA at the leading cell pole is essential for the directionality of the cell. It was recently shown that MglA is targeted to the leading cell pole by a response regulator protein RomR (Keilberg *et al.*, 2012; Zhang *et al.*, 2012). How MglB localizes to the lagging cell pole has yet to be identified, but our findings provide rationale for how the MglA GTPase cycle is essential for MglA localization. Furthermore, the inability of cells to move further than one cell length once MglA is locked in its GTP-bound state encouraged us to hypothesize that the components necessary for gliding are able to assemble, but once they reach the lagging cell pole they do not disassemble due to the inability of MglB to inactivate MglA.

3.1.2 MglA is required for FACs localization

In this study we show that MglA is a component of the gliding motility machinery found at focal adhesion sites, and that its GTPase cycle is essential in regulating the formation and dissociation of the adhesion complexes during motility. Gliding motility in *M. xanthus* has been shown to depend on multiple, periodically spaced protein complexes that are stationary relative to the substratum as the cell moves (Mignot *et al.*, 2007b; Nan *et al.*, 2011; Nan *et al.*, 2010; Sun *et al.*, 2011). AglQ, AglR, AglS, AglZ, AgmU, GltD, and GltF have been shown to be a part of these motility complexes. Currently, there exist two parallel models to explain how gliding motility

works. In one, the PMF driven motor consisting of the AglQ/R/S complex is coupled to other gliding machinery proteins, some of which span different cell wall compartments and provide a direct link to the substratum as depicted in Figure 6 (Luciano *et al.*, 2011; Sun *et al.*, 2011). At positions where these focal adhesion clusters are formed in the cell, there is additional evidence of gel-like slime compounds being deposited that are required for proper gliding (Ducret *et al.*, 2012). In the second model, the AglQ/R/S motor is moving along an endless helical loop filament, most likely formed by AgmU/GltD, and collisions of proteins along this filament at ventral side of the cell appear to form fixed adhesions in the cell, leading to accumulation of "high drag cargo" that pushes on the cell wall without breaking it and makes deformations in the membrane that contact the substratum, as shown in Figure 7 (Nan *et al.*, 2011; Nan *et al.*, 2013). Recently, a cytoplasmic component of the gliding machinery, the pseudoresponse regulator AglZ, was found to localize to multiple periodically spaced positions in the cell, and dynamically co-localizes with a polystyrene bead attached to cell surface (Sun *et al.*, 2011). The bead attached to the dorsal side of the cell moved in the same direction like AglZ, suggesting that the rearward translocation of the motor apparatus leads to forward movement of the cells. This observation strongly supports the existence of outer membrane components that provide direct attachment of the focal adhesions to the substratum.

In order for a cell to move by gliding, at least two conditions must be met. First, it has to exert force onto the substratum at the sites where the focal adhesion complexes form to power cell movement; and, second, the focal adhesions should not be permanently stuck at the same positions as they would inhibit motility in this way. Rather, the adhesions have to coordinate assembly and disassembly at specific sites so not to impede motility. Previous evidence that associates MglA to the gliding motility machinery has been published in multiple works, but whether MglA is part of the adhesion complexes was never clearly defined (Mauriello *et al.*, 2010a; Yang *et al.*, 2004; Zhang *et al.*, 2010). We addressed this further by examining proteins known to localize to FACs in addition to MglA.

In the absence of MglA, AglZ FACs become diffuse and cells are unable to glide, and moreover, instead of forming multiple clusters as in wildtype, AglZ forms only one large FAC in the presence of $MglA^{Q82L}$ active protein variant (Zhang *et al.*, 2010; Zhang *et al.*, 2012). Interestingly, AglZ-YFP behaviour in $MglA^{Q82L}$ background

is similar to the oscillatory behaviour between the poles of YFP-MglA^{Q82A} protein (Miertzschke *et al.*, 2011; Zhang *et al.*, 2010). The AglZ-YFP cluster did not disassemble upon reaching the lagging cell pole, but rather induced a cellular reversal, leading to a continuous pendulum-like motion of the cells suggesting that the gliding motility machinery does not get deactivated at the lagging cell pole. To further understand whether other gliding machinery components of FACs have different localizations and dynamics in presence of MglA-GTP, we localized the AglQ-mCherry motor subunit in MglA^{Q82A} background. AglQ-mCherry instead of forming multiple adhesion clusters as seen in a wildtype background, formed mostly one large internal cluster that remained at a stationary position relative to the substratum as the cell moved (Figure 16A, 17C), similar to the localization of AglZ-YFP in the MglA^{Q82L} background. These findings together with the previously published observation that AglZ and AglQ co-localize to focal adhesion clusters in a wildtype background (Sun *et al.*, 2011) suggested a direct connection between MglA and the focal adhesion clusters. Furthermore, a direct MglA–AglZ interaction has been shown using multiple approaches including yeast two hybrid assays and pull-down experiments with purified and cross-linked proteins, suggesting a direct link between MglA and the gliding machinery via AglZ (Mauriello *et al.*, 2010b; Yang *et al.*, 2004).

Consistent with other Ras-like G-proteins, MglA is active in its GTP bound state (Figure 2) and deactivated by its specific GAP, MglB, which localizes to the lagging cell pole preventing MglA-GTP accumulation (Leonardy *et al.*, 2010; Miertzschke *et al.*, 2011; Patryn *et al.*, 2010; Zhang *et al.*, 2010; Zhang *et al.*, 2012). In wildtype cells, this regulation complicates the study of MglA dynamics and its function in gliding motility. To circumvent this problem, we took advantage of the point mutant MglA^{Q82A}, which locks the protein in the GTP bound state and is insensitive to MglB. The intriguing observation that YFP-MglA^{Q82A} displays a prominent internal cluster that appears to stay fixed relative to the substratum as the cell moves (Figure 13D) led us to hypothesize that MglA in its active form is a component of the gliding motility machinery adhesion clusters. Indeed, when we co-localized AglZ-mCherry with YFP-MglA^{Q82A}, we found that both proteins co-localize at the prominent cluster which retained a fixed position as the cell moved (Figure 15). Furthermore, we co-localized the component of the gliding motor AglQ-mCherry with YFP-MglA^{Q82A} and found that they co-localized at the internal cluster (Figure 16A). The localization and dynamics of

the co-localizing cluster is very similar to that of the YFP-MglA^{Q82A} cluster described in Figure 13D. The AglQ-mCherry and YFP-MglA^{Q82A} co-localizing cluster retained a stationary position relative to the substratum in the cell during gliding, and upon reaching the lagging cell pole the cell reversed the direction (Figure 16A). The localization analyses of AglZ, AglQ and MglA for the first time gave strong support to the idea that MglA is a component of the FACs. Furthermore, our results demonstrate that MglA locked in the active state (Q82A point mutation) leads to a formation of a large focal adhesion complex (rather than multiple smaller ones in wildtype) which cannot be dissolved at the lagging cell pole, most probably due to the inability of MglB to inactivate MglA^{Q82A} and thereby the other components in the complex. It remains to be elucidated how the wildtype cells form multiple adhesions at the front of the cell, and whether the disassembly of these complexes when they reach the rear of the cell leads to their recycling and re-assembly at the front by an as yet uncharacterized mechanism.

3.1.3 AglZ and AglQ depend on MglA for localization to FACs

The localization of AglZ to focal adhesion clusters has been shown to depend on MglA (Zhang *et al* 2012). The non-polar AglZ-YFP is diffuse in the absence of MglA and in the presence of MglA$^{T26/27N}$, an inactive form of MglA (Leonardy *et al.*, 2010; Zhang *et al.*, 2012). In contrast, AglZ-YFP forms one large focal adhesion cluster in the presence of constitutively active MglA^{Q82L} (Zhang *et al.*, 2010) or MglA^{Q82A} (Figure 10).

We found that in the absence of AglZ, YFP-MglA^{Q82A} did not form a internal cluster, suggesting that AglZ is specifically required for the localization of YFP-MglA^{Q82A} to the focal adhesion cluster, Figure 22. The non-motile phenotype of the Δ*aglZ* mutant can be rescued by a null mutation in the Frz chemosensory system that regulates motility and cellular reversals (Mauriello *et al.*, 2009). Since AglZ is thought to be a regulatory protein in addition to a component of the gliding motility machinery, we wanted to test whether we could recover the formation and dynamics of YFP-MglA^{Q82A} FAC in the Δ*aglZ frzE::*Tn5Ω226 in DK1622 wildtype background. In DZ2 wildtype background deletion of *aglZ* in *frzE::*Tn5Ω226 background leads to recovery of motility (Mauriello *et al.*, 2009). In DK1622, the Δ*aglZ frzE::*Tn5Ω226 strain carrying YFP-MglA^{Q82A} was non-motile, and the fluorescent protein did not form FACs (Figure 23). To confirm this, further analyses of a strain carrying a clean in-frame deletion of *frzE* in combination with Δ*aglZ* should be examined in DK1622

background, as the observed differences might be due to wildtype background used in our study, or YFP tagged versions of MglA.

In the absence of the AglQ motor subunit, YFP-MglA^{Q82A} formed an internal cluster that was similar to the focal adhesion clusters by appearance (Figure 18), but it stayed immobilized in the non-motile cell over time, compared to wildtype where the cluster appears to move between the poles in an oscillatory pattern. Thus, in contrast to functional focal adhesion clusters which enable motility but disrupt the irregular reversals of the direction of motility, the internal YFP-MglA^{Q82A} cluster did not exhibit the dynamics in cells lacking the gliding motor (Figure 18). These results suggest that the recruitment of MglA to the gliding machinery complex does not specifically require AglQ; in the absence of AglQ the motility apparatus is most likely able to assemble, but its dynamics are abolished. This hypothesis is in line with published evidence that in Δ*aglQ*, the formation of the AglZ-YFP clusters can also occur in a manner similar to the internal YFP-MglA^{Q82A} cluster formed in Δ*aglQ*. In the absence of AglQ, AglZ-YFP polar clusters are still dynamic (even though the cells are non-motile), but the internal clusters are completely immobile (Sun *et al.*, 2011).

Previously, cells with a AglQ mutation of D28 to asparagine were found to be non-motile, and fluorescently tagged AglQ^{D28N}-mCherry localized to multiple paralyzed clusters throughout the cells (in DZ2 wildtype background) (Sun *et al.*, 2011). We predicted that YFP-MglA^{Q82A} is linked to the paralyzed AglQ^{D28N} motor subunit, and the localization analyses support that this is most likely the case (Figure 21A). In presence of the AglQ^{D28N}, YFP-MglA^{Q82A} polar clusters were not affected, but instead of forming one prominent internal focal adhesion cluster there were multiple adhesions that were not dynamic. To confirm the spatial and temporal co-localization of YFP-MglA^{Q82A} non-functional multiple clusters with AglQ^{D28N}, we co-localized them and found somewhat ambiguous results. Both AglQ^{D28N}-mCherry and YFP-MglA^{Q82A} fusions formed multiple clusters in the cell as previously described for single labelled strains, but interestingly, while the cluster often/sometimes co-localized, they also were often found as stand-alone clusters in the cell (Figure 22B). Partial overlap of the paralyzed motor subunit with active and immobilized YFP-MglA^{Q82A} supports the hypothesis that AglQ is not necessary for the formation of the focal adhesion clusters (Figure 18), but that a fully functional motor is necessary for cluster formation and localization of YFP-MglA^{Q82A} protein to the central adhesion cluster (Figure 21A, B).

Adding the antibiotic nigericin to the cells leads to a partial dispersal of the FACs of AglQ-mCherry motor subunit, and it blocks proton motive force thereby inhibiting the gliding motor function and blocking motility within minutes (Sun *et al.*, 2011). The rotation and dynamics of the AgmU/GltD component of the gliding apparatus are also specifically blocked in the presence of nigericin (Nan *et al.*, 2011). In our experiments, addition of nigericin to AglQ-mCherry harbouring cells led to more pronounced, but completely paralyzed, clusters resembling FACs (Figure 19). This result is consistent with the localization of the paralyzed motor mutant AglQ^{D28N}-mCherry at fixed positions in the cell. Therefore, we speculated that nigericin-induced paralysis of the gliding machinery would have an effect on YFP-MglA^{Q82A} localization and dynamics. Surprisingly, we observed that the FAC of YFP-MglA^{Q82A} was dissolved in most cells in the presence of nigericin, whereas the polar clusters were unaffected (Figure 20A). The effect of nigericin is reversible, and after rinsing it away with TPM buffer, gliding motility resumed and YFP-MglA^{Q82A} relocalized to the central focal adhesion cluster (Figure 20A). The analyses of YFP-MglA^{Q82A} localization and dynamics revealed that in the presence of the paralyzed motor mutant, AglQ^{D28N}, YFP-MglA^{Q82A} localizes to multiple defective adhesion clusters, whereas blocking the PMF with nigericin leads to a dispersal of YFP-MglA^{Q82A} from the FACs. In both experiments the polar clusters of YFP-MglA^{Q82A} were unaffected. One possible explanation for why we observe a dissolution of the focal adhesion cluster of MglA^{Q82A} when nigericin is added could be that this compound has pleiotropic effects in the cell; thus, in addition to blocking the function of AglQ by inhibiting PMF, it could also act to immediately block an additional unknown component which is needed to keep MglA^{Q82A} localized to an adhesion complex. On the other hand, bearing a paralyzed AglQ^{D28N} could result in multiple defective YFP-MglA^{Q82A} clusters in the cell because a fully functional AglQ itself is necessary to keep YFP-MglA^{Q82A} in one prominent FAC. In conclusion, paralyzing the gliding motor by constructing an AglQ^{D28N} variant, or by injecting nigericin to the cells interferes with YFP-MglA^{Q82A} localization to the focal adhesion cluster due to AglQ itself, or a component which acts in the interface between AglQ and MglA.

In addition to assaying whether localization of YFP-MglA^{Q82A} to the focal adhesion cluster depends on AglZ and AglQ, we tested whether the formation of AglQ-mCherry in FACs depends on the presence of MglA. The strain expressing AglQ-

mCherry in Δ*mglA* background showed mostly diffuse localization of AglQ in the cell envelope, and rarely formed a small distorted cluster resembling a focal adhesion cluster (Figure 17B). This finding tells us that the formation of the motor subunit clusters depends on MglA and that in its absence the protein is mostly diffuse in the envelope and unable to localize into focal adhesion clusters.

Together with the previously published result that AglZ-YFP is completely diffuse in the cytoplasm in a Δ*mglA* mutant (Zhang *et al.*, 2012), our results strongly suggest that in the absence of MglA, FACs do not form. This gave us a clue that MglA itself is responsible for recruiting the components of the gliding apparatus to the FACs. Additionally, in the presence of GTP-locked variants MglA$^{Q82A/L}$, focal adhesion components form one prominent cluster that cannot disassemble at the lagging cell pole, unlike wildtype focal adhesion clusters (Figures 13, 15, and 16). This further confirms that the nucleotide-bound state of MglA regulates the size, number, assembly and disassembly of the FACs in the cell. Exactly how all the components of the gliding apparatus are linked is not yet clear. It also remains to be elucidated how the membrane associated complex is held stationary during gliding.

3.2 MreB is essential for gliding motility and FACs

Previous findings that the MreB-inhibiting antibiotic A22 blocks gliding motility and dissolves the focal adhesion clusters of AglZ and wildtype MglA (Mauriello *et al.*, 2010b), prompted us to investigate the role of MreB in these processes in further detail.

3.2.1 MreB inhibition by A22 inhibits the formation of AglQ and MglA^{Q82A} FACs

MreB is a bacterial actin homolog that is important in different cellular processes, but it is currently understood to act as a cytosolic scaffold for the PG synthesizing machinery as its primary function (Carballido-Lopez, 2006; Shaevitz and Gitai, 2010; White and Gober, 2012). The A22 antibiotic competitively binds the ATP binding pocket of MreB, thus preventing its polymerization and leading to disassembly of existing polymers (Bean *et al.*, 2009). This effect on MreB leads to cells becoming spherical and eventually to cell death (Figure 24A, 24B).

We tested the effect of A22 on gliding and localization of YFP-MglA^{Q82A} because of the previously seen effects of A22 on gliding motility and FACs of AglZs. In presence of A22, DK1622 wildtype cells stopped gliding at MIC (24C). Also, we found that the bipolar localization of YFP-MglA^{Q82A} was unaffected. However, the

localization to the large internal FAC was absent in most of the cells (Figure 25A, B). We found a significant decrease in cell velocity during A22 treatment, which was almost completely recovered once A22 was rinsed with TPM buffer (Figure 25E). In the A22-insensitive strain carrying the MreB^{V323A} variant, we found no dispersal of YFP-MglA^{Q82A} localization to the internal focal adhesion cluster (Figure 25 C, D) and no blocking of motility (Figure 25E). From these data we conclude that intact MreB cytoskeletal elements are necessary for the localization and maintenance of YFP-MglA^{Q82A} to the FAC.

To further examine the role of MreB in focal adhesion localization and formation, we tested the behavior of AglQ-mCherry FACs in the presence of A22. This experiment revealed that AglQ completely disperses from the FACs 1-2 min post A22 injection (Figure 26) just as observed for YFP-MglA^{Q82A} localization (Figure 25A). The A22 injection experiment on a double labeled strain carrying YFP-MglA^{Q82A}/AglQ-mCherry led to a rapid dispersal of their co-localization to FAC, suggesting a simultaneous collapse of the gliding apparatus once MreB is perturbed with A22 (Figure 27). Taken together, A22 injection experiments show that MreB cytoskeletal elements are essential for the recruitment of the regulator MglA and the motor subunit AglQ to the FACs.

3.3 MreB interacts with MglA-GTP to confer gliding motility

3.3.1 MreB polymerizes and forms filaments *in vitro*

MreB was previously shown to interact with AglZ in an *in vitro* pull-down assay using purified proteins (Mauriello *et al.*, 2010b). Based on the observations that polymerized MreB is necessary to localize AglZ (Mauriello *et al.*, 2010b), AglQ and MglA (Figures 20, 21, 22) to FACs, we hypothesized that MreB is acting as a scaffold for the recruitment of the FAC components to the correct sites in the cell by MglA itself. To test whether MglA and MreB interact directly, we performed *in vitro* interaction experiments using purified MglA and MreB.

Polymerization of purified MreB-His$_6$ (Figure 28) was tested in presence of different nucleotides and at multiple times and temperatures, followed by high speed sedimentation. MreB was recovered in the pellet fraction in a temperature- and time-dependent manner, independent of the presence or absence of nucleotides (Figure 29). When analyzed by electron microscopy, we found that MreB-ATP readily formed filaments at 37°C (Figure 30A), and only amorphous and disorganized structures were observed when the protein was incubated with ADP (Figure 30B). Thus, under our

experimental conditions MreB-ATP formed long and thick filaments that often interacted to form multi-filamentous bundles.

3.3.2 Polymerized MreB interacts directly with MglA-GTP

We used wildtype His-tagged purified MglA or MglA^{Q82L} (Figure 31) pre-charged with GDP or GTP before further analyses of interactions with MreB. MglA ^{Q82L} phenocopies the localization and dynamics of MglA^{Q82A} *in vivo*, and behaves similar to it *in vitro*. Both MglA protein variants recovered in the pellet only slightly when they were pre-incubated with GTP, indicating a possible stronger interaction of MglA to itself in presence of GTP. Moreover, when polymerized MreB (ATP, 37 °C) was added to wildtype MglA or MglA^{Q82L}, both proteins were readily recovered in the pellet fraction together with MreB (Figure 32). Importantly, this interaction was specific to GTP-bound MglA proteins because neither GDP-MglA nor GDP-MglA^{Q82L} was significantly recovered in the pellet fraction when MreB was present in the reaction (Figure 32). Finally, when mixed with increasing concentrations of MreB, wildtype MglA-GTP was recovered in the pellet in an MreB concentration-dependent manner (Figure 33). Altogether, these experiments demonstrate that MglA interacts directly with polymerized MreB in a GTP-dependent manner (Figures 32 and 33), which together with our genetic and cell biology data suggests a pathway in which active MglA is involved in recruiting motility complexes to specific places in the cell by its direct interaction with polymerized MreB.

3.4 The function of MreB in gliding motility is separable from its function in PG biosynthesis

3.4.1 Preliminary data show that PG biosynthesis inhibiting drugs do not interfere with gliding motility

MreB is suggested to function as a scaffold for the PG synthesis machinery, and during cell growth it forms short and dynamic patches which move in trajectories nearly perpendicular to the cell long axis (Dominguez-Escobar *et al.*, 2011; Garner *et al.*, 2011; van Teeffelen *et al.*, 2011). It is proposed that MreB dynamics are powered by the PG synthesis machinery, and supported by the evidence that antibiotics which block PG synthesis block MreB dynamics.

We questioned whether PG elongation-specific blocking antibiotics have an effect on *M. xanthus* cells, and whether they affect gliding motility. In numerous other bacteria,

cell wall growth can be inhibited by addition of mecillinam, which is known to specifically bind and prevent the function of pencillin-binding protein 2 (PBP2) during PG synthesis (for reviews on antibiotics' modes of action refer to (Lovering *et al.*, 2012; Walsh and Wencewicz, 2013). We found that the mecillinam MIC for *M. xanthus* cells is 10 µg/ml (Figure 34). Additionally, phosphomycin, which blocks the first cytosolic step of PG synthesis, has a MIC at 40 µg/ml (Supplementary Figure 9). Both mecillinam and phosphomycin have been shown to block the dynamics of MreB patches within minutes of their addition to *E. coli* and *B. subtilis* cells (Dominguez-Escobar *et al.*, 2011; Garner *et al.*, 2011; van Teeffelen *et al.*, 2011). Furthermore, it was shown that A22, which inhibits MreB polymerization, cefsulodin, which binds PBP1A/B and, cephalexin, which binds PBP3, do not lead to reduction of MreB dynamics in *E.coli* (van Teeffelen *et al.*, 2011). We tested the effect of A22, mecillinam, phosphomycin, cefsulodin and cephalexin at MIC on gliding motility of wildtype *M. xanthus* cells after 10-15 min post addition of the antibiotics. We found that A22 blocks motility, contrary to all the other drugs which do not inhibit gliding motility (Figures 35A, 36). To test whether mecillinam had an effect on the localization and maintenance of FACs, we performed time-lapse analyses of cells harbouring YFP-MglA^{Q82A} and AglQ-mCherry. In presence of mecillinam, localization and dynamics of YFP-MglA^{Q82A} and AglQ-mCherry at FACs (Figure 35B and 35C, respectively) were not affected.

Two different laboratories have shown that gliding motility in *M. xanthus* is not affected when cellular filamentation is induced by cephalexin treatment up to 8 hours (Sliusarenko *et al.*, 2007; Sun *et al.*, 1999). Sliusarenko and colleagues also reported that in the cephahexin-treated elongated cells AglZ-YFP clusters were still able to form. Taken together, our results on the effects of antibiotics on gliding motility strongly support that all three drugs that have an effect on blocking PG synthesis during elongation and cellular growth do not affect motility.

Therefore, we propose that MreB has independent functions in gliding motility and PG synthesis in *M. xanthus*. One of the unsolved questions still remains, whether MreB forms only a scaffold for the motility machinery complexes or if MreB itself exerts force actively onto the cell envelope to allow gliding. As MreB is linked to the cell cortex, it would be a possibility that in addition to forming a scaffold for PG synthesizing machinery, it also acts to accumulate a number of proteins involved in

force transduction. These complexes may be regulated to exert force and engage the entire motility apparatus at the sites where the appropriate cell-substrate contact exists.

3.4.2 Preliminary results indicate that PBP2 could be used a proxy for MreB dynamics in *M. xanthus*

Thus far an MreB fluorescent fusion has not be obtained for *M. xanthus*. Therefore, to indirectly track MreB *in vivo*, we focused on using penicillin-binding protein 2 (PBP2) (Figure 37) as a marker for MreB localization given the well-established association between MreB dynamics and PG elongation machinery complex. In *E. coli*, *C. crescentus and B. subtilis*, the dynamics of MreB are driven by PG synthesis, and can be inhibited by addition of mecillinam, which binds and changes the catalytic site in PBP2 in the elongation machinery of PG. In these reports, the dynamics of MreB is identical to the dynamics of PBP2 and other components of the PG elongation machinery, and it can be inhibited by antibiotics blocking PG elongation (Dominguez-Escobar *et al.*, 2011; Garner *et al.*, 2011; van Teeffelen *et al.*, 2011).

Consequently, we reasoned that the PBP2 localization can be used as a proxy for MreB behavior in *M. xanthus*. We have shown that mecillinam inhibits cell growth by inhibiting PG synthesis, but it does not interfere with gliding motility (Figures 35A and 36). Therefore, we focused on tracking fluorescently tagged PBP2 in presence of mecillinam. In wildtype background (*pbp2+*), PBP2-sfGFP localized to multiple clusters within the cell and this localization pattern was not affected in presence of mecillinam, which specifically blocks PBP2, or other antibiotics used (A22, phosphomycin, cefsulodin and cephalexin) (Figure 38). Interestingly, the time-lapse microscopy of PBP2-sfGFP taken every 30 sec, led to an interesting observation that 25% of the total clusters of PBP2 were highly mobile (Figure 39A). This suggested that PBP2 in *M. xanthus* is dynamic, so we further analyzed if we can inhibit the dynamics using its specific inhibitor, mecillinam. After the addition of mecillinam the dynamics of PBP2-sfGFP were highly reduced (Figure 39D). Since these initial results showed that mecillinam reduced PBP2-sfGFP dynamics without blocking gliding motility (Figures 35A, 36 and 39D), we wanted to examine whether the MreB polymerization perturbing compound A22, which inhibits motility within minutes of its addition, has an effect on PBP2-sfGFP dynamics. It was previously shown that A22 does not affect the dynamics of MreB polymers and PG synthesis machinery even though it blocks polymerization of newly synthesized MreB molecules in *E. coli* (van Teeffelen *et al.*, 2011). Under our experimental conditions, in the presence of A22 at the MIC, the

dynamics of PBP2-sfGFP clusters were not affected (Figures 39B). Furthermore, we tested whether PBP2-sfGFP clusters are affected in the presence of cephalexin, cefsulodin and phosphomycin, and found that phosphomycin and cefsulodin completely reduce the clusters dynamics (Figure 39E, F), whearas cephalexin has an intermediate effect (Figure X). We observed similar effects of cefsulodin and phosphomycin when velocities and mean square displacements were calculated (Figure 39C).

To verify the inhibitory effects by PG-inhibition drugs on PBP2-sfGFP cluster dynamics, we analyzed the velocity and mean squared displacement of clusters in untreated and treated cells (Figure 40). We found that mecillinam significantly reduced the velocities of PBP2-sfGFP clusters (Figure 40A, red bars) and that the adding mecillinam reduced the total distance travelled by the clusters with time (Figure 40B, red lines). When the same analyses were performed on multiple clusters from the A22 treated cells, we saw no major effect on PBP2-sfGFP cluster velocities or mean squared displacement (Figures 40A, B, blue bars and lines). Cephalexin had an intermediate reducing effect on PBP2-sfGFP clusters (Figure 40A, B, green bars and lines). Lastly, the effects on cesfuslodin and phosphomycin were similar on PBP2-sfGFP velocities and mean squared displacement, with a trend showing major reduction in both values compared to untreated cells.

Further analyses of PBP2-sfGFP protein localization and dynamics are needed, as there is endogenous PBP2 present in the genome, and we also observed that changing the buffer conditions of the agar pad influences the localization of the protein.

Taken together, our results strongly support the idea that the function of MreB in gliding of *M. xanthus* is separate from the function in PG synthesis. Therefore, we suggest that, polymeric MreB in addition to its function as a scaffold for the PG synthesis machinery has an independent function as a scaffold for the gliding motility machinery supporting focal adhesion complex formation and stability.

3.5 Conclusion

In this work we demonstrate that bacterial small G-protein MglA is essential for gliding of *M. xanthus* by interfacing between the gliding machinery complexes and MreB bacterial actin homolog. In order to move by gliding, *M. xanthus* cells require intact MreB cytoskeletal elements, and MglA which can cycle between active and inactive forms. Our findings strongly suggest that MglA regulates the recruitment of

proteins to FACs at the sites in the cell where MreB forms a scaffolding platform enabling gliding. Perturbing MreB polymerization causes the scaffold to disintegrate, leading to loss of support for MglA and thus in turn the inability of AglQ, AglZ and MglA to localize to FACs. We show that MglA in its active state interacts with polymerizing MreB, which in turn regulates the turnover of the FACs in the cell.

In the absence of MglA the FACs cannot form, whereas in presence of wildtype MglA they form at the front of the cell, and fall apart at the lagging cell pole upon deactivation by the GAP, MglB (Figure 41B). Thus, the regulation of the assembly and disassembly of the FACs depends on the nucleotide-bound state of MglA. In absence of the MglA GTPase cycle the formation of the FACs is perturbed and only one prominent internal FAC forms (depicted in Figure 41B). This large FAC cannot be disassembled at the lagging cell pole due to the inability of MglB to stimulate MglA GTP hydrolysis (summarized in Figure 41B). Therefore, we propose that activated MglA drives the formation of FACs at specific sites in the cell. Furthermore, in the presence of antibiotics that block peptidoglycan (PG) synthesis and inhibit MreB dynamics, gliding motility and focal adhesion complex formation are not affected. Thus, we suggest a model in which MreB acts as a scaffold to spatially organize FACs, and this function of MreB is separable from its role in PG synthesis during growth (Figure 41C).

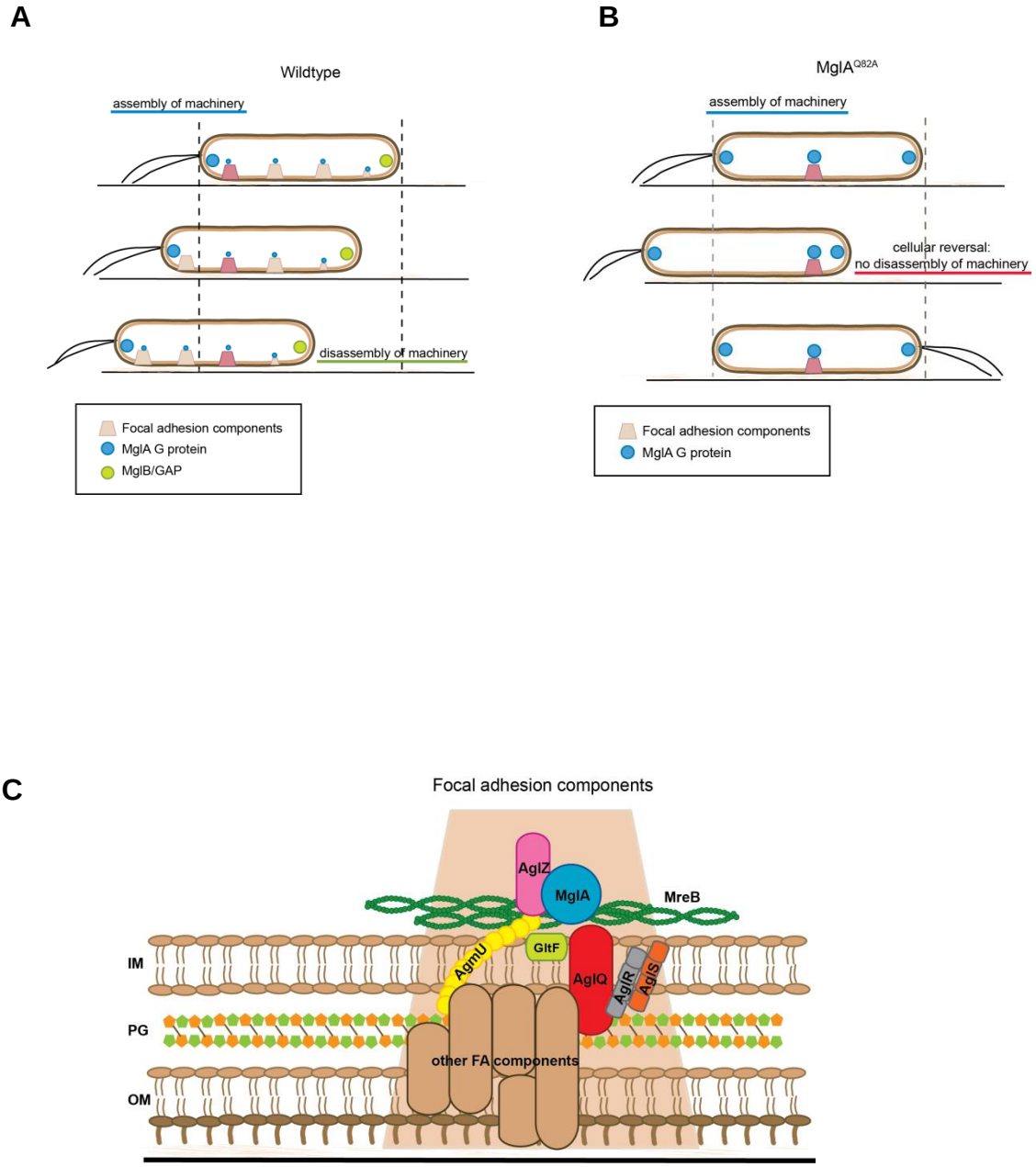

Figure 41. A model for the function of MreB as a scaffold for gliding machinery. (A) In wildtype cells multiple focal adhesion complexes (FACs) are periodically spaced along the cell body during gliding. MglA forms a cluster at the leading cell pole and multiple small internal clusters that co-localize with FACs. Upon reaching MglB at the lagging cell pole the FACs disassemble. Cellular reversals occur irregularly and cells can move for long distances. (B) In active MglA^{Q82A} background, one prominent internal FAC is formed. YFP-MglA^{Q82A} co-localizes with the FAC, and upon reaching the lagging cell pole there is no FAC disassembly; cells instead reverse the direction of gliding immediately, thus moving a net distance of one cell length. (C) Enlarged model of the components of the FACs components during motility. MreB serves as a scaffold for the machinery assembly, and MglA is essential for recruiting the adhesion complexes through its interaction with MreB.

The identification of the components in the FACs and a characterization of some of their interactions and inter-dependent localizations and dynamics has allowed for development of a working, yet incomplete model of the molecular motor complex

driving motility (Figure 41C). Bioinformatics and experimental data from recent studies propose that the gliding motility machinery consists of multiple cell envelope spanning components (Figure 41), thus paving the path for further clarification of the how the machinery functions. Further studies are needed to elucidate the proteins involved in cellular adhesion to the substrate, and to understand how force is generated and transduced from the cell cytoplasm through the membranes via the FACs. Furthermore, identification of MglA GEF proteins and effectors would help elucidate how the motility machinery is regulated.

In summary, our results on regulation of gliding motility in a bacterium by controlling FACs through small Ras-like G-protein MglA together with actin-like bacterial cytoskeleton MreB, share general functional similarities with eukaryotic cell migration (Figure 42).

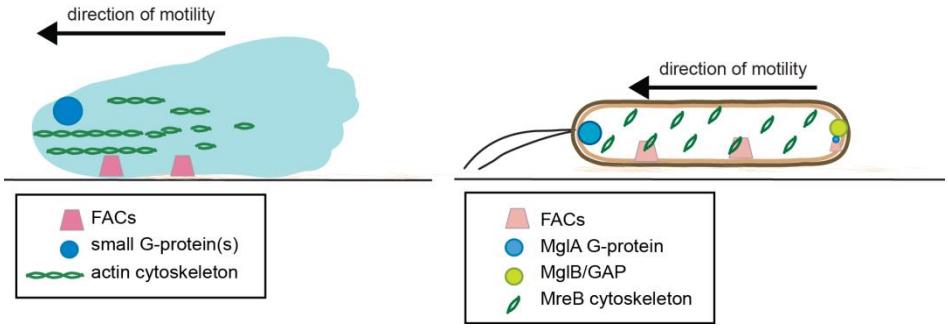

Figure 42. Surface-dependent motility parallels between a eukaryotic cell (on the left) and a bacterial M. *xanthus* cell (on the right). Major components involved in motility of both cell types are labeled.

Although the specific components of the machineries, signals and pathways regulating motility in bacterial and eukaryotic cell types are highly different, small G-proteins, focal adhesion complexes and actin homolog presence and requirement for gliding in *M. xanthus* strongly support that bacteria require complex intracellular spatial and dynamic organization to accomplish a processes such as cellular motility (parallels outlined in Figure 42).

4 Supplementary results

4.1.1 MreB co-immunoprecipitates specifically with active MglA forms from the cell lysates

To check if MreB interacts with MglA *in vivo*, we performed a co-immunoprecipitation experiment using GFP antibodies on cell lysates of the strains expressing: only GFP, YFP-MglA, YFP-MglA^{G21V}, YFP-MglA^{Q82A} and YFP-MglA$^{T26/7N}$ (Figure S1). When anti-MreB Western was performed on elution fractions from the co-IP we found MreB was pulled-down with YFP-MglA (wildtype protein), and the active YFP-MglA^{G21V} and YFP-MglA^{Q82A} forms, but not in the negative control expressing GFP only, and more interestingly not in the YFP-MglA$^{T26/7N}$ inactive form of MglA.

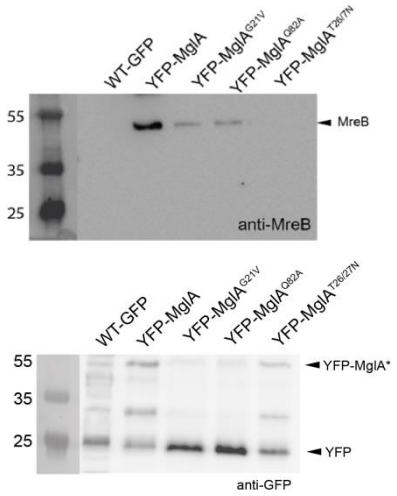

Figure S1. MreB co-precipitates with wildtype and active MglA variants specifically. Anti-MreB western on elution fractions from the co-IP from the cell lysates indicated above.

4.1.2 Purified MreB does not interact with an unspecific cytoplasmic protein

To verify that MreB in presence of ATP interacts with MglA protein specifically, we tested whether an unrelated *E. coli* FdhD-His$_6$ purified dehydrogense protein can interact with MreB-His$_6$ *in vitro*, Figure S2.

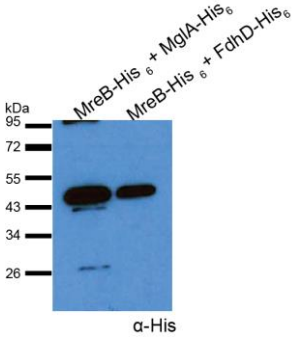

Figure S2. MreB interacts with MglA specifically, *in vitro*. Anti-His Western showing MglA-His$_6$ and MreB-His$_6$ at above 26kDa and above 45kDa, respectively, in the first lane. In the second lane only MreB can be recovered after polymerization with FdhD-His$_6$.

Western analyses using His-tag specific antibodies showed that in the MglA-His_6 fraction with MreB-His_6 both proteins can be pulled-down, whereas in the fraction containing FdhD-His_6, only MreB-His_6 is present in the pellet alone.

4.1.3 MreB localization in the cell can partially be inhibited by A22

To examine the localization of MreB in *M. xanthus*, we used immuno-fluorescence microscopy with affinity-purified MreB antibodies. Using this technique we found that MreB localizes to multiple clusters over the cell length (Figure S3, top left panel), similar to what has previously been reported in *M. xanthus* and in other organisms. With increasing time (from 5 to 10 minutes) of cells treatment with smaller than MIC (10 µM) or MIC of A22 (184µM) concentrations, we found a greater dissolution of the MreB localization in wildtype background and no major effect on the A22-insensitive allele, Figure S3.

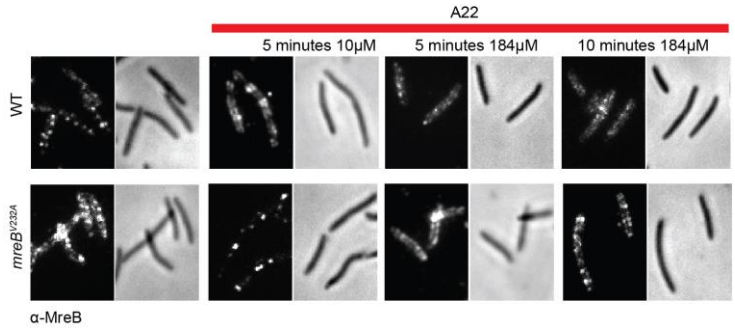

Figure S3. MreB localizes to multiple clusters over the cell. In presence of A22 , the clusters of MreB become less structured and more diffuse with increasing time and drug concentration. Bottom panel $MreB^{V323A}$ A22-insensitive allele.

However, we never observed a full diffusion of A22 in presence of the concentrations and times we used, probably due to the technical drawbacks of immunofluoresence which might often lead to cluster like fluoresenct structures in the cell.

4.1.4 Active MglA partially co-localizes with MreB

To assay if there is a sub-cellular link between MglA and MreB, we analyzed if YFP-$MglA^{Q82A}$ co-localizes with MreB, using immunofluoresence on the fixed cells (Figure S4). With this assay we found a partial co-localization of MglA and MreB, where the prominent focal adhesion cluster of YFP-$MglA^{Q82A}$ is observed to partly overlap with a few of the MreB clusters found at that position.

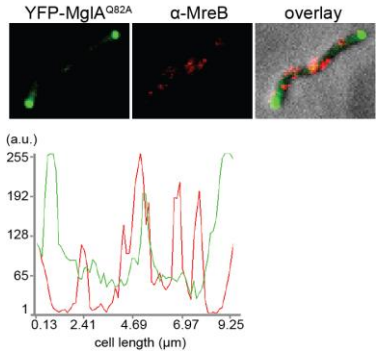

Figure S4. MreB partially co-localizes with YFP-MglA^{Q82A} at the focal adhesion site. In green YFP-MglA^{Q82A}, in red MreB clusters, and grey overlay. Bottom panel the intensity of the fluorescence in each channel revealing co-localization of both red and green at a specific point in the cell where YFP-MglA^{Q82A} FA cluster localizes.

4.1.5 YFP-MglA fusions which complement the Δ*mglA* phenotype are expressed

To check if the MglA fluorescent fusions used in this study are expressed under *pilA* promoter at the *attB* site, we performed anti-MglA Western blot analyses (Figure S5). We found partial degradation of the fusion protein, but no major over-expression was observed in any of the strains.

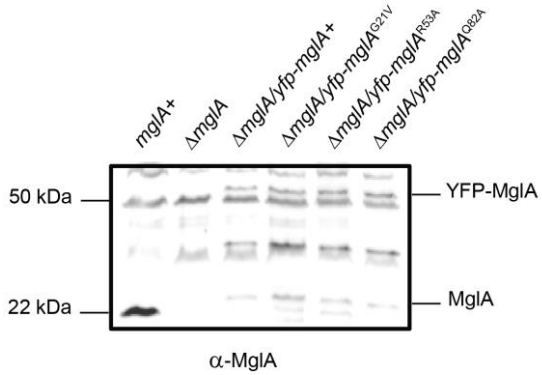

Figure S5. Immunoblot of YFP-MglA* accumulation in Δ*mglA*. Wildtype and the active forms of MglA (G21V, R53A and Q82A) tagged to YFP N-terminally are expressed under *pilA* promoter. Higher band shows fusion protein, and the lower band cleaved MglA only.

4.1.6 PBP2-sfGFP fusion protein is expressed in the wildtype background

To test whether PBP2-sfGFP construct under *pilA* promoter is expressed, we performed Western blot analyses using GFP antibodies. In all of the checked clones full size fusion protein was made, and a slight band of GFP degradation product was detected (Figure S6).

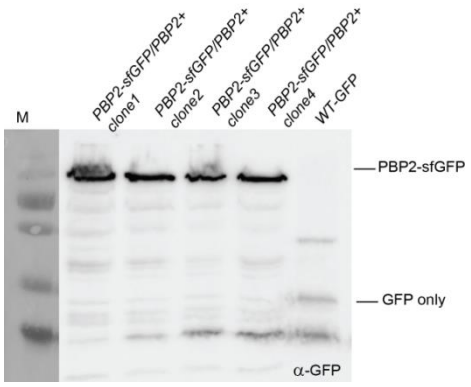

Figure S6. Immunoblot analyses of PBP2-sfGFP expressing strains. PBP2-sfGFP fusion protein is made, and slightly degraded (higher than 25kDa band).

4.1.7 PG biosynthesis inhibiting drugs affect *M. xanthus* cells

Prior to testing the effects of different antibiotics on cellular gliding, or PBP2 localization, we tested whether they have an effect on cell shape and growth (for antibiotics specific roles refer to the Discussion, Chapter 3.4.1).

Cefsulodin had a minimal inhibitory growth concentration at 20 µg/ml (Figure S7A, B).

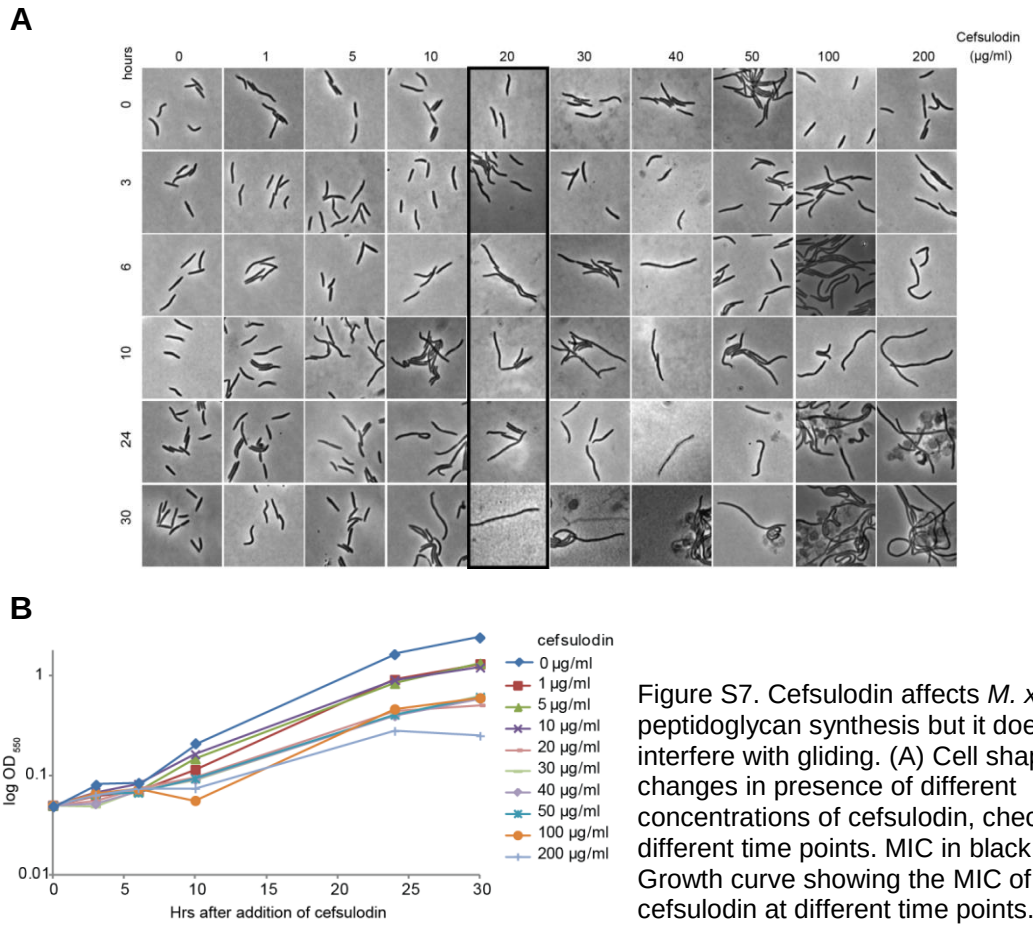

Figure S7. Cefsulodin affects *M. xanthus* peptidoglycan synthesis but it does not interfere with gliding. (A) Cell shape changes in presence of different concentrations of cefsulodin, checked at different time points. MIC in black box. (B) Growth curve showing the MIC of cefsulodin at different time points.

Cephalexin has an effect on peptidoglycan synthesis and causes cell death at 30 µg/ml; however, this or higher concentrations of cephalexin do not inhibit gliding motility (Figure S8).

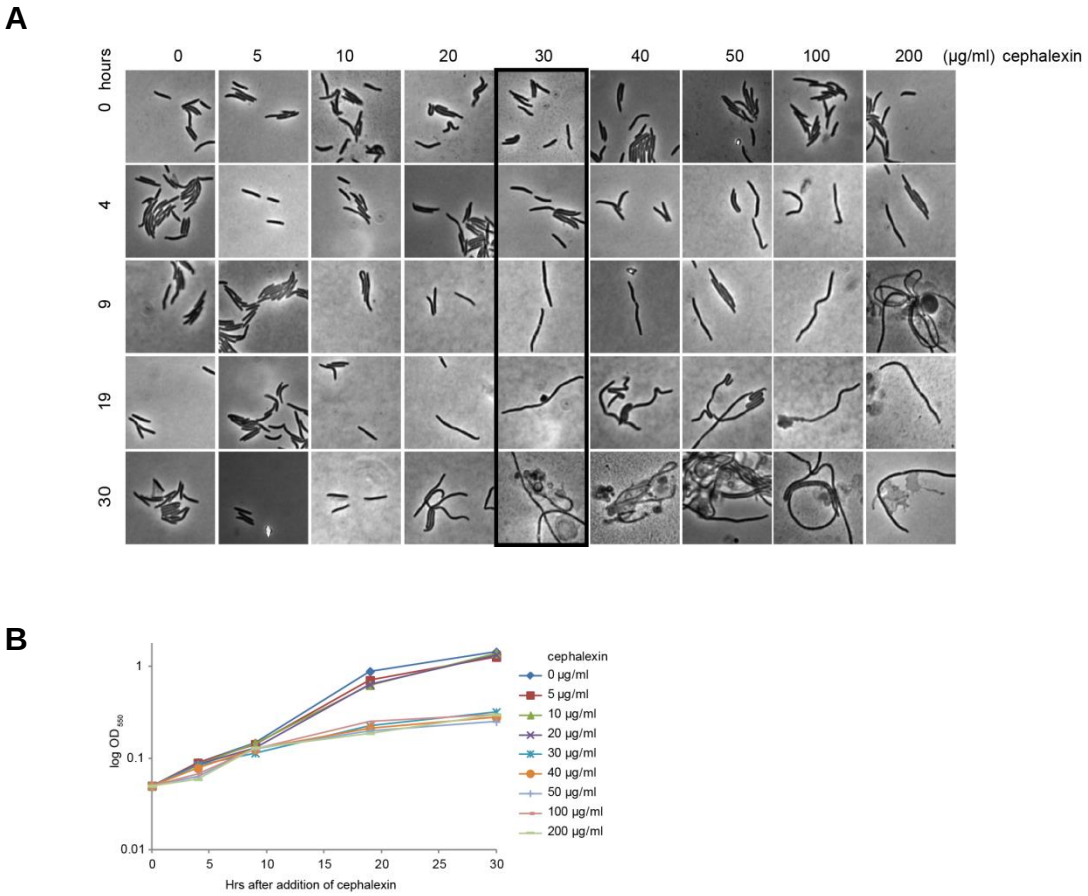

Figure S8. Cephalexin inhibits peptidoglycan synthesis but it does not have an effect on gliding. (A) Effect of cephalexin on cell shape changes due to its action. MIC in black box. (B) Growth curve showing MIC of cephalexin.

Phosphomycin had an effect on cell growth and prevented peptidoglycan biosynthesis (as visible by the cell shape changes), but it did not interfere with gliding motility (Figure S9).

A

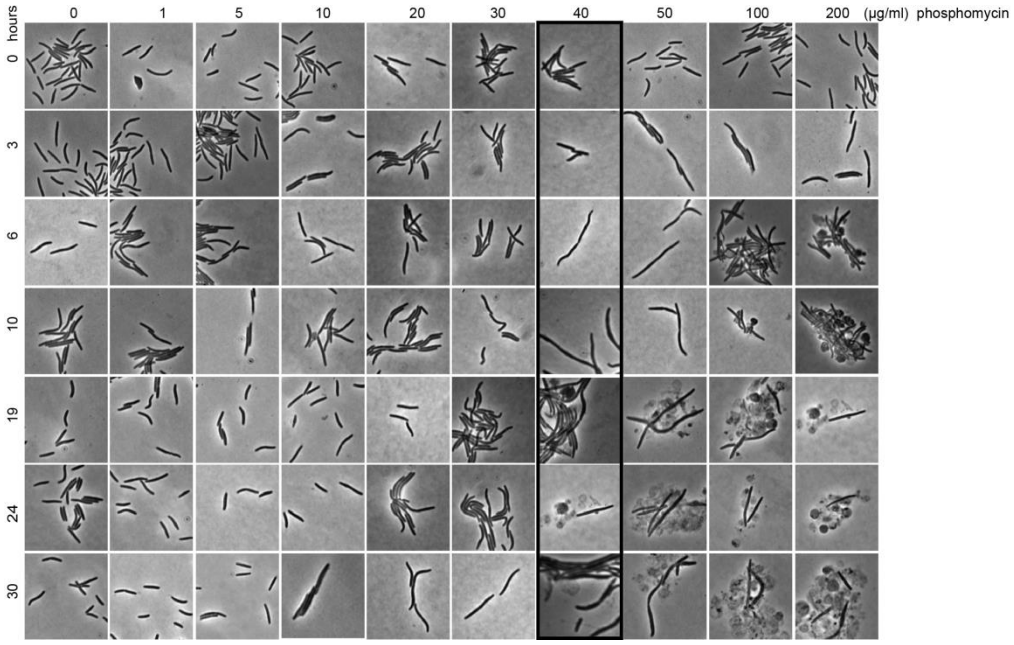

B

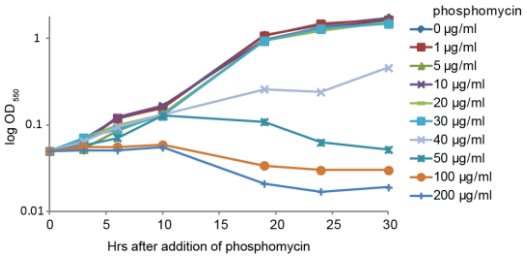

Figure S9. Phosphomycin inhibits peptidoglycan synthesis but it does not have an effect on gliding. (A) Effect of phosphomycin on cell shape changes due to its action. MIC in black box. (B) Growth curve showing MIC of cephalexin.

4.1.8 SgnC, mxan4438 and MasK

We intially sought to analyze the sgnC, mxan4438 and masK genes products functions in motility, as they were implicated in motility by other studies. However, deletions of these genes did not affect gliding motility and we did not further characterize them.

5 Materials and Methods

5.1 Reagents and equipment

A list of antibiotics, enzymes and reagents, as well as their producers is shown in Table 1. Technical equipment and software used for data analyses, and their manufacturers are listed in Table 2.

Table 1. Antibiotics, enzymes and other reagents.

Antibiotics	**Supplier**
Kanamacyin, chloramphenicol, ampicilin, gentamycin, oxytetracyclin, tetracycline, A22, nigericin, mecillinam, phosphomycin, cefsulodin, piperacillin, moenomycin, aztreonam, cefoxitin, vancomycin, cephalexin	Sigma-Aldrich (Schnelldorf), Roth (Karlsruhe), Merck Millipore (Darmstadt)
Enzymes	
Pfu Ultra II® DNA Polymerase	Stratagene (Amsterdam)
AccuPrime CG rich DNA Polymerase	Invitrogen (Karlsruhe)
Taq-Polymerase in Eppendorf® MasterMix, 5 Prime Master Mix	Eppendorf (Hamburg), 5 PRIME GmbH Hamburg
Restriction endonucleases, T4 DNA ligase, Antarctic phosphatase	New England Biolabs (Frankfurt), MBI Fermentas (St Leon-Rot)
Buffer J PCR mix	Epicentre (Hess.-Oldendorf).
Reagents	
Chitosan from shrimp	Sigma Aldrich (Schnelldorf)
Agar, solid and liquid media components	Difco (Heilderbeg), Roth (Karlsruhe), Sigma-Aldrich (Schnelldorf)
SDS-PAGE and DNA size standard markers	MBI Fermentas (St Leon-Rot), Bioline (Luckenwalde)
Oligonucleotides	Eurofins MWG Operon (Ebersberg)
Rabbit anti-sera	Eurogentec (Seraing, Belgium)
Goat anti-rabbit IgG, goat anti-rabbit IgG DyLight549	Roche (Manheim)
Anti-GFP monoclonal antibody	Roche (Manheim)
Kits	
Super Signal Chemiluminescent detection	Pierce Thermo Scientific (Dreiech)
DNA/RNA purification, gel extraction	Qiagen (Hilden), Research (HiSS-

and plasmid mini preparation	Diagnostics, Freiburg), Macherey Nagel Nucleo Spin (Oensingen), Epicentre
SlowFade Antifade kit	Molecular Probes Invitrogen (Darmstadt)

Table 2. Technical equipment used in the study

Device and application	**Manufacturer**
Molecular and cellular applications	
Branson sonifier for cell disruption	Heinemann (Shwabisch Gmund)
SLM Aminico French Pressure Cell Press FA- 078 for cell disruption	Gaithersburg, USA
MasteCycler personal, MasteCycler epgradient for PCRs	Eppendorf (Hamburg)
Gene pulser X cell for electroporation	Bio-Rad (Munich)
Mini-PROTEAN 3 cell for protein electrophoresis	Bio-Rad (Munich)
TE77 semi-dry transfer for Western blotting	Amersham Biosciences (Munich)
Ultraspec 2100 Pro Spectrophotometer for optical densities	Amersham Biosciences (Munich)
Nanodrop ND-1000 UV-Vis for nucleic acid absorption	Nanodrop (Wilmington)
Imaging	
Diagnostic microscope 12 well slides for immunofluorescence	Pierce Thermo Scientific (Dreiech)
Carbon-film covered grids for electron microscopy	PLANO (Wetzlar)
Leica DM600B, DM IRE2 and DMI6000B light microscopes for imaging	Leica Microsystems (Wetzlar)
MZ75 stereomicroscope, Nikon Eclipse TE 2000-E Light microscope for imaging	Nikon (Düsseldor)
TE2000-E-PFS Nikon Light microscope for imaging	Nikon, France
Fuji Photo Film FPM 100A Luminescent Image analyzer LAS4000	Fujifilm (Düsseldorf)

Jeol JEM 1400 120kV	Jeol, USA
Software	
Vector NTI 11 for DNA and protein sequence analyses	Invitrogen (Darmstadt)
Image J 1.43 for image processing	NIH provided free software
Metamorph® v 7.5 for image processing	Molecular Devices, Union City, USA
Built-in macros for cell tracking	A. Ducret, T. Mignot, CNRS Marseille

5.2 Microbiological methods

5.2.1 Media and cultivation of *E. coli* and *M. xanthus* strains

E. coli cells were grown on LB plates or in LB liquid medium (Table 3) at 37°C, and *M. xanthus* cells were grown in 1% CTT liquid and /or agar supplemented media (Table 3) at 37°C. Antibiotics and other additives for both species were supplemented where necessary at concentrations indicated in Table 4. All media and solutions were autoclaved for 20 min at 121˚C. Antibiotic solutions were filtered using 0.22 μm pore size filters (Millipore, Schwalbach) and added to the pre-cooled to 55˚C media. Liquid cultures were incubated shaking with 220 rpm.

Table 3. Growth media for *E. coli* and *M. xanthus*.

Medium	**Composition / Source of reference**
E. coli	
Luria Bertani (LB)	1% (w/v) tryptone, 0.5% (w/v) yeast extract, 1% (w/v) NaCl
LB agar plates	LB medium, 1% (w/v) agar
M. xanthus	
1% CTT	1% (w/v) BactoTM casitone, 10 mM Tris-HCl pH 8.0, 1 mM potassium phosphate buffer pH 7.6, 8 mM $MgSO_4$
1% CTT agar plates	1% CTT medium, 1.5% agar
Motility assays	

A (gliding motility of single cells) on agar	0.5% CTT, 1.5% agar (Hodgkin and Kaiser, 1977)
S (type 4 pili) motility of groups of cells	0.5% CTT, 0.5% agar (Hodgkin and Kaiser, 1977)
Microscopy assays surfaces	
A 50 microscopy agar	10 mM MOPS pH 7.2, 10 mM $CaCl_2$, 10 mM $MgCl_2$, 50 mM NaCl, 1.5% or 0.7% (w/v) agar
A (gliding motility of single cells) on chitosan	15 mg/ml chitosan in 2M acetic acid (Ducret *et al.*, 2009)
TPM agar for microscopy	10 mM Tris-HCl pH 7.6, 1 mM KH_2PO_4pH 7.6, 8 mM $MgSO_4$ 1.5% (w/v) agar

Table 4. Antibiotics and additional compounds used for growth / selection and induction in liquid and solid media where appropriate.

E. coli		
Antibiotic	**Final concentration**	**Solvent**
Ampicilin sodium sulfate	100 µg/ml	Water
Chloramphenicol	50 µg/ml	99.99% Ethanol
Kanamycin sulfate	100 µg/ml	Water
Additional compounds		
IPTG	0.5 mM	Water
Tetracyclin	15 µg/ml	99.99% Ethanol
M. xanthus		
Antibiotic	**Final concentration**	**Solvent**
Kanamycin sulfate	50 µg/ml	Water
Oxytetracyclin	10 µg/ml	99.99% Methanol
Gentamycin sulfate	10 µg/ml	Water
Additional compounds		
Galactose	3 %	Water

Table 5. *E. coli* strains used in this study.

Strain	Relevant characteristics	Source of reference
Top 10	F- mcrA Δ(mrr-hsdRMS-mcrBC), 80lacZΔM15ΔlacX74, deoR, recA1, arsD139 Δ(ara-leu)7697, galU, galK, rpsL (StrR) endA1, nupG	Invitrogen (Karsruhe)
Rosetta 2 (DE3)	F-ompT hsdSB(rB-mB) gal dcm(DE3) pRARE2(CmR)	Novagen Merck (Darmstadt)

Table 6. *M. xanthus* strains used in this study.

Strain	Relevant characteristics	Source of reference
DK1622	WT	(Kaiser, 1979)
DK1300	*ΔsglG*	(Hodgkin and Kaiser, 1979)
DK1217	*ΔaglB*	(Hodgkin and Kaiser, 1979)
DK6204	*ΔmglBA*	(Hartzell and Kaiser, 1991b)
MxH2265	*ΔaglZ*	(Yang *et al.*, 2004)
SA3387	*ΔmglB*	(Leonardy *et al.*, 2010)
SA4420	*ΔmglA*	This study, (Miertzschke *et al.*, 2011)
SA4440	Δ*mglA/attB::*P_{pilA}-*yfp-mglA*$^{+}$ (pSL60) Kan^{R}	This study, (Miertzschke *et al.*, 2011)
SA3829	Δ*mglA/attB::*P_{pilA}-*yfp-mglA*^{Q82A} (pTS10) Kan^{R}	This study, (Miertzschke *et al.*, 2011)
SA3396	Δ*mglA/attB::*P_{pilA}-*yfp-mglA*^{Q82L} (pSL73) Kan^{R}	This study

SA4451	Δ*mglA/attB::*P_{pilA}-*yfp-mglA*^{G21V} (pSL61) Kan^R	This study, (Miertzschke *et al.*, 2011)
SA4445	Δ*mglA/attB::*P_{pilA}-*yfp-mglA*^{R53A}(pEH42) Kan^R	This study, (Miertzschke *et al.*, 2011)
SA3385	Δ*mglBA/attB::*P_{pilA}-*yfp-mglA*$^{+}$ (pSL60) Kan^R	This study, (Miertzschke *et al.*, 2011)
SA3823	Δ*mglBA/attB::*P_{pilA}-*yfp-mglA*^{G21V} (pSL61) Kan^R	This study, (Miertzschke *et al.*, 2011)
SA4449	Δ*mglBA/attB::*P_{pilA}-*yfp-mglA*^{R53A}(pEH42) Kan^R	This study, (Miertzschke *et al.*, 2011)
SA3831	Δ*mglBA/attB::*P_{pilA}-*yfp-mglA*^{Q82A} (pTS10) Kan^R	This study, (Miertzschke *et al.*, 2011)
SA3918	Δ*agmK (gltI)*	D. Keilberg, MPI Marburg
SA3919	Δ*agmX(gltJ)*	D. Keilberg, MPI Marburg
TM793	Δ*mglA mreB*^{V323A} */attB::*P_{pilA}-*yfp-mglA*^{Q82A} (pTS10) Kan^R	This study
TM796	Δ*mglA* Δ*aglQ/attB::*P_{pilA}-*yfp-mglA*^{Q82A} (pTS10) Kan^R	This study
TM801	Δ*mglA aglQ-mCherry*	This study
TM798	Δ*mglA aglQ-mcherry/attB::*P_{pilA}-*yfp-mglA*^{Q82A} (pTS10) Kan^R	This study
TM821	Δ*mglA* Δ*aglZ/attB::*P_{pilA}-*yfp-mglA*^{Q82A} (pTS10) Kan^R	This study
TM805	Δ*mglA* Δ*agmX(gltJ)/attB::*P_{pilA}-*yfp-mglA*^{Q82A} (pTS10) Kan^R	This study
TM806	Δ*mglA* Δ*agmX/(gltJ)*	This study
TM815	Δ*mglA* Δ*agmK(gltI)/attB::*P_{pilA}-*yfp-mglA*^{Q82A} (pTS10), Kan^R	This study
SA5293	Δ*aglQ*	This study, (Sun *et al.*, 2011)
TM813	Δ*mglA* Δ*aglQ*	This study

TM812	Δ*mglA* Δ*aglZ*	This study
TM816	Δ*mglA* Δ*agmK(gltI)*	This study
TM818	Δ*aglZfrzE::tn5Ω226* Tet^R	This study
TM819	Δ*mglA* Δ*aglZfrzE::tn5Ω226* Tet^R	This study
TM820	Δ*mglAaglZfrzE::tn5Ω226/attB::*P_{pilA}*-yfp-mglA*^{Q82A} (pTS10) Tet^R, Kan^R	This study
SA4460	Δ*mglA* Δ*aglQ/attB::*P_{nat}*-aglQ*^{D28N}-P_{pilA}*-yfp-mglA*^{Q82A} (pEH100) Kan^R	This study
SA4463	*attB::*P_{pilA}*-pbp2-sfGFP* (pEH110) Tet^R	This study
SA4452	*aglQ-mCherry*	This study
SA4464	*aglZ::aglZ-mCherry* Kan^R	This study
SA4465	Δ*mglA aglZ::aglZ-mCherry/attB::*P_{pilA}*-yfp-mglA*^{Q82A} (pEH108) Kan^R, Tet^R	This work
SA4466	Δ*mglA aglQ*^{D28N}*-mCherry/attB::*P_{pilA}*-yfp-mglA*^{Q82A} (pTS10) Kan^R	This work
SA4467	Δ*aglQ aglZ::aglZ-mCherry* Kan^R	This work
SA4468	*aglQ*^{D28N}*-mCherry*	This work
SA4469	*aglZ::aglZ-mCherry* Δ*aglQ* Kan^R	This work
SA4470	*aglZ::aglZ-mCherry* Δ*aglQ* Δ*mglA /attB::*P_{pilA}*-yfp-mglA*^{Q82A} (pEH108) Kan^R, Tet^R	This work
SA4471	*aglZ::aglZ-mCherry mglA*^{Q82A} Kan^R	This work
SA4472	*aglQ-mCherry mglA*^{Q82A}	This work
SA4401	*MXAN_4438::StrepR* StrepR	This work

SA4403	Δ*MXAN_6627 (sngC)*	This work
SA4411	*mglA::StrepR* StrepR	This work
SA3078	Δ*masK*	I Bulyha, MPI Marburg
SA4438	Δ*masK* Δ*mglA*	This work
SA4415	Δ*masK mglA*$^{T26/27N}$	This work
SA4412	Δ*masK mglA::StrepR* StrepR	This work

[1] plasmids in brackets were integrated at the Mx8 *attB* site.

5.2.2 Storage of *E. coli* and *M. xanthus* strains

E. coli and *M. xanthus* cells on plates were stored up to four weeks at 4°C and 18°C respectively. For long term storage of cells in the -80°C**,** *M. xanthus* cells were grown to OD_{550}=0.8-1 and mixed with glycerol at 4% final concentration; for *E. coli* cells glycerol was added to a final concentration of 10%, and after mixing with glycerol, both bacterial species were snap frozen in liquid nitrogen before being transferred to a freezer.

5.2.3 Motility assays of *M. xanthus* strains

To assay motility of *M. xanthus*, cells growing in exponential phase (7×10^8cells/ml) were harvested by centrifugation at 4700 rpm for 5 min and resuspended in 1% CTT medium to a 7×10^9cells/ml density. Typically, 5 µl of cells were spotted on 0.5% and 1.5% agar motility plates, which favor type 4 pili (S) and gliding (A) motility respectively (Hodgkin and Kaiser, 1977). After 24 hours of incubation at 32°C, the morphology of the colony edge was examined using a Leica MZ75 stereomicroscope at 8 × and 50 × magnifications. Images were captured on Leica DFC280 camera.

5.2.4 Determining minimal inhibitory concentrations of antibiotics

Prior to testing the effects of different antibiotics on gliding motility and protein localizations in the cell, the minimal inhibitory concentrations were determined in growing liquid cultures at different concentrations of the drug. The OD_{550} was checked

and cells' shape changes were examined every 3 hours post addition of the antibiotic for at least 24 hours, on a DM6000B microscope, using a Leica Plan Apo100/NA 1.4 objective. In this study, minimal inhibitory concentrations were determined for A22 (Calbiochem, Merck Millipore), mecillinam, cefoxitin, vancomycin, chloramphenicol, phosphomycin and cephalexin (Sigma Aldrich).

5.3 Molecular biology methods

5.3.1 Primers and plasmids

Table 7. List of primers used in this study.

Name	Nucleotide sequence (5'-3')
oMglAQ82Lforw	ACGGTGCCCGGTCTGGTCTTCTACGAC
oMglAQ82Lrev	GTCGTAGAAGACCAGACCGGGCACCGT
oAglZ-9	ATCCGGGATCCATGGTGAGCAAGGGCGAG
oAglZ-1	ATCGGGAATTCGAGGCCAAGCTCCAGACG
oDmglA1	ATCGGGAATTCCATCGGAGCGTCGCCATG
oDmglA2	ATCGGTCTAGAAATCTTGCAGTTGATTTC
oDmglA3	ATCGGTCTAGAGCCGTGGCCAAGCTCGTC
oDmglA4	ATCGGAAGCTTGTTGAAGACCTCGAAGAG
omcherry-1	ATACGGATCCATGGTGAGCAAGGGCGAGGAG
omcherry-2	ATACAAGCTTTTACTTGTACAGCTCGTC
o6861fwd	ATCAAGCTTGCTCGCGACGAGGAGTAGGAAGTCC
o6861rev	ATCGGATCCGCCCATCGCCGCGGACACCGACACCTGG
o6861fwd-2	ACGTCTAGACCGCCCAAGGAGCTCACGACACGTCA
o6861rev-2	ACGGAATTCCCCTTGAAGGTGTTGGCCGTG
oMcherryfw	ATCGGATCCATGGTGAGCAAGGGCGAGGAGGAT
oMcherryrev	ATCTCTAGATTACTTGTACAGCTCGT
oMglArevEco	ATCAGAATTCTCAACCACCCTTCTTGAGCTCGGTGAG
oPilAfwdXba	ATCATCTAGAGCGGCGTTGAACGAGGGGACGCTGG
o2647fwdsfGFP	ATACTCTAGAGTGACCCCACCCACCTTGGGCAACACGA
o2647revsfGFP	ATACGGATCCATCCGCAGTTGCACGCGTGCGGTCCTC
oMglApilAfwd	ATCCGGGATCCATGTCCTTCATCAATTAC

oMglApilArev	ATACAAGCTTTCAACCACCCTTCTTGAGCT
oMglAR53Afwd	TCCACGGAGACGGACGCCACGCTCTTCTTC
oMglAR53Arev	GAAGAAGAGCGTGGCGTCCGTCTCCGTGGA
oMglAQ82Aforw	ACGGTGCCCGGTGCAGTCTTCTACGA
oMglAQ82Arev	GTCGTAGAAGACTGCACCGGGCACCGT
oYFP-9	ATCCGGGATCCCTTGTCCAACTCGTCCAC
oYFP	ATCGGAAGCTTCTACTTGTACAGCTCGTC
o6861DNfwd	AACCTCACGGCATTCATCAACCTGATGGCG
o6861DNrev	CGCCATCAGGTTGATGAATGCCGTGAGGTT
oABlocFwd	ACAAGCTTGCATGCCTGCAGATAAGCATGAATA
oABlocrev	ATGAATTCGAGCTCGGTACCCGGGGATCCTCTAGA
oMglB upst rev	ACTCTAGACTCGCTGAAGAGGTTGTCGAT
o6861 downst fwd	ACGTCTAGACCGCCCAAGGAGCTCACGACACGTCA
o6861 downst rev	ACGGAATTCCCCTTGAAGGTGTTGGCCGTG
o6861 fwd	ATCAAGCTTGCTCGCGACGAGGAGTAGGAAGTCC
o6861 rev	ATCGGATCCGCCCATCGCCGCGGACACCGACACCTGG
oMcherry fw	ATCGGATCCATGGTGAGCAAGGGCGAGGAGGAT
oMcherry rev	ATCTCTAGATTACTTGTACAGCTCGT
o1927fwdXba	ATACTCTAGATTGCAGCGGGAGGCCTTCGACC
mglA int PCR fwd	TGCGGGAAGACGACCAACCTTCAGT
mglA int PCR rev	ACGGCCTGGTACTCCGGGATGTTGC
oUpstr mglA	CCAAGGACGCGAACGCGAAG
oDown mglA	CGACACGCACGGTACGACCT
mglA FWD pilA	GATCACTCTAGAATGTCCTTCATCAATTACTCAT
mglA REV pilA	ATACAAGCTTTCAACCACCCTTCTTGAGCTCG
oMcherry fwd	ATACGGATCCATGGTGAGCAAGGGCGAGGAG
oMcherry rev	ATACAAGCTTTTACTTGTACAGCTCGTC
mglA int PCR fwd	TGCGGGAAGACGACCAACCTTCAGT
mglA int PCR rev	ACGGCCTGGTACTCCGGGATGTTGC
oAglZMXAN2992for	CAGCGTCCGCCTCGGCTCCA
oAglZdownrev	CCGCGGTGGCGGACGCTTGAG

Table 8. Primers used to verify integration at Mx8 phage attachment site and sequencing and general plasmid sequencing.

Name	Nucleotide sequence (5'-3')
attBright	GGAATGATCGGACCAGCTGAA
attBleft	CGGCACACTGAGGCCACATA
attPright	CGGCACACTGAGGCCACATA
attPleft	GGGAAGCTCTGGGTACGAA
M13 fwd	GTCGTGACTGGGAAAACCCTGGCG
M13 rev	CTGGGGTGCCTAATGAGTGAGCTA
GFy045	TTTACACTTTATGCTTCCGGCT
pSW105fwd	GGCTTGGAGTGCGCACCT
pSW105rev	ACGACGTTGTAAAACGAC

Table 9. List of plasmids used in this study.

Plasmid	Relevant characteristics	Source or reference
pET24 a(+)	Used for overproduction of C-terminal His6-tagged proteins in *E.coli*,T7 promoter, Kan^R	Novagen Merck Darmstadt
pET45 b(+)	Used for overproduction of N-terminal His6-tagged proteins in *E.coli*, T7 promoter, Amp^R	Novagen Merck Darmstadt
pBJ114	*galK* containing vector for double homologous recombination in *M.xanthus*, Kan^R	(Julien *et al.*, 2000)
pBJ113	*galK* containing vector for double homologous recombination in *M.xanthus*, Kan^R	(Julien *et al.*, 2000)
pSW105	Used for ectopic integraton at phage Mx8 *att* site, with expression from *pilA* promoter, Kan^R	(Jakovljevic *et al.*, 2008)
pBluescript II SK-	Used for cloning in *E. Coli*, blue-white seletion, Amp^R	Fermentas
pSWU30	Used for integraton at phage Mx8 *attB* site, Tet^R	(Wu and Kaiser, 1997)
pSW19	Used for integration at phage Mx8 *attB* site, Kan^R	(Julien *et al.*, 2000)
pSL73	pSW105 allowing expression of *yfp-mglA*^{Q82L}	This study
pSL60	pSW105 allowing expression of *yfp-mglA*$^{+}$	(Miertzschke *et al.*, 2011)

pTS10	pSW105 allowing expression of *yfp-mglA*^{Q82A}	(Miertzschke *et al.*, 2011)
pSL16	pBJ114 bearing deletion cassette for *mglA*	(Miertzschke *et al.*, 2011)
pSL61	pSW105 allowing expression of *yfp-mglA*^{G21V}	(Miertzschke *et al.*, 2011)
pEH42	pSW105 allowing expression of *yfp-mglA*^{R53A}	This study
pTS9	pBJ114 allowing expression of *yfp-mglA*^{Q82A} at native site	T. Schöner, BA Thesis 2010
pTS8	pBJ114 allowing expression of *mglA*^{Q82A} at native site	T. Schöner, BA Thesis 2010
pSC100	pSW105 allowing C-terminal sfGFP allowing	C. Freidreich, MPI Marburg
pFM1	pBJ113 bearing mr*eB*^{V323A} variant for native site integration	(Mauriello *et al.*, 2010b)
pZY2	pET24a(+) with His_6-*mglA*	(Zhang *et al.*, 2010)
pZY3	pET24a(+) bearing *mglA*^{Q82L} variant	(Zhang *et al.*, 2010)
pBJdAglQ	pBJ113 bearing in-frame deletion cassette for *aglQ*	(Sun *et al.*, 2011)
pSW19AglQD28N	pSW19 allowing expression of *aglQ*^{D28N} variant from native promoter	(Sun *et al.*, 2011)
pFM3	pET24a(+) bearing *mreB*-His_6 gene without the N-terminal amphipatic helix	This study
pEH48	pBluescript II SK- bearing *mCherry* gene and upstream homologous region of *aglQ*	This work
pEH51	pBJ114 allowing expression of *aglQ-mCherry* at native site	This work
pEH100	pSW105 allowing expression of *aglQ*^{D28N} from native and *yfp-mglA*^{Q82A} from *pilA* promoter	This work
pEH105	pSWU30 allowing expression of *pbp2-sfGFP* from *pilA* promoter	This work
pMB10	pBJ114 bearing *aglZ-mCherry* fusion for homologous integration at native site	M. Buhremster, BA Thesis 2010
pEH107	pBJ114 bearing *aglQ*^{D28N}*-mCherry* replacement of native gene	This work
pEH108	pSWU30 allowing expression of *yfp-mglA*^{Q82A} from *pilA* promoter, Tet^R	This work

5.3.2 General method for generating in-frame deletions

In frame deletions of genes in *M. xanthus* were generated in a two-step homologous recombination event, described in detail by Shi and colleagues (Shi *et al.*, 2008) and represented in Figure 27. Briefly, 500bp long fragments directly up- and down-stream of the target gene were amplified by PCR using A - B (upstream) and C - D (downstream) primers pairs. Primers B and C were designed to possess complementary ends which allow fusing AB and CD fragments in a subsequent PCR reaction using A and D primers. The final AD fragment was cloned into pBJ114/3 vector's compatible restriction sites, and further sequenced with M13 primers prior to electroporation in *M. xanthus*. The plasmids pBJ114/3 confers Kan resistance to the cells once integrated in the chromosome up- or downstream of the gene of interest via homologous recombination. To obtain markarless in-frame deletion, a second round of homologous recombination was induced by adding galactose to the media in which cells were grown, as the pBJ plasmids contain a counter-selection marker gene *galK* (galactokinase-encoding gene originating from *E. coli*). The product of *galK* phosphorylates galactose in the cells, whose high levels can become toxic to *M. xanthus* cells. This results in cells excising (looping-out) the plasmid in order to stay viable. After having looped-out the pBJ plasmid, some transformants will contain the in-frame deletion and some the wildtype genomic situation. To initiate second round of homologous recombination, cells containing Kan resistant pBJ plasmid insertions were grown in liquid CTT medium without antibiotic to OD_{550}=0.5-0.7, and different aliquots of cultures were plated on CTT media containing 3% galactose (w/v). Transformants obtained from those plates were selected and transferred to a CTT and CTT Kan containing agar plates, in parallel. Colonies which were unable to grow on CTT Kan were used to verify correct in-frame deletions by PCR.

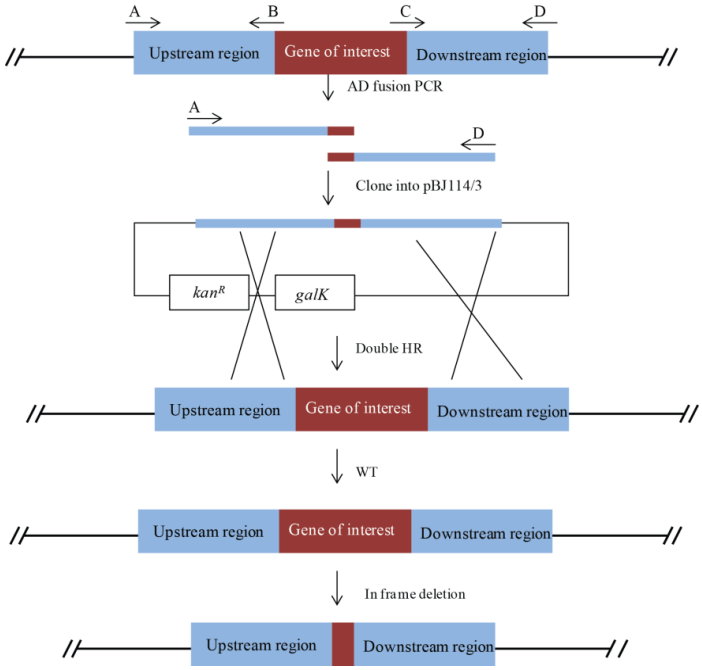

Figure 43. Schematic representation of in-frame deletion method in *M. xanthus*

5.3.3 Generating point mutations in genes of interest

All point mutations constructed in this study were made by using chromosomal wildtype DNA as a template for PCR reactions. To create the desired nucleotide substitution, the overlapping primers carrying a mutation of interest were used in one PCR reaction. Plasmids integrating at native sites to replace wildtype genes additionally had upstream and downstream regions of the gene cloned in the plasmid, to allow integration and loop-out steps (described in detail in the section above). Genes encoding *mCherry*, *yfp* or *sf-gfp* were cloned at the C or N-terminus where needed. Plasmids integrating at *attB* site were carrying *PpilA* or native promoters, as described in detail in the section below.

5.3.4 Constructions of plasmids in *E. coli* and their subsequent use in *M. xanthus*

Plasmids were propagated in *E. coli* TOP10 (F^-, *mcrA*, Δ(*mrr-hsd*RMS-*mcr*BC), φ80*lac*ZΔM15, Δ*lac*X74, *deo*R, *rec*A1, *ara*D139, Δ(*ara-leu*)7679, *gal*U, *gal*K, *rps*L, *end*A1, *nup*G) unless otherwise stated. Primers used are listed in Table SII. All DNA fragments generated by PCR were verified by sequencing. DK1622 was used as the wild type *M. xanthus* strain throughout the study. All strains constructed were confirmed by PCR. Strains containing plasmids were constructed by electroporation of the plasmid into the relevant strain. Plasmids were integrated by site-specific

recombination at the Mx8 *attB* site or in the native site on the chromosome by homologous recombination. Constructs cloned in pSW105 and pSWU30 plasmids for *attB* site integration are under P*pilA* promoter, unless otherwise stated. The construction of pSL16 plasmid using oDmglA1, oDmglA2, oDmglA3 and oDmglA4 primers for *mglA* deletion was previously described by (Miertzschke *et al.*, 2011).The construction of pSL60 and pSL61 plasmids was described previously (Leonardy *et al.*, 2010). The plasmid pEH42 and pTS10 were constructed by replacing the *BamHI HindIII* sequence in pSL60 by a mutated form of MglA, leaving the N-terminal YFP-linker fusion as originally constructed. The MglA point mutations were constructed by using nested PCR, whereby two products of separate PCR reactions were fused in a third PCR which results in a point mutation using primers containing homologouss regions. To obtain the pEH42 plasmid, *mglA*^{R53A} point mutation was constructed with primers oMglApilArev and oMglAR53Afwd in one reaction and oMglApilAfwd and oMglAR53Arev in the second reaction using wildtype chromosomal DNA.These two products were then used as template for the PCR using oMglApilAfwd (*BamHI)* and oMglApilArev(*HindIII)* primers which amplify the mutated *mglA* gene. The same procedure was done for constructing the pTS10 plasmid, where oMglAQ82Aforw and oMglAQ82Arev primers were used in a PCR reaction to construct the desired point mutation, which was then cloned into the *BamHI HindIII* sites of the pSL60 backbone.

To construct the strain SA4420, an in-frame deletion of *mglA* was constructed by electroporation of the pSL16 plasmid in DK1622 strain. The plasmid integration was confirmed to be upstream of *mglA*, and the plasmid was looped-out downstream of the gene of interest, by counter-seletion on the galactose containing CTT. The strains SA4440, SA4451, SA4455 SA3289 were constructed by integrating pSL60, pSL61, pEH42 and pTS10 complementation plasmids into the attachment site of the SA4420 strain, respectively. The strains SA3385, SA3823, SA4449 and SA3831 were constructed by integrating the pSL60, pSL61, pEH42 and pTS10 into the attachment site of the DK6204 strain, respectively.

The pSL16 plasmid was used to create the in-frame deletion of mglA gene in the following strain backgrounds: Δ*aglZ,* Δ*aglQ,* Δ*agmK(gltI),* Δ*agmX(gltJ),* Δ*aglZfrzE::tn5Ω226, aglQ-mCherry*, *aglZ::aglZ-mCherry* and *mreB*^{V323A} backgrounds. Δ*agmK(gltI),* Δ*agmX(gltJ)* single deletion strains were provided by D. Keilberg, (unpublished data) and Δ*aglZ* was constructed and provided by the Hartzell lab, U Idaho (Yang *et al.*, 2004). (Yang *et al.*, 2004). Construction of frzE::tn5Ω226 in

DK1622 wildtype and Δ*aglZ* backgrounds was done by electroporation of chromosomal DNA from DZF3377 strain carrying a transposon inserted in *frzE* gene (Ω226, tet^R) (Sun *et al.*, 2011). Construction of pBJ113-$MreB^{V323A}$ plasmid for native site replacement of *mreB* gene was previously described and provided by Mignot Lab, CNRS Marseille (Mauriello *et al.*, 2010b). Constructions of pBJdAglQ plasmid and $aglQ^{D28N}$ variant were previously detailed in work by (Sun *et al.*, 2011) and provided by Mignot Lab, CNRS Marseille. Construction of pET24a(+) His_6-tagged wildtype and $mglA^{Q82L}$ and mreB-His_6 without the amphipatic N-terminal helix for over-expression were previously described by (Zhang *et al.*, 2010), (Mauriello *et al.*, 2010b) and plasmids were provided by Franco Lab CNRS Sophia Antipolis and /or Mignot Lab, CNRS Marseille.

Generation of pEH51 plasmid involved a series of following cloning steps: first, upstream homologous region of *aglQ* was constructed using a PCR with o6861fwd and o6861rev primers. This product was cloned into *HindIII/BamHI* site of pBluescript II SK- vector to which a PCR product of *mCherry* gene using oMcherryfw and oMcherryrev was added in order to generate pEH48 plasmid. The downstream homologous region of *aglQ* was made using a PCR with o6861fwd-1 and o6861rev-1 primers and this product was inserted into pEH48. To generate pEH51 sequences from pEH48 containing upstream and downstream homologues regions to *aglQ*, and *mCherry* gene were cut using *HindIII/EcoRI* and ligated into pBJ114 vector background to allow native *aglQ* replacement by the tagged version. To generate pBM10 plasmid, a PCR reaction using oMcherry-1 and o-Mcherry-2 primers yielded *mCherry* gene to replace *yfp* at *BamHI/HindIII* sites in previously described pSL65 plasmid containing *aglZ* (Leonardy *et al.*, 2010). To generate pEH100, first $aglQ^{D28N}$ variant and its native promoter were cut from pSW19AglQD28N plasmid using *BamHI/HindIII* restriction enzymes. Second, *yfp-*$mglA^{Q82A}$ under *pilA* promoter was generated by PCR using oPilAfwdXba and omglArevEco primers using pTS10 as a template. This product was ligated into pSWU30 *NdeI/EcoRI* site, and the digested $aglQ^{D28N}$ variant with native promoter was added into *BamHI/HindIII* sites to generate a final pEH100 plasmid. To generate pEH105, *pbp2(mxan2647)* full-length was generated by PCR using wildtype chromosomal DNA with o2647fwdsfGFP and o2647revsfGFP primers. This product was digested with *XbaI/BamHI* and ligated into pSWU30 plasmid containing *pilA* promoter and C-terminal *sfGFP* gene (pSC100, unpublished plasmid). To obtain the

pSL73 plasmid, *mglA*^{Q82L} point mutation was constructed with primers oMglApilArev and oMglAQ82Lforw in one reaction and oMglApilAfwd and oMglAQ82Lrev in the second reaction using wildtype chromosomal DNA.These two products were then used as template for the PCR using oMglApilAfwd and oMglApilArev primers which amplify the mutated *mglA* gene. To construct pEH107 *aglQ*^{D28N}*-mCherry* gene variant was amplified from pSWU19D28NC plasmid (Sun *et al.,* 2011) together with its native promoter using o6861fwd and oMcherryrev primers. The PCR product was digested with *XbaI/HindIII* and cloned into pEH51 background where *aglQ-mcherry* was cut out by *XbaI/HindIII and replaced* by the *aglQ*^{D28N}*-mCherry* variant. This plasmid was used to allow integration into wildtype and Δ*mglA* backgrounds. To construct pEH108 plasmid, the P$_{pilA}$*-yfp-mglA*^{Q82A} was amplified in a PCR reaction using oMglArevEco and oPilaXbaFwd primers. This product was digested with *XbaI/EcoRI* and ligated into pSWU30 plasmid with tetracycline resistance. To construct pEH107 aglQD28Ngene variant was amplified from pSWU19D28NC plasmid (Sun et al 2011) together with its native promoter. The PCR product was digested with BamHI/HindIII and cloned into pBJ114 to allow integration into M. xanthus genome. Replacement of wildtype aglQ with aglQD2N8-mCherry was done in wildtype and ΔmglA backgrounds.

5.3.5 DNA preparation from *E. coli* and *M. xanthus* cells

E. coli plasmid DNA was isolated using QIAprep Spin Miniprep (Quiagen) or Macherey Nagel Nucleo Spin (Oensingen) kit. Chromosomal DNA from *M. xanthus* was isolated using MasterPure DNA kit (Epicenter) following the instructions from the manufacturer. Crude DNA preparation from cell extracts for check PCRs was done by boiling samples for 5 minutes in 30 µl water, followed by quick centrifugation of the cell debris.

5.3.6 Polymerize chain reaction (PCR)

Amplification of DNA sequences using PCR reactions was done in 50 µl volume reactions using PfuUltraII polymerase (Stratagene) or Buffer J (Epicentre). The PCR reaction mix includes the following:

Genomic or plasmid DNA	1 µl (final concentration 50-100ng)
10 µM Primer (each)	1 µl
dNTPs (10mM)	1 µl

10x PfuII Ultra buffer	5 µl
DMSO	5 µl
PfuUltraII Polymerase	0.5 µl
H_2O deionized	36.5 µl

Alternatively Bufer J (Epicentre) containing dNTPs was used instead of 10x PfuII Ultra buffer.

To check for correct plasmid integration, gene deletions or mutations at native site colony PCRs were performed in 20 µl volume reactions using the following:

Crude genomic DNA	2 µl
10 µM Primer (each)	1 µl
Eppendorf Master Mix	8 µl
DMSO	2 µl
H2O deionized	7 µl

The PCR programs used in this study are represented in Table 9. Conditions for specific PCR reactions were modified according to type of DNA polymerase used, predicted primer annealing temperatures and expected product sizes.

Table 9. PCR programs used in this study.

Step	Temperature	Time
Standard / Check PCR program		
Initial denaturation	94°C	3 min
Denaturation cycles	94°C	30 sec x 30
Primer annealing[1] cycles	5°C below predicted Tm	30 sec x 30
Elongation cycles	72°C	30 sec x 30
Final elongation	72°C	5 min
Hold	4°C	
Touch down PCR		

Initial denaturation Denaturation Primer annealing Elongation	94°C 94°C 68°C 72°C	3 min 30 sec x 9 cycles 30 sec x 9 cycles 30 sec x 9 cycles
Denaturation Primer annealing Elongation	94°C 60°C 72°C	30 sec x 9 cycles 30 sec x 9 cycles 30 sec x 9 cycles
Denaturation Primer annealing Elongation Final elongation Hold	94°C 55°C 72°C 72°C 4°C	30 sec x 20 cycles 30 sec x 20 cycles 30 sec x 20 cycles 5 min

[1] Primer annealing temperature for check PCRs used with standard primers was 55°C.

5.3.7 Agarose gel electrophoresis

All PCR products were checked for correct sizes by mixing with 5x loading buffer (Bioline), and running gel electrophoresis at 120 V in 1% agarose in TAE buffer. Ethidium bromide was added to agarose at a final concentration of 0.01% (v/v). Agarose gels were imaged using 2UV transilluminator (UVP-Bio-Doc-It-System, UniEquip) at 365 nm.

5.3.8 Restriction and ligation of DNA fragments

Restriction digests on plasmid or linear DNA was done for 2 hours according to the specific requirements for the enzyme used. Restricted DNA was purified with DNA Clean&Concentrator-5 kit (ZymoResearch Hiss Diagnostics), or from an agarose gel where multiple fragments had to be separated prior to purification.

Ligation reactions were performed using T4 DNA ligase, in a reaction which contained appropriate vector and 3x more in molar excess of the corresponding insert DNA. Ligations were done at room temperature for 1 hour, followed by enzyme heat inactivation at 65°C for 20 min.

5.3.9 Preparation of chemically- and electro-competent *E. coli* cells

To prepare chemically- and / or electro-competent *E. coli* cells, overnight cultures were diluted 1:200 in 1L LB medium. At OD_{600}=0.5 cells were harvested by centrifugation at 4700 rmp for 20 min at 4°C. To proceed with making cells chemically

competent, cells were resuspended and washed in 200 ml of 50 mM $CaCl_2$, twice. The washing steps were repeated in 100 and 50 ml volumes of 50 mM $CaCl_2$, and finally the pellet was resuspended in 20 ml 50 mM $CaCl_2$ and 10% Glycerol. To make cells electro-competent, after harvesting cell pellet was washed in 500 ml ice cold sterile 10% glycerol, twice. The washing steps were repeated in 100 and 50 ml volumes of ice cold 10% glycerol, and finally the cell pellet was resuspended in 2 ml sterile 10% glycerol. Cells were snap frozen in 50 µl aliquots and kept at the -80°C.

5.3.10 Transformation of chemically- and electro-competent *E. coli* cells

For transformation of chemically competent cells, 10 µl of ligation reaction or plasmid DNA (previously dialyzed against sterile water on a VSWP Milipore membrane for 30 min) was transferred to an aliquot of competent cells, on ice. Cells and DNA were incubated on ice for 20 min and then heat shocked at 42°C for 1 min 30 sec. Next, cells were incubated on ice for 5 min, after which 1 ml LB medium was added for a subsequent 1 hour recovery at 37°C, 230 rpm shaking. After 1 hour incubation cells were centrifuged at 5000 rpm for 1 min and 100 µl cell suspension was plated on LB agar plate containing appropriate antibiotic.

To transform electro-competent cells, 10 µl of ligation reaction or plasmid DNA (previously dialyzed against sterile water on a VSWP Milipore membrane for 30 min) was transferred to an aliquot of competent cells, on ice. The mixture was transferred into an electroporation cuvette (Bio-Rad, Munich) and pulsed with 25 µF, 1.8 kV, and 200 Ω, immediately after which 1 ml of LB medium was added for cells recovery, and cells were transferred to 37°C, 230 rpm for 1 hour. After 1 hour incubation cells were centrifuged at 5000 rpm for 1 min and 100 µl cell suspension was plated on LB agar plate containing appropriate antibiotic.

After incubating transformed *E. coli* cells at 37°C over-night, single colonies were transferred onto fresh plates, and correct clones were checked by check digestion reaction followed by electrophoresis gel, and finally sequencing of the DNA fragments of expected sizes.

5.3.11 Sequencing of DNA

Sequencing of purified plasmids or PCR products was sent to Eurofins MWG Operon according to company's instructions. Primers used for sequencing were either standard primers synthesized and kept at the company, or aliquots of the primers used in

this study were sent to the company. Sequences received were aligned using Vector NTI 11 (Invitrogen) software.

5.4 Microscopy methods

5.4.1 Live imaging of cells on agar surface

For assaying cell motility and protein localizations in the cell, exponentially growing cultures of *M. xanthus* were grown to OD_{550} = 0.5-0.8 in liquid CTT medium at 32°C. Next, 5-10 µl of cells were transferred to a microscope slide containing 1% agar in A50 buffer (Table 3), immediately covered with a cover slip and left for 15 min at room temperature to attach to the surface. Images were captured using the automated and inverted epifluorescence microscopes TE2000-E-PFS (Nikon, France) (Ducret *et al.*, 2009) or Leica DM6000B (Bulyha *et al.*, 2013) and / or the upright DM IRE2 light microscope (Leonardy *et al.*, 2010). For time lapse recordings, snap shots were taken every 1 min, unless otherwise stated. All images were captured using Metamorph v 7.5 (Molecular Devices) software.

For each experiment, stacks of images were first normalized to correct for background fluctuations over time or over different fields. If required, the background intensity of phase contrast images was subtracted to optimize auto-thresholding operations. Cells boundary were detected using a specifically developed plug-in for ImageJ. Briefly, cells were detected using an auto-thresholding function and sub-pixel resolution refined cell contours were obtained using a cubic spline fitting algorithm. Cells were tracked over the time an optimized nearest-neighbor linking algorithm. From cells trajectories, the distance between two temporal points, the cumulated distance and the distance from the origin were extracted and used to compute the average speed. For each condition tested, the average speed of at least 40 individual cell trajectory was calculated. Cell velocities and automated analyses of fluorescence were performed by Prof. T. Mignot and Dr. A. Ducret, CNRS Marseille.

For fluorescent microscopy, GFP, YFP or mCherry/TxR filters were used for checking fluorescent protein localizations in the cell. The analyses of fluorescently tagged proteins were done using Metamorph v7.5 or Image J 1.4.

To determine the exact position of PBP2-sfGFP clusters in the cells, time lapse recordings were done every 30 seconds for 6 min. For each cluster, x and y coordinates were collected for every time point, with the long axis of the cell corresponding to 0°.

Calculations of PBP2-sfGFP cluster velocities, angles and mean square displacements were performed by Prof. P. Lenz, Philipps University, Marburg, and the data on velocities and mean square displacements combined in histograms was done by Dr. A. Treuner-Lange, MPI Marburg.

5.4.2 Live imaging of cells on chitosan coated chambers

Apart from using 1% agar (in A50 buffer) containing surface on glass slides for microscopy analyses, chitosan-coated chambers are preferred surfaces on which *M. xanthus* cells move by gliding (Ducret *et al.*, 2009). The later surface was used as preferred apparatus for injection and reversible effects experiments. Briefly, 1 ml of the freshly prepared chitosan solution (chitosan from shrimp, Sigma) 15 mg/ml in 2 M acetid acid was carefully injected in the custom made silicone microscopic chamber. After 30 min, the unattached chitosan was rinsed with 1 ml of water and second with 1 ml of TPM buffer (10 mM Tris-HCl, 1 mM KH_2PO_4, pH 7.6, 8 mM $MgSO_4$). Next, 1 ml of cells grown to OD_{550} = 0.5-0.8 were briefly centrifuged and the cell pellet was resuspended in 500 µl of TPM buffer; the cell suspension was injected in the chitosan-coated chamber and cells were left to attach at room temperature. After 30 min incubation, unattached cells were rinsed off with TPM buffer and the cells were visualized using TE2000-E-PFS (Nikon, France) using appropriate filters every 30 sec.

5.4.3 Drug injection experiments and time-lapse recordings

To test immediate effects of A22 MreB perturbing compound (Calbiochem Merck Milipore) and nigericin (Sigma Aldrich) on cells harboring fluorescently labeled MglA and AglQ proteins, both drugs (prepared within 2 weeks from the date of experiment) were injected individually at concentrations previously determined to block gliding motility within minutes of their addition. 10 µg/ml A22 was manually injected 5 minutes post starting the time-lapse movie. When the cells stopped gliding, 1.5 ml TPM buffer was manually injected to rinse the antibiotic from the chamber, and the reversibility of the blocking gliding effect would be scored by recording the time-lapse for 15-20 additional minutes.

To test the effects of mecillinam, phosphomycin, cefsulodin, cefoxitin, vancomycin, chloramphenicol, cephalexin, piperacillin, moenomycin and aztreonam (Sigma Aldrich), on gliding motility, minimal inhibitory concentrations specific for each drug were added to 1% agar-containing A-50 buffered pad on a microscope slide. Next, 1 ml of exponentially growing *M. xanthus* cells was shortly mixed with the same

concentration of the specific drug, and 5-10 µl of the cell suspension was transferred onto the microscope slide. 10-20 min long time-lapse recordings taken every one minute with appropriate filters were done after 10-15 min of cells' incubation on the agar pad containing the drug, at room temperature. The effects of A22, phosphomycin, mecillinam, cephalexin, chloramphenicol, vancomycin, cefsulodin and cefoxitin on PBP2-sfGFP localization and dynamics were assayed using the A50 buffered 1% agar mixed with drug method with 5-10 min long time-lapse.

5.4.4 Immunofluorescence microscopy and data analyses

Immunofluorescence microscopy was done according to the previously protocol described (Mignot *et al.*, 2005). In short, *M. xanthus* cells were grown to a 7×10^8 density, and 500 µl cell suspension was either treated with 10 µg/ml A22 for 10 and 20 minutes, or directly fixed, as follows: 10 µl of cells previously fixed with 1.6% paraformaldehyde and 0.008% glutaraledehyde were spotted on freshly coated poly-L-lysine 12well slides (Thermo Scientific). Fixed cells were then permeabilzed with GTE buffer (50 mM glucose, 20 mM Tris, 10mM EDTA, pH 7.5) for 5 min, and probed with 1:200 dilution of anti-MreB polyclonal antibodies in PBS buffer (137 mM NaCl, 2.7 mM KCl, 10 mM Na_2HPO_4, 1.8 mM KH_2PO_4, pH 7.4) supplemented with 2% BSA, at 4°C overnight. Next, secondary DyLight 549-conjugated goat anti-rabbit antibodies (Pierce Thermo Scientific) were added for 1 hour at room temperature, and lastly, SlowFade Antifade reagent (Invitrogen) was added.

Images were captured using Leica DM6000B upright light microscope with Leica Plan Apo 100x 1.40 phase contrast oil objective, and fluorescently tagged MglA protein was visualized using a Leica YFP filter where appropriate**.**

5.4.5 Transmission electron microscopy

Purified MreB protein incubated at different conditions was analyzed for formation of structures under a JEOL 1400 transmission electron microscope equipped with a Morada Olympus CCD camera, by Dr. S. Lacas-Gervais Universite de Nice, Nice, France. Briefly, MreB-His_6 protein (105 µM) was incubated at 4°C or 37°C for 30 minutes in G-buffer (40 mM HEPES, 300 mM KCl, 2 mM $MglCl_2$, 1 mM DTT, pH 7.7) containing 2 mM ATP. Next, 5 µl of the reaction was put on carbon-coated copper electron microscopic grids. Excess liquid was blotted off, and then stained with 2% uranylacetate solution for a few seconds.

5.5 Biochemical methods

5.5.1 Overexpression and purification of MreB, MglA and MglA^{Q82L} proteins

Detailed protocol for over-expression and purification of MglA His_6-tagged proteins was previously described (Zhang *et al.*, 2010), and followed in our study. All three proteins, MglA-His_6, MglA^{Q82L}-His_6, and MreB-His_6 were expressed from a pET28a vector (Novagen), in BL21DE Expression of all three of the recombinant proteins was induced by growing cells at room temperature for 20 hours in presence of 0.5 mM IPTG (isopropyl-h-d-thiogalacto-pyranoside). Cells containing MglA-His_6 and MglA^{Q82L}-His_6 were harvested by centrifugation at 8000 rpm for 10 min, resuspended in a buffer containing 50 mM NaH_2PO_4 pH 8.0, 300 mM NaCl, 10 mM imidazole, and lysed with French press. Note that only in the lysis, purification and elution buffers of MglA-His_6 protein, GDP nucleotides to a final concentration of 30 µM were added. Supernatants were incubated with Nickel beads (Biorad) for 2 hours at 4° C, after which beads were collected and loaded into 5 ml HisTrapTM column (GE Healthcare). Proteins were eluted using a buffer containing 50 mM NaH_2PO_4 pH 8.0, 300 mM NaCl, 250 mM imidazole, and 30 µM GDP for MglA-His_6.

C41 (DE3) (Miroux and Walker, 1996) cells containing plasmid expressing MreB-His_6 were lysed in TrisHCl 20 mM, pH 7.4, NaCl 300 mM, $MgCl_2$ 1 mM, 0.1% CHAPS, Imidazole 10 mM, protease inhibitor tablet (Roche), and PMSF 0.25 mM, and lysed with French press. Cell lysates were centrifuged twice (8000 rpm, 4° C, 30 min) to remove debris prior to purification. Supernatant was incubated with Nickel beads (Biorad) for 2 hours at 4° C, after which beads were collected and loaded into 5 ml HisTrapTM column (GE Healthcare). Elution was performed using a buffer containing 20 mM TrisHCl, 300 mM NaCl, 1 mM $MgCl_2$, 0.25 mM PMSF, pH 7.4 and increasing concentrations of imidazole from 100 to 250 mM Imidazole. All protein purities, stabilities and quantifications were analyzed using SDS-PAGE and Bradford assay.

5.5.2 Determining protein concentration

To determine protein concentration the Bio-Rad protein kit (Munich) was used following the instructions of the manufacturer. In short, 20 µl of the sample was added to 980 µl of the 1:15 dilution of the Bradford solution and incubated at room temperature in the dark, 10 min. In parallel, BSA (bovine serum albumin) was used as a protein standard for standard curve preparation. Next, absorbance at 595 nm was

measured with Ultrospec 2100 pro spectrophotometer (Amersham Biosciences), and based on the values from the standard curve slope, the protein concentrations for proteins of interest were determined.

5.5.3 SDS polyacrylamide gel electrophoresis (SDS-PAGE)

Proteins were separated under denaturing conditions with 12% or 14% gels using the SDS-PAGE (Laemmli, 1970) method. First, samples were mixed with 5x loading buffer (50% (v/v) glycerol, 250 mM Tris-HCl pH 6.8, 10 mM EDTA, 10% (w/v) SDS, 0.5 M DTT, 1% (w/v) bromphenol blue) and heated at 95˚C for 5 min, quickly spun and loaded on the gel. Gel electrophoresis was carried out in Bio-Rad electrophoresis chambers (Bio Rad, Munich) at 120-150 V in 1X Trish Glycine SDS buffer (Bio Rad, Munich). Prestained protein markers from Fermentas (St Leon-Rot) were used to estimate the protein sizes. Proteins were visualized by staining for 30 min at room temperature in Coomassie brilliant blue (Sambrook and Russell, 2001).

5.5.4 Immunoblot analyses

For immunoblot / Western analyses, the earlier described standard protocol was followed (Sambrook and Russell, 2001). Proteins of approximately 5 - 15 µg were loaded per lane of SDS-PAGE, and proteins were transferred to nitrocellulose membrane using Hoefer TE77 semi-dry blotting system (Amersham Biosciences, Munich) with a constant current of 0.8 mA/cm^2. Transfer buffers are listed in Table 10. After transfer was complete, the nitrocellulose membranes were blocked in 1x TTBS buffer (0.05% (v/v) Tween 20, 20 mM TrisHCl, 137 mM NaCl pH 7) supplemented with 5% (w/v) non-fat milk powder, at 4˚C, overnight. Next, membranes were incubated with a specific dilution of primary antibody (1:1000 anti-MglA, 1:300 anti-MreB, 1:500 anti-GFP) in 1xTTBS buffer containing 2% (w/v) non-fat milk powder, for 2-6 hours at 4˚C. MreB antibodies were provided by Dr. P. Higgs, MPI Marburg. Then, membranes were washed 2 x 5 min in 1xTTBS buffer, and lastly, incubated for 1 hour at 4˚C with 1:15000 dilution of secondary anti-rabbit IgG, or secondary anti-mouse IgG horseradish peroxide coupled antibodies (Pierce/Thermo Scientific). To visualize proteins of interest coupled to antibodies, secondary antibodies were washed twice in 1xTTBS buffer, and the chemiluminescent substrate was incubated on the membrane for 1 min prior to exposure on the luminescent analyzer LAS-4000 (Fujifilm).

Table 10. Transfer buffers for immunoblot analyses.

Membrane (anode side)		Gel (cathode side)	
Chemical / 1 L H_20	Final concentration	Chemical / 1 L H_20	Final concentration
3.03 g Tris	25 mM	6.06 g Tris	50 mM
14.4 g Glycine	192 mM	28.8 g Glycine	384 mM
0.1g SDS	0.01 %	2 g SDS	0.2%
250 ml methanol	25%	100 ml methanol	10%

5.5.5 Polymerization and sedimentation assays

Purified pre-spun *M. xanthus* MreB-His_6 at a final concentration of 5 µM was polymerized in presence of HEPES 40 mM, pH 7.7, KCl 300mM, $MglCl_2$ 2mM , ATP (or ADP, GDP, GTP) at 2mM final concentration, and DTT 1mM at 37° C for 1 hour. The reactions were centrifuged in a TLA100.1 rotor (Beckman) at 70 000g for 15 minutes, 4° C. The supernatant and pellet were separated for analyses and separately mixed with equal amounts of SDS loading buffer. Equivalent amounts of the total reaction, supernatants and pellets were analyzed on a 14% SDS-polyacrylamide gel, which was stained with Coomassie Blue G250.

5.5.6 Nucleotide exchange

MglA-His_6 and $MglA^{Q82L}$-His_6 proteins at 2 µM final concentrations were pre-charged with GDP/GTP in a buffer containing HEPES 160mM, KCl 300mM, $MglCl_2$ 2mM, pH 7.7, and GDP or GTP at 1mM for 30 minutes at 20 °C.

5.5.7 *In vitro* interactions of purified proteins

MreB-His_6 (5 µM) was polymerized as described above, and then incubated with MglA-His_6 or $MglA^{Q82L}$-His_6 (2 µM) pre-charged with GDP or GTP, as described in the 5.5.6 section. The reaction was incubated for 30 min at 20 °C and the sedimentation assay performed as described in 5.5.5 section.

5.5.8 Bioinformatics analyses

Gene and protein sequences were obtained from a microbial genomes resource TIGR (http://cmr.jcvi.org/tigr-scripts/CMR/CmrHomePage.cgi); analyses were performed using BlastN, BlasP and psiBlastp algorithms from the NCBI (http://blast.ncbi.nlm.nih.gov/Blast.cgi) or SMART algorithm from EMBL

(http://smart.embl-heidelberg.de). Selected sequences were aligned and analyzed using Vector NTI Advance 11 (Invitrogen).

6 References

Abercrombie , M., Heaysman, J.E., and Pegrum, S.M. (1970). Locomotion of Fibroblasts in Culture .1. Movements of Leading Edge. Experimental Cell Research *59*, 393.

Abercrombie, M., Heaysman, J.E., and Pegrum, S.M. (1971). The locomotion of fibroblasts in culture. IV. Electron microscopy of the leading lamella. Exp Cell Res *67*, 359-367.

Arnold, J.W., and Shimkets, L.J. (1988). Cell-Surface Properties Correlated with Cohesion in *Myxococcus xanthus*. Journal of Bacteriology *170*, 5771-5777.

Ataide, S.F., Schmitz, N., Shen, K.A., Ke, A.L., Shan, S.O., Doudna, J.A., and Ban, N.N. (2011). The Crystal Structure of the Signal Recognition Particle in Complex with Its Receptor. Science *331*, 881-886.

Ausmees, N., Kuhn, J.R., and Jacobs-Wagner, C. (2003). The bacterial cytoskeleton: an intermediate filament-like function in cell shape. Cell *115*, 705-713.

Balaban, M., Joslin, S.N., and Hendrixson, D.R. (2009). FlhF and Its GTPase Activity Are Required for Distinct Processes in Flagellar Gene Regulation and Biosynthesis in *Campylobacter jejuni*. Journal of Bacteriology *191*, 6602-6611.

Balaban, N.Q., Schwarz, U.S., Riveline, D., Goichberg, P., Tzur, G., Sabanay, I., Mahalu, D., Safran, S., Bershadsky, A., Addadi, L., *et al.* (2001). Force and focal adhesion assembly: a close relationship studied using elastic micropatterned substrates. Nature Cell Biology *3*, 466-472.

Bange, G., Petzold, G., Wild, K., Parlitz, R.O., and Sinning, I. (2007). The crystal structure of the third signal-recognition particle GTPase FlhF reveals a homodimer with bound GTP. Proceedings of the National Academy of Sciences of the United States of America *104*, 13621-13625.

Baum, J., Papenfuss, A.T., Baum, B., Speed, T.P., and Cowman, A.F. (2006). Regulation of apicomplexan actin-based motility. Nature Reviews Microbiology *4*, 621-628.

Bean, G.J., Fllckinger, S.T., Westler, W.M., McCully, M.E., Sept, D., Weibel, D.B., and Amann, K.J. (2009). A22 Disrupts the Bacterial Actin Cytoskeleton by Directly Binding and Inducing a Low-Affinity State in MreB. Biochemistry *48*, 4852-4857.
Berg, H.C., and Anderson, R.A. (1973). Bacteria Swim by Rotating Their Flagellar Filaments. Nature *245*, 380-382.

Bergman, L.W., Kaiser, K., Fujioka, H., Coppens, I., Daly, T.M., Fox, S., Matuschewski, K., Nussenzweig, V., and Kappe, S.H.I. (2003). Myosin A tail domain interacting protein (MTIP) localizes to the inner membrane complex of Plasmodium sporozoites. Journal of Cell Science *116*, 39-49.

Bershadsky, A.D., and Kozlov, M.M. (2011). Crawling cell locomotion revisited. Proceedings of the National Academy of Sciences of the United States of America *108*, 20275-20276.

Bi, E., Dai, K., Subbarao, S., Beall, B., and Lutkenhaus, J. (1991). FtsZ and cell division. Res Microbiol *142*, 249-252.

Bigelow, D.M., Olsen, M.W., and Gilbertson, R.L. (2005). Labyrinthula terrestris sp nov., a new pathogen of turf grass. Mycologia *97*, 185-190.

Blackhart, B.D., and Zusman, D.R. (1985). Frizzy Genes of *Myxococcus xanthus* Are Involved in Control of Frequency of Reversal of Gliding Motility. Proceedings of the National Academy of Sciences of the United States of America *82*, 8767-8770.

Blair, D.F., and Berg, H.C. (1990). The MotA protein of *E. coli* is a proton-conducting component of the flagellar motor. Cell *60*, 439-449.

Block, J., Stradal, T.E.B., Hanisch, J., Geffers, R., Kostler, S.A., Urban, E., Small, J.V., Rottner, K., and Faix, J. (2008). Filopodia formation induced by active mDia2/Drf3. Journal of Microscopy-Oxford *231*, 506-517.

Bowden, M.G., and Kaplan, H.B. (1998). The *Myxococcus xanthus* lipopolysaccharide O-antigen is required for social motility and multicellular development. Molecular Microbiology *30*, 275-284.

Bowman, G.R., Comolli, L.R., Zhu, J., Eckart, M., Koenig, M., Downing, K.H., Moerner, W.E., Earnest, T., and Shapiro, L. (2008). A polymeric protein anchors the chromosomal origin/ParB complex at a bacterial cell pole. Cell *134*, 945-955.

Brown, E.D. (2005). Conserved P-loop GTPases of unknown function in bacteria: an emerging and vital ensemble in bacterial physiology. Biochem Cell Biol *83*, 738-746.

Bulyha, I., Hot, E., Huntley, S., and Sogaard-Andersen, L. (2011). GTPases in bacterial cell polarity and signalling. Current Opinion in Microbiology *14*, 726-733.

Bulyha, I., Lindow, S., Lin, L., Bolte, K., Wuichet, K., Kahnt, J., van der Does, C., Thanbichler, M., and Sogaard-Andersen, L. (2013). Two small GTPases act in concert with the bactofilin cytoskeleton to regulate dynamic bacterial cell polarity. Dev Cell *25*, 119-131.

Bulyha, I., Schmidt, C., Lenz, P., Jakovljevic, V., Hone, A., Maier, B., Hoppert, M., and Sogaard-Andersen, L. (2009). Regulation of the type IV pili molecular machine by dynamic localization of two motor proteins. Molecular Microbiology *74*, 691-706.

Burchard, R.P. (1982). Trail following by gliding bacteria. J Bacteriol *152*, 495-501.

Burmann, F., Ebert, N., van Baarle, S., and Bramkamp, M. (2011). A bacterial dynamin-like protein mediating nucleotide-independent membrane fusion. Molecular Microbiology *79*, 1294-1304.

Burrows, L.L. (2005). Weapons of mass retraction. Molecular Microbiology *57*, 878-888.

Bustamante, V.H., Martinez-Flores, I., Vlamakis, H.C., and Zusman, D.R. (2004). Analysis of the Frz signal transduction system of *Myxococcus xanthus* shows the importance of the conserved C-terminal region of the cytoplasmic chemoreceptor FrzCD in sensing signals. Molecular Microbiology *53*, 1501-1513.

Caldon, C.E., and March, P.E. (2003). Function of the universally conserved bacterial GTPases. Curr Opin Microbiol *6*, 135-139.

Carballido-Lopez, R. (2006). The bacterial actin-like cytoskeleton. Microbiology and Molecular Biology Reviews *70*, 888.

Carballido-Lopez, R., Formstone, A., Li, Y., Ehrlich, S.D., Noirot, P., and Errington, J. (2006). Actin homolog MreBH governs cell morphogenesis by localization of the cell wall hydrolase LytE. Developmental Cell *11*, 399-409.

Carruthers, V.B., Sherman, G.D., and Sibley, L.D. (2000). The Toxoplasma adhesive protein MIC2 is proteolytically processed at multiple sites by two parasite-derived proteases. Journal of Biological Chemistry *275*, 14346-14353.

Charest, P.G., and Firtel, R.A. (2007). Big roles for small GTPases in the control of directed cell movement. Biochem J *401*, 377-390.

Choi, C.K., Vicente-Manzanares, M., Zareno, J., Whitmore, L.A., Mogilner, A., and Horwitz, A.R. (2008). Actin and alpha-actinin orchestrate the assembly and maturation of nascent adhesions in a myosin II motor-independent manner. Nat Cell Biol *10*, 1039-1050.

Chrzanowska Wodnicka, M., and Burridge, K. (1996). Rho-stimulated contractility drives the formation of stress fibers and focal adhesions. Journal of Cell Biology *133*, 1403-1415.

Clausen, M., Jakovljevic, V., Sogaard-Andersen, L., and Maier, B. (2009). High-Force Generation Is a Conserved Property of Type IV Pilus Systems. Journal of Bacteriology *191*, 4633-4638.

Cooper, J.A., and Schafer, D.A. (2000). Control of actin assembly and disassembly at filament ends. Current Opinion in Cell Biology *12*, 97-103.

Correa, N.E., Peng, F., and Klose, K.E. (2005). Roles of the regulatory proteins FlhF and FlhG in the *Vibrio cholerae* flagellar transcription hierarchy. Journal of Bacteriology *187*, 6324-6332.

Cowles, K.N., and Gitai, Z. (2010). Surface association and the MreB cytoskeleton regulate pilus production, localization and function in *Pseudomonas aeruginosa*. Mol Microbiol *76*, 1411-1426.

Craig, L., Volkmann, N., Arvai, A.S., Pique, M.E., Yeager, M., Egelman, E.H., and Tainer, J.A. (2006). Type IV pilus structure by cryo-electron microscopy and crystallography: Implications for pilus assembly and functions. Molecular Cell *23*, 651-662.

Danuser, G. (2009). Testing the lamella hypothesis: the next steps on the agenda. Journal of Cell Science *122*, 1959-1962.

Derman, A.I., Becker, E.C., Truong, B.D., Fujioka, A., Tucey, T.M., Erb, M.L., Patterson, P.C., and Pogliano, J. (2009). Phylogenetic analysis identifies many uncharacterized actin-like proteins (Alps) in bacteria: regulated polymerization, dynamic instability and treadmilling in Alp7A. Mol Microbiol *73*, 534-552.

Dobrowolski, J.M., Carruthers, V.B., and Sibley, L.D. (1997). Participation of myosin in gliding motility and host cell invasion by Toxoplasma gondii. Molecular Microbiology *26*, 163-173.

Dobrowolski, J.M., and Sibley, L.D. (1996). Toxoplasma invasion of mammalian cells is powered by the actin cytoskeleton of the parasite. Cell *84*, 933-939.

Dominguez-Escobar, J., Chastanet, A., Crevenna, A.H., Fromion, V., Wedlich-Soldner, R., and Carballido-Lopez, R. (2011). Processive Movement of MreB-Associated Cell Wall Biosynthetic Complexes in Bacteria. Science *333*, 225-228.

Dong, J.H., Wen, J.F., and Tian, H.F. (2007). Homologs of eukaryotic Ras superfamily proteins in prokaryotes and their novel phylogenetic correlation with their eukaryotic analogs. Gene *396*, 116-124.

Drum, R.W., and Hopkins, J.T. (1966). Diatom Locomotion - an Explanation. Protoplasma *62*, 1-&.

Ducret, A., Maisonneuve, E., Notareschi, P., Grossi, A., Mignot, T., and Dukan, S. (2009). A Microscope Automated Fluidic System to Study Bacterial Processes in Real Time. Plos One *4*.

Ducret, A., Valignat, M.P., Mouhamar, F., Mignot, T., and Theodoly, O. (2012). Wet-surface-enhanced ellipsometric contrast microscopy identifies slime as a major adhesion factor during bacterial surface motility. Proceedings of the National Academy of Sciences of the United States of America *109*, 10036-10041.

Duxbury, T., Humphrey, B.A., and Marshall, K.C. (1980). Continuous Observations of Bacterial Gliding Motility in a Dialysis Microchamber - Effects of Inhibitors. Archives of Microbiology *124*, 169-175.

Dye, N.A., Pincus, Z., Theriot, J.A., Shapiro, L., and Gitai, Z. (2005). Two independent spiral structures control cell shape in *Caulobacter*. Proceedings of the National Academy of Sciences of the United States of America *102*, 18608-18613.

Dzink-Fox, J.L., Leadbetter, E.R., and Godchaux, W. (1997). Acetate acts as a protonophore and differentially affects bead movement and cell migration of the gliding

bacterium Cytophaga johnsonae (Flavobacterium johnsoniae). Microbiology-Uk *143*, 3693-3701.

Elson, E.L., Felder, S.F., Jay, P.Y., Kolodney, M.S., and Pasternak, C. (1999). Forces in cell locomotion. Cell Behaviour: Control and Mechanism of Motility, 299-314.

Esue, O., Cordero, M., Wirtz, D., and Tseng, Y. (2005). The assembly of MreB, a prokaryotic homolog of actin. Journal of Biological Chemistry *280*, 2628-2635.

Esue, O., Wirtz, D., and Tseng, Y. (2006a). GTPase activity, structure, and mechanical properties of filaments assembled from bacterial cytoskeleton protein MreB. J Bacteriol *188*, 968-976.

Esue, O., Wirtz, D., and Tseng, Y. (2006b). GTPase activity, structure, and mechanical properties of filaments assembled from bacterial cytoskeleton protein MreB. Journal of Bacteriology *188*, 968-976.

Figge, R.M., Divakaruni, A.V., and Gober, J.W. (2004). MreB, the cell shape-determining bacterial actin homologue, co-ordinates cell wall morphogenesis in Caulobacter crescentus. Molecular Microbiology *51*, 1321-1332.

Formstone, A., and Errington, J. (2005). A magnesium-dependent mreB null mutant: implications for the role of mreB in *Bacillus subtilis*. Mol Microbiol *55*, 1646-1657.
Friedl, P., and Gilmour, D. (2009). Collective cell migration in morphogenesis, regeneration and cancer. Nat Rev Mol Cell Biol *10*, 445-457.

Garner, E.C., Bernard, R., Wang, W.Q., Zhuang, X.W., Rudner, D.Z., and Mitchison, T. (2011). Coupled, Circumferential Motions of the Cell Wall Synthesis Machinery and MreB Filaments in B. subtilis. Science *333*, 222-225.

Gaskins, E., Gilk, S., DeVore, N., Mann, T., Ward, G., and Beckers, C. (2004). Identification of the membrane receptor of a class XIV myosin in Toxoplasma gondii. Journal of Cell Biology *165*, 383-393.

Gerding, M.A., Ogata, Y., Pecora, N.D., Niki, H., and de Boer, P.A. (2007). The trans-envelope Tol-Pal complex is part of the cell division machinery and required for proper outer-membrane invagination during cell constriction in *E. coli*. Mol Microbiol *63*, 1008-1025.

Gitai, Z., Dye, N., and Shapiro, L. (2004). An actin-like gene can determine cell polarity in bacteria. Proc Natl Acad Sci U S A *101*, 8643-8648.

Green, J.C.D., Kahramanoglou, C., Rahman, A., Pender, A.M.C., Charbonnel, N., and Fraser, G.M. (2009). Recruitment of the Earliest Component of the Bacterial Flagellum to the Old Cell Division Pole by a Membrane-Associated Signal Recognition Particle Family GTP-Binding Protein. Journal of Molecular Biology *391*, 679-690.

Guillou, H., Depraz-Depland, A., Planus, E., Vianaya, B., Chaussy, J., Grichine, A., Albiges-Rizo, C., and Block, M.R. (2008). Lamellipodia nucleation by filopodia

depends on integrin occupancy and downstream Rac1 signaling. Experimental Cell Research *314*, 478-488.

Gupton, S.L., and Waterman-Storer, C.M. (2006). Spatiotemporal feedback between actomyosin and focal-adhesion systems optimizes rapid cell migration. Cell *125*, 1361-1374.

Harshey, R.M. (2003). Bacterial motility on a surface: Many ways to a common goal. Annual Review of Microbiology *57*, 249-273.

Hartzell, P., and Kaiser, D. (1991a). Function of Mgla, a 22-Kilodalton Protein Essential for Gliding in *Myxococcus xanthus*. Journal of Bacteriology *173*, 7615-7624.

Hartzell, P., and Kaiser, D. (1991b). Upstream Gene of the Mgl Operon Controls the Level of Mgla Protein in *Myxococcus xanthus*. Journal of Bacteriology *173*, 7625-7635.

Hasselbring, B.M., and Krause, D.C. (2007). Cytoskeletal protein P41 is required to anchor the terminal organelle of the wall-less prokaryote *Mycoplasma pneumoniae*. Molecular Microbiology *63*, 44-53.

Heintzelman, M.B., and Schwartzman, J.D. (1999). Characterization of Myosin-A and Myosin-C: Two class XIV unconventional myosins from Toxoplasma gondii. Cell Motility and the Cytoskeleton *44*, 58-67.

Henderson, G.P., and Jensen, G.J. (2006). Three-dimensional structure of M*ycoplasma pneumoniae*'s attachment organelle and a model for its role in gliding motility. Molecular Microbiology *60*, 376-385.

Heng, Y.W., and Koh, C.G. (2010). Actin cytoskeleton dynamics and the cell division cycle. International Journal of Biochemistry & Cell Biology *42*, 1622-1633.

Herm-Gotz, A., Weiss, S., Stratmann, R., Fujita-Becker, S., Ruff, C., Meyhofer, E., Soldati, T., Manstein, D.J., Geeves, M.A., and Soldati, D. (2002). Toxoplasma gondii myosin A and its light chain: a fast, single-headed, plus-end-directed motor. Embo Journal *21*, 2149-2158.

Hettmann, C., Herm, A., Geiter, A., Frank, B., Schwarz, E., Soldati, T., and Soldati, D. (2000). A dibasic motif in the tail of a class XIV apicomplexan myosin is an essential determinant of plasma membrane localization. Molecular Biology of the Cell *11*, 1385-1400.

Hodgkin, J., and Kaiser, D. (1977). Cell-to-Cell Stimulation of Movement in Nonmotile Mutants of *Myxococcus*. Proceedings of the National Academy of Sciences of the United States of America *74*, 2938-2942.

Hodgkin, J., and Kaiser, D. (1979). Genetics of Gliding Motility in *Myxococcus xanthus* (Myxobacterales) - 2 Gene Systems Control Movement. Molecular & General Genetics *171*, 177-191.

Hu, K., Ji, L., Applegate, K.T., Danuser, G., and Waterman-Stirer, C.M. (2007). Differential transmission of actin motion within focal adhesions. Science *315*, 111-115.

Inclan, Y.F., Laurent, S., and Zusman, D.R. (2008). The receiver domain of FrzE, a CheA-CheY fusion protein, regulates the CheA histidine kinase activity and downstream signalling to the A- and S-motility systems of *Myxococcus xanthus*. Molecular Microbiology *68*, 1328-1339.

Inclan, Y.F., Vlamakis, H.C., and Zusman, D.R. (2007). FrzZ, a dual CheY-like response regulator, functions as an output for the Frz chemosensory pathway of *Myxococcus xanthus*. Molecular Microbiology *65*, 90-102.

Insall, R.H., and Machesky, L.M. (2009). Actin Dynamics at the Leading Edge: From Simple Machinery to Complex Networks. Developmental Cell *17*, 310-322.

Jakovljevic, V., Leonardy, S., Hoppert, M., and Sogaard-Andersen, L. (2008). PilB and PilT are ATPases acting antagonistically in type IV pilus function in *Myxococcus xanthus*. Journal of Bacteriology *190*, 2411-2421.

Jarrell, K.F., and McBride, M.J. (2008). The surprisingly diverse ways that prokaryotes move. Nature Reviews Microbiology *6*, 466-476.

Jewett, T.J., and Sibley, L.D. (2003). Aldolase forms a bridge between cell surface adhesins and the actin cytoskeleton in apicomplexan parasites. Molecular Cell *11*, 885-894.

Jones, L.J., Carballido-Lopez, R., and Errington, J. (2001). Control of cell shape in bacteria: helical, actin-like filaments in *Bacillus subtilis*. Cell *104*, 913-922.

Julien, B., Kaiser, A.D., and Garza, A. (2000). Spatial control of cell differentiation in *Myxococcus xanthus*. Proceedings of the National Academy of Sciences of the United States of America *97*, 9098-9103.

Kaiser, D. (1979). Social Gliding Is Correlated with the Presence of Pili in *Myxococcus xanthus*. Proceedings of the National Academy of Sciences of the United States of America *76*, 5952-5956.

Kaiser, D., and Welch, R. (2004). Dynamics of fruiting body morphogenesis. Journal of Bacteriology *186*, 919-927.

Kappe, S., Bruderer, T., Gantt, S., Fujioka, H., Nussenzweig, V., and Menard, R. (1999). Conservation of a gliding motility and cell invasion machinery in Apicomplexan parasites. Journal of Cell Biology *147*, 937-943.

Keilberg, D., Wuichet, K., Drescher, F., and Sogaard-Andersen, L. (2012). A Response Regulator Interfaces between the Frz Chemosensory System and the MglA/MglB GTPase/GAP Module to Regulate Polarity in *Myxococcus xanthus*. Plos Genetics *8*.

Kim, Y.K., and McCarter, L.L. (2000). Analysis of the polar flagellar gene system of *Vibrio parahaemolyticus*. Journal of Bacteriology *182*, 3693-3704.

Kimmel, A. R., and Parent, C.A. (2003). *Dictyostelium discoideum* cAMP chemotaxis pathway. Science *300*, 1525-1527.

King, C.A. (1981). Cell-Surface Interaction of the Protozoan Gregarina with Concanavalin-a Beads - Implications for Models of Gregarine Gliding. Cell Biology International Reports *5*, 297-305.

King, C.A. (1988). Cell Motility of Sporozoan Protozoa. Parasitology Today *4*, 315-319.

King, C.A., Whitehead, C., Pringle, N., Cooper, L., and Baines, I.C. (1986). Motility of Protozoan Gregarines - a Model for Studying Mechanochemical Force Transduction at the Cell-Surface. Cell Motility and the Cytoskeleton *6*, 243-243.

Koch, M.K., and Hoiczyk, E. (2013). Characterization of myxobacterial A-motility: insights from microcinematographic observations. J Basic Microbiol.

Komatsu, M., Takano, H., Hiratsuka, T., Ishigaki, Y., Shimada, K., Beppu, T., and Ueda, K. (2006). Proteins encoded by the conservon of *Streptomyces coelicolor* A3(2) comprise a membrane-associated heterocomplex that resembles eukaryotic G protein-coupled regulatory system. Mol Microbiol *62*, 1534-1546.

Krendel, M., and Mooseker, M.S. (2005). Myosins: Tails (and heads) of functional diversity. Physiology *20*, 239-251.

Kroos, L., Hartzell, P., Stephens, K., and Kaiser, D. (1988). A Link between Cell-Movement and Gene-Expression Argues That Motility Is Required for Cell Cell Signaling during Fruiting Body Development. Genes & Development *2*, 1677-1685.

Kruse, T., Moller-Jensen, J., Lobner-Olesen, A., and Gerdes, K. (2003). Dysfunctional MreB inhibits chromosome segregation in *Escherichia coli*. Embo Journal *22*, 5283-5292.

Kuhn, J., Briegel, A., Morschel, E., Kahnt, J., Leser, K., Wick, S., Jensen, G.J., and Thanbichler, M. (2010). Bactofilins, a ubiquitous class of cytoskeletal proteins mediating polar localization of a cell wall synthase in Caulobacter crescentus. EMBO J *29*, 327-339.

Kusumoto, A., Shinohara, A., Terashima, H., Kojima, S., Yakushi, T., and Homma, M. (2008). Collaboration of FlhF and FlhG to regulate polar-flagella number and localization in *Vibrio alginolyticus*. Microbiology-Sgm *154*, 1390-1399.

Laemmli, U.K. (1970). Cleavage of structural proteins during the assembly of the head of bacteriophage T4. Nature *227*, 680-685.

Lauffenburger, D.A., and Horwitz, A.F. (1996). Cell migration: A physically integrated molecular process. Cell *84*, 359-369.

Laukaitis, C.M., Webb, D.J., Donais, K., and Horwitz, A.F. (2001). Differential dynamics of alpha 5 integrin, paxillin, and alpha-actinin during formation and disassembly of adhesions in migrating cells. Journal of Cell Biology *153*, 1427-1440.

Le Clainche, C., and Carlier, M.F. (2008). Regulation of actin assembly associated with protrusion and adhesion in cell migration. Physiological Reviews *88*, 489-513.

Lee, J., Ishihara, A., Theriot, J.A., and Jacobson, K. (1993). Principles of Locomotion for Simple-Shaped Cells. Nature *362*, 167-171.

Leonardy, S., Miertzschke, M., Bulyha, I., Sperling, E., Wittinghofer, A., and Sogaard-Andersen, L. (2010). Regulation of dynamic polarity switching in bacteria by a Ras-like G-protein and its cognate GAP. Embo Journal *29*, 2276-2289.

Lew, A.E., Dluzewski, A.R., Johnson, A.M., and Pinder, J.C. (2002). Myosins of Babesia bovis: molecular characterisation, erythrocyte invasion, and phylogeny. Cell Motility and the Cytoskeleton *52*, 202-220.

Lleo, M.M., Canepari, P., and Satta, G. (1990). Bacterial-Cell Shape Regulation - Testing of Additional Predictions Unique to the 2-Competing-Sites Model for Peptidoglycan Assembly and Isolation of Conditional Rod-Shaped Mutants from Some Wild-Type Cocci. Journal of Bacteriology *172*, 3758-3771.

Lovering, A.L., Safadi, S.S., and Strynadka, N.C.J. (2012). Structural Perspective of Peptidoglycan Biosynthesis and Assembly. Annual Review of Biochemistry, Vol 81 *81*, 451-478.

Low, H.H., and Lowe, J. (2006). A bacterial dynamin-like protein. Nature *444*, 766-769.

Luciano, J., Agrebi, R., Le Gall, A.V., Wartel, M., Fiegna, F., Ducret, A., Brochier-Armanet, C., and Mignot, T. (2011). Emergence and Modular Evolution of a Novel Motility Machinery in Bacteria. Plos Genetics *7*.

Mattick, J.S. (2002). Type IV pili and twitching motility. Annual Review of Microbiology *56*, 289-314.

Mattila, P.K., and Lappalainen, P. (2008). Filopodia: molecular architecture and cellular functions. Nature Reviews Molecular Cell Biology *9*, 446-454.

Mauriello, E.M., Nan, B., and Zusman, D.R. (2009). AglZ regulates adventurous (A-) motility in Myxococcus xanthus through its interaction with the cytoplasmic receptor, FrzCD. Mol Microbiol *72*, 964-977.

Mauriello, E.M.F., Mignot, T., Yang, Z.M., and Zusman, D.R. (2010a). Gliding Motility Revisited: How Do the Myxobacteria Move without Flagella? Microbiology and Molecular Biology Reviews *74*, 229-+.

Mauriello, E.M.F., Mouhamar, F., Nan, B., Ducret, A., Dai, D., Zusman, D.R., and Mignot, T. (2010b). Bacterial motility complexes require the actin-like protein, MreB and the Ras homologue, MglA. Embo Journal *29*, 315-326.

Mayer, J.A., and Amann, K.J. (2009). Assembly properties of the *Bacillus subtilis* actin, MreB. Cell Motil Cytoskeleton *66*, 109-118.

Mazza, P., Noens, E.E., Schirner, K., Grantcharova, N., Mommaas, A.M., Koerten, H.K., Muth, G., Flardh, K., van Wezel, G.P., and Wohlleben, W. (2006). MreB of *Streptomyces coelicolor* is not essential for vegetative growth but is required for the integrity of aerial hyphae and spores. Mol Microbiol *60*, 838-852.

McBride, M.J. (2004). Cytophaga-flavobacterium gliding motility. Journal of Molecular Microbiology and Biotechnology *7*, 63-71.

McBride, M.J., and Braun, T.F. (2004). GldI is a lipoprotein that is required for *Flavobacterium johnsoniae* gliding motility and chitin utilization. Journal of Bacteriology *186*, 2295-2302.

McBride, M.J., Braun, T.F., and Brust, J.L. (2003). *Flavobacterium johnsoniae* GldH is a lipoprotein that is required for gliding motility and chitin utilization. Journal of Bacteriology *185*, 6648-6657.

Mejillano, M.R., Kojima, S., Applewhite, D.A., Gertler, F.B., Svitkina, T.M., and Borisy, G.G. (2004). Lamellipodial versus filopodial mode of the actin nanomachinery: Pivotal role of the filament barbed end. Cell *118*, 363-373.

Miertzschke, M., Koerner, C., Vetter, I.R., Keilberg, D., Hot, E., Leonardy, S., Sogaard-Andersen, L., and Wittinghofer, A. (2011). Structural analysis of the Ras-like G protein MglA and its cognate GAP MglB and implications for bacterial polarity. EMBO J *30*, 4185-4197.

Mignot, T., Merlie, J.P., Jr., and Zusman, D.R. (2005a). Regulated pole-to-pole oscillations of a bacterial gliding motility protein. Science *310*, 855-857.

Mignot, T., Merlie, J.P., and Zusman, D.R. (2007a). Two localization motifs mediate polar residence of FrzS during cell movement and reversals of Myxococcus xanthus. Molecular Microbiology *65*, 363-372.

Mignot, T., Shaevitz, J.W., Hartzell, P.L., and Zusman, D.R. (2007b). Evidence that focal adhesion complexes power bacterial gliding motility. Science *315*, 853-856.

Minamino, T., Imada, K., and Namba, K. (2008). Molecular motors of the bacterial flagella. Curr Opin Struct Biol *18*, 693-701.

Miroux, B., and Walker, J.E. (1996). Over-production of proteins in *Escherichia coli*: Mutant hosts that allow synthesis of some membrane proteins and globular proteins at high levels. Journal of Molecular Biology *260*, 289-298.

Mizuno, Y., Makioka, A., Kawazu, S., Kano, S., Kawai, S., Akaki, M., Aikawa, M., and Ohtomo, H. (2002). Effect of jasplakinolide on the growth, invasion, and actin cytoskeleton of Plasmodium falciparum. Parasitology Research *88*, 844-848.

Mogilner, A., and Keren, K. (2009). The shape of motile cells. Curr Biol *19*, R762-771.

Morrissette, N.S., and Sibley, L.D. (2002). Cytoskeleton of apicomplexan parasites. Microbiology and Molecular Biology Reviews *66*, 21-+.

Muller, F.D., Schink, C.W., Hoiczyk, E., Cserti, E., and Higgs, P.I. (2012). Spore formation in *Myxococcus xanthus* is tied to cytoskeleton functions and polysaccharide spore coat deposition. Molecular Microbiology *83*, 486-505.

Murray, T.S., and Kazmierczak, B.I. (2006). FlhF is required for swimming and swarming in *Pseudomonas aeruginosa*. Journal of Bacteriology *188*, 6995-7004.

Nakane, D., Sato, K., Wada, H., McBride, M.J., and Nakayama, K. (2013). Helical flow of surface protein required for bacterial gliding motility. Proc Natl Acad Sci U S A *110*, 11145-11150.

Nan, B., Chen, J., Neu, J.C., Berry, R.M., Oster, G., and Zusman, D.R. (2011). Myxobacteria gliding motility requires cytoskeleton rotation powered by proton motive force. Proc Natl Acad Sci U S A *108*, 2498-2503.

Nan, B., Mauriello, E.M., Sun, I.H., Wong, A., and Zusman, D.R. (2010). A multi-protein complex from Myxococcus xanthus required for bacterial gliding motility. Mol Microbiol *76*, 1539-1554.

Nan, B.Y., Bandaria, J.N., Moghtaderi, A., Sun, I.H., Yildiz, A., and Zusman, D.R. (2013). Flagella stator homologs function as motors for myxobacterial gliding motility by moving in helical trajectories. Proceedings of the National Academy of Sciences of the United States of America *110*, E1508-E1513.

Nelson, S.S., Bollampalli, S., and McBride, M.J. (2008). SprB is a cell surface component of the *Flavobacterium johnsoniae* gliding motility machinery. Journal of Bacteriology *190*, 2851-2857.

Nobes, C.D., and Hall, A. (1995). Rho, Rac, and Cdc42 Gtpases Regulate the Assembly of Multimolecular Focal Complexes Associated with Actin Stress Fibers, Lamellipodia, and Filopodia. Cell *81*, 53-62.

Nurse, P., and Marians, K.J. (2013). Purification and Characterization of *Escherichia coli* MreB Protein. Journal of Biological Chemistry *288*, 3469-3475.

Ohtani, N., and Miyata, M. (2007). Identification of a novel nucleoside triphosphatase from *Mycoplasma mobile*: a prime candidate motor for gliding motility. Biochemical Journal *403*, 71-77.

Opas, M. (1995). Cellular adhesiveness, contractility, and traction: Stick, grip, and slip control. Biochemistry and Cell Biology-Biochimie Et Biologie Cellulaire *73*, 311-316.

Opitz, C., and Soldati, D. (2002). 'The glideosome': a dynamic complex powering gliding motion and host cell invasion by Toxoplasma gondii. Molecular Microbiology *45*, 597-604.

Pandza, S., Baetens, M., Park, C.H., Au, T., Keyhan, M., and Matin, A. (2000). The G-protein FlhF has a role in polar flagellar placement and general stress response induction in *Pseudomonas putida*. Molecular Microbiology *36*, 414-423.

Pate, J.L., and Chang, L.Y.E. (1979). Evidence That Gliding Motility in Prokaryotic Cells Is Driven by Rotary Assemblies in the Cell Envelopes. Current Microbiology *2*, 59-64.

Patryn, J., Allen, K., Dziewanowska, K., Otto, R., and Hartzell, P.L. (2010). Localization of MglA, an essential gliding motility protein in *Myxococcus xanthus*. Cytoskeleton (Hoboken) *67*, 322-337.

Pelicic, V. (2008). Type IV pili: e pluribus unum? Molecular Microbiology *68*, 827-837.

Petit, V., and Thiery, J.P. (2000). Focal adhesions: structure and dynamics. Biol Cell *92*, 477-494.

Pinder, J.C., Fowler, R.E., Dluzewski, A.R., Bannister, L.H., Lavin, F.M., Mitchell, G.H., Wilson, R.J.M., and Gratzer, W.B. (1998). Actomyosin motor in the merozoite of the malaria parasite, Plasmodium falciparum: implications for red cell invasion. Journal of Cell Science *111*, 1831-1839.

Pollard, T.D., and Borisy, G.G. (2003). Cellular motility driven by assembly and disassembly of actin filaments (vol 112, pg 453, 2002). Cell *113*, 549-549.

Pollard, T.D., and Cooper, J.A. (2009). Actin, a central player in cell shape and movement. Science *326*, 1208-1212.

Pollard, T.D., Satterwhite, L., Cisek, L., Corden, J., Sato, M., and Maupin, P. (1990). Actin and Myosin Biochemistry in Relation to Cytokinesis. Annals of the New York Academy of Sciences *582*, 120-130.

Ponti, A., Machacek, M., Gupton, S.L., Waterman-Storer, C.M., and Danuser, G. (2004). Two distinct actin networks drive the protrusion of migrating cells. Science *305*, 1782-1786.

Popp, D., Narita, A., Maeda, K., Fujisawa, T., Ghoshdastider, U., Iwasa, M., Maeda, Y., and Robinson, R.C. (2010). Filament Structure, Organization, and Dynamics in MreB Sheets. Journal of Biological Chemistry *285*, 15858-15865.

Postle, K., and Kadner, R.J. (2003). Touch and go: tying TonB to transport. Molecular Microbiology *49*, 869-882.

Praefcke, G.J.K., and McMahon, H.T. (2004). The dynamin superfamily: Universal membrane tubulation and fission molecules? Nature Reviews Molecular Cell Biology *5*, 133-147.

Rafelski, S.M., and Theriot, J.A. (2004). Crawling toward a unified model of cell motility: Spatial and temporal regulation of actin dynamics. Annual Review of Biochemistry *73*, 209-239.

Raftopoulou, M., and Hall, A. (2004). Cell migration: Rho GTPases lead the way. Developmental Biology *265*, 23-32.

Ridley, A.J., and Hall, A. (1992a). Distinct Patterns of Actin Organization Regulated by the Small Gtp-Binding Proteins Rac and Rho. Cold Spring Harbor Symposia on Quantitative Biology *57*, 661-671.

Ridley, A.J., and Hall, A. (1992b). The Small Gtp-Binding Protein Rho Regulates the Assembly of Focal Adhesions and Actin Stress Fibers in Response to Growth-Factors. Cell *70*, 389-399.

Ridley, A.J., Schwartz, M.A., Burridge, K., Firtel, R.A., Ginsberg, M.H., Borisy, G., Parsons, J.T., and Horwitz, A.R. (2003). Cell migration: Integrating signals from front to back. Science *302*, 1704-1709.

Robson, K.J.H., Frevert, U., Reckmann, I., Cowan, G., Beier, J., Scragg, I.G., Takehara, K., Bishop, D.H.L., Pradel, G., Sinden, R., *et al.* (1995). Thrombospondin-Related Adhesive Protein (Trap) of Plasmodium-Falciparum - Expression during Sporozoite Ontogeny and Binding to Human Hepatocytes. Embo Journal *14*, 3883-3894.

Robson, K.J.H., Hall, J.R.S., Jennings, M.W., Harris, T.J.R., Marsh, K., Newbold, C.I., Tate, V.E., and Weatherall, D.J. (1988). A Highly Conserved Amino-Acid-Sequence in Thrombospondin, Properdin and in Proteins from Sporozoites and Blood Stages of a Human Malaria Parasite. Nature *335*, 79-82.

Rorth, P. (2009). Collective cell migration. Annu Rev Cell Dev Biol *25*, 407-429.

Russell, D.G., and Sinden, R.E. (1981). The Role of the Cytoskeleton in the Motility of Coccidian Sporozoites. Journal of Cell Science *50*, 345-359.

Salje, J., van den Ent, F., de Boer, P., and Lowe, J. (2011). Direct membrane binding by bacterial actin MreB. Mol Cell *43*, 478-487.

Sambrook, J.J., and Russell, D.D.W. (2001). Molecular cloning: a laboratory manual. Vol. 2 (Cold Spring Harbor Laboratory Press).

Sander, E.E., and Collard, J.G. (1999). Rho-like GTPases: Their role in epithelial cell-cell adhesion and invasion. European Journal of Cancer *35*, 1302-1308.

Sander, E.E., ten Klooster, J.P., van Delft, S., van der Kammen, R.A., and Collard, J.G. (1999). Rac downregulates Rho activity: Reciprocal balance between both GTPases determines cellular morphology and migratory behavior. Journal of Cell Biology *147*, 1009-1021.

Sato, K., Naito, M., Yukitake, H., Hirakawa, H., Shoji, M., McBride, M.J., Rhodes, R.G., and Nakayama, K. (2010). A protein secretion system linked to bacteroidete gliding motility and pathogenesis. Proc Natl Acad Sci U S A *107*, 276-281.

Satyshur, K.A., Worzalla, G.A., Meyer, L.S., Heiniger, E.K., Aukema, K.G., Misic, A.M., and Forest, K.T. (2007). Crystal structures of the pilus retraction motor PilT suggest large domain movements and subunit cooperation drive motility. Structure *15*, 363-376.

Scheffzek, K., and Ahmadian, M. (2005). GTPase activating proteins: structural and functional insights 18 years after discovery. Cellular and Molecular Life Sciences *62*, 3014-3038.

Scott, A.E., Simon, E., Park, S.K., Andrews, P., and Zusman, D.R. (2008). Site-specific receptor methylation of FrzCD in *Myxococcus xanthus* is controlled by a tetra-trico peptide repeat (TPR) containing regulatory domain of the FrzF methyltransferase. Mol Microbiol *69*, 724-735.

Seto, S., Uenoyama, A., and Miyata, M. (2005). Identification of a 521-kilodalton protein (Gli521) involved in force generation or force transmission for *Mycoplasma mobile* gliding. Journal of Bacteriology *187*, 3502-3510.

Shaevitz, J.W., and Gitai, Z. (2010). The Structure and Function of Bacterial Actin Homologs. Cold Spring Harbor Perspectives in Biology *2*.

Shaw, M.K., and Tilney, L.G. (1999). Induction of an acrosomal process in Toxoplasma gondii: Visualization of actin filaments in a protozoan parasite. Proceedings of the National Academy of Sciences of the United States of America *96*, 9095-9099.

Shi, X., Wegener-Feldbrugge, S., Huntley, S., Hamann, N., Hedderich, R., and Sogaard-Andersen, L. (2008). Bioinformatics and experimental analysis of proteins of two-component systems in *Myxococcus xanthus*. J Bacteriol *190*, 613-624.

Shih, Y.L., Kawagishi, I., and Rothfield, L. (2005). The MreB and Min cytoskeletal-like systems play independent roles in prokaryotic polar differentiation. Mol Microbiol *58*, 917-928.

Sibley, L.D. (2004). Intracellular parasite invasion strategies. Science *304*, 248-253.

Singer, M., and Kaiser, D. (1995). Ectopic production of guanosine penta- and tetraphosphate can initiate early developmental gene expression in *Myxococcus xanthus*. Genes Dev *9*, 1633-1644.

Sliusarenko, O., Zusman, D.R., and Oster, G. (2007). The motors powering A-motility in *Myxococcus xanthus* are distributed along the cell body. Journal of Bacteriology *189*, 7920-7921.

Small, J.V., Isenberg, G., and Celis, J.E. (1978). Polarity of Actin at Leading-Edge of Cultured-Cells. Nature *272*, 638-639.

Sogaard-Andersen, L. (2011). Directional intracellular trafficking in bacteria. Proceedings of the National Academy of Sciences of the United States of America *108*, 7283-7284.

Soldati, D., and Meissner, M. (2004). Toxoplasma as a novel system for motility. Current Opinion in Cell Biology *16*, 32-40.

Soufo, H.J., and Graumann, P.L. (2003). Actin-like proteins MreB and Mbl from *Bacillus subtilis* are required for bipolar positioning of replication origins. Curr Biol *13*, 1916-1920.

Spoerner, M., Herrmann, C., Vetter, I.R., Kalbitzer, H.R., and Wittinghofer, A. (2001). Dynamic properties of the Ras switch I region and its importance for binding to effectors. Proceedings of the National Academy of Sciences of the United States of America *98*, 4944-4949.

Spratt, B.G. (1975). Distinct Penicillin Binding-Proteins Involved in Division, Elongation, and Shape of Escherichia-Coli-K12. Proceedings of the National Academy of Sciences of the United States of America *72*, 2999-3003.

Srivastava, P., Demarre, G., Karpova, T.S., McNally, J., and Chattoraj, D.K. (2007). Changes in nucleoid morphology and origin localization upon inhibition or alteration of the actin homolog, MreB, of V*ibrio cholerae*. J Bacteriol *189*, 7450-7463.

Stewart, M.J., and Vanderberg, J.P. (1988). Malaria Sporozoites Leave Behind Trails of Circumsporozoite Protein during Gliding Motility. Journal of Protozoology *35*, 389-393.

Stewart, M.J., and Vanderberg, J.P. (1991). Malaria Sporozoites Release Circumsporozoite Protein from Their Apical End and Translocate It Along Their Surface. Journal of Protozoology *38*, 411-421.

Sun, H., Yang, Z.M., and Shi, W.Y. (1999). Effect of cellular filamentation on adventurous and social gliding motility of *Myxococcus xanthus*. Proceedings of the National Academy of Sciences of the United States of America *96*, 15178-15183.

Sun, H., Zusman, D.R., and Shi, W.Y. (2000). Type IV pilus of *Myxococcus xanthus* is a motility apparatus controlled by the frz chemosensory system. Current Biology *10*, 1143-1146.

Sun, M.Z., Wartel, M., Cascales, E., Shaevitz, J.W., and Mignot, T. (2011). Motor-driven intracellular transport powers bacterial gliding motility. Proceedings of the National Academy of Sciences of the United States of America *108*, 7559-7564.

Sun, S.X., Walcott, S., and Wolgemuth, C.W. (2010). Cytoskeletal cross-linking and bundling in motor-independent contraction. Curr Biol *20*, R649-654.

Swulius, M.T., and Jensen, G.J. (2012). The helical MreB cytoskeleton in *Escherichia coli MC1000/pLE7* is an artifact of the N-Terminal yellow fluorescent protein tag. J Bacteriol *194*, 6382-6386.

Uenoyama, A., and Miyata, M. (2005). Gliding ghosts of *Mycoplasma mobile*. Proceedings of the National Academy of Sciences of the United States of America *102*, 12754-12758.

van den Ent, F., Amos, L.A., and Lowe, J. (2001). Prokaryotic origin of the actin cytoskeleton. Nature *413*, 39-44.

van Teeffelen, S., Wang, S.Y., Furchtgott, L., Huang, K.C., Wingreen, N.S., Shaevitz, J.W., and Gitai, Z. (2011). The bacterial actin MreB rotates, and rotation depends on cell-wall assembly. Proceedings of the National Academy of Sciences of the United States of America *108*, 15822-15827.

Verkhovsky, A.B., Svitkina, T.M., and Borisy, G.G. (1999). Self-polarization and directional motility of cytoplasm. Current Biology *9*, 11-20.

Vetter, I.R., and Wittinghofer, A. (2001). Signal transduction - The guanine nucleotide-binding switch in three dimensions. Science *294*, 1299-1304.

Vicente-Manzanares, M., Koach, M.A., Whitmore, L., Lamers, M.L., and Horwitz, A.F. (2008). Segregation and activation of myosin IIB creates a rear in migrating cells. Journal of Cell Biology *183*, 543-554.

Vicente-Manzanares, M., Ma, X.F., Adelstein, R.S., and Horwitz, A.R. (2009). Non-muscle myosin II takes centre stage in cell adhesion and migration. Nature Reviews Molecular Cell Biology *10*, 778-790.

Vollmer, W., Blanot, D., and de Pedro, M.A. (2008). Peptidoglycan structure and architecture. Fems Microbiology Reviews *32*, 149-167.

Waidner, B., Specht, M., Dempwolff, F., Haeberer, K., Schaetzle, S., Speth, V., Kist, M., and Graumann, P.L. (2009). A novel system of cytoskeletal elements in the human pathogen *Helicobacter pylori*. PLoS Pathog *5*, e1000669.

Walsh, C.T., and Wencewicz, T.A. (2013). Flavoenzymes: Versatile catalysts in biosynthetic pathways. Natural Product Reports *30*, 175-200.

Wang, S., Arellano-Santoyo, H., Combs, P.A., and Shaevitz, J.W. (2010). Actin-like cytoskeleton filaments contribute to cell mechanics in bacteria. Proc Natl Acad Sci U S A *107*, 9182-9185.

Webb, D.J., Donais, K., Whitmore, L.A., Thomas, S.M., Turner, C.E., Parsons, J.T., and Horwitz, A.F. (2004). FAK-Src signalling through paxillin, ERK and MLCK regulates adhesion disassembly. Nature Cell Biology *6*, 154-+.

Wehrle-Haller, B. (2012). Assembly and disassembly of cell matrix adhesions. Curr Opin Cell Biol *24*, 569-581.

Wennerberg, K., Rossman, K.L., and Der, C.J. (2005). The Ras superfamily at a glance. Journal of Cell Science *118*, 843-846.

Wetzel, D.M., Hakansson, S., Hu, K., Roos, D., and Sibley, L.D. (2003). Actin filament polymerization regulates gliding motility by apicomplexan parasites. Molecular Biology of the Cell *14*, 396-406.

White, C.L., and Gober, J.W. (2012). MreB: pilot or passenger of cell wall synthesis? Trends in Microbiology *20*, 74-79.

Wittmann, T., and Waterman-Storer, C.M. (2001). Cell motility: can Rho GTPases and microtubules point the way? Journal of Cell Science *114*, 3795-3803.

Wolgemuth, C., Hoiczyk, E., Kaiser, D., and Oster, G. (2002a). How myxobacteria glide. Current Biology *12*, 369-377.

Wolgemuth, C.W., Hoiczyk, E., Kaiser, D., and Oster, G. (2002b). How gliding bacteria glide. Biophysical Journal *82*, 402a-402a.

Wu, S.S., and Kaiser, D. (1997). Regulation of expression of the pilA gene in *Myxococcus xanthus*. Journal of Bacteriology *179*, 7748-7758.

Yam, P.T., Wilson, C.A., Ji, L., Hebert, B., Barnhart, E.L., Dye, N.A., Wiseman, P.W., Danuser, G., and Theriot, J.A. (2007). Actin-myosin network reorganization breaks symmetry at the cell rear to spontaneously initiate polarized cell motility. Journal of Cell Biology *178*, 1207-1221.

Yang, R.F., Bartle, S., Otto, R., Stassinopoulos, A., Rogers, M., Plamann, L., and Hartzell, P. (2004). AglZ is a filament-forming coiled-coil protein required for adventurous gliding motility of *Myxococcus xanthus*. Journal of Bacteriology *186*, 6168-6178.

Youderian, P., Burke, N., White, D.J., and Hartzell, P.L. (2003). Identification of genes required for adventurous gliding motility in *Myxococcus xanthus* with the transposable element mariner. Mol Microbiol *49*, 555-570.

Young, G.M., Smith, M.J., Minnich, S.A., and Miller, V.L. (1999). The *Yersinia enterocolitica* motility master regulatory operon, flhDC, is required for flagellin production, swimming motility, and swarming motility. Journal of Bacteriology *181*, 2823-2833.

Young, K.D. (2003). Bacterial shape. Molecular Microbiology *49*, 571-580.

Yuda, M., Sawai, T., and Chinzei, Y. (1999). Structure and expression of an adhesive protein-like molecule of mosquito invasive-stage malarial parasite. Journal of Experimental Medicine *189*, 1947-1952.

Zaidel-Bar, R., Milo, R., Kam, Z., and Geiger, B. (2007). A paxillin tyrosine phosphorylation switch regulates the assembly and form of cell-matrix adhesions. Journal of Cell Science *120*, 137-148.

Zhang, X.Y.Z., Goemaere, E.L., Thome, R., Gavioli, M., Cascales, E., and Lloubes, R. (2009). Mapping the Interactions between *Escherichia coli* Tol Subunits ROTATION OF THE TolR TRANSMEMBRANE HELIX. Journal of Biological Chemistry *284*, 4275-4282.

Zhang, Y., Franco, M., Ducret, A., and Mignot, T. (2010). A Bacterial Ras-Like Small GTP-Binding Protein and Its Cognate GAP Establish a Dynamic Spatial Polarity Axis to Control Directed Motility. Plos Biology *8*.

Zhang, Y., Guzzo, M., Ducret, A., Li, Y.Z., and Mignot, T. (2012). A Dynamic Response Regulator Protein Modulates G-Protein-Dependent Polarity in the Bacterium *Myxococcus xanthus*. Plos Genetics *8*.

Zigmond, S.H. (2004). Beginning and ending an actin filament: Control at the barbed end. Current Topics in Developmental Biology, Vol 63 *63*, 145-188.

Acknowledgments

This thesis is a result of a challenging jorney, upon which many people have contributed and given their support.

First, I would like to thank my advisor Prof. Dr. L. Sogaard-Andersen, for the opportunity to work in her lab, and for providing her mentorship and expertise. Her guidance and constructive criticism prompted my scholarly development. Also, I am thankful to all the past and present members of Sogaard-Andersen laboratory, who've been helpful in different ways.

Second, I am deeply indepted to Dr. Tam Mignot at CNRS in Marseille, for his fundamental and steady influence throughout my doctoral work in his laboratory, and after that. I am eternally grateful for his valuble feedback, advice and unreserved support and encouragement, which allowed me to grow as a research scientist, and as a person. I admire his ability to balance research interests and personal pursuits.

I would also like to thank Dr. Adrien Ducret, for his extremely important discussions and input for my research, and for becoming a valued friend and support in Marseille.

Third, I would like to thank the collaborator Dr. Michel Franco at CNRS in Nice, for great support and guidance, and a wonderful atmosphere during my short stay in his laboratory.

I would also like to express sincere gratitude to the members of my thesis committe, Prof. Michael Boelker, Prof. Renate Renkawitz-Pohl, and Prof. Martin Thanbichler, for all the productive discussions, and valuble suggestions all throughout my doctoral work.

Next, I would like to thank Dr. Iryna Bulyha, Dr. Anna Mcloon, Dr. Kristin Wuichet, and Dr. Tobias Petters, for their helpful comments on my thesis. I am very grateful for having wonderful friends, Iryna, Anna K., Mattia, Nuria, Carmen, Toby and Amra, who were immensely helpful and supportive during my doctoral work.

Furthermore, I owe special thanks go to Steffi Lindow and Dr. Astrid Brandis-Heep, for their constant support, encouragement and help whenever needed.

Also, many thanks to Christian Benglesdorff, Dr. Manfred Irlmer and Reinhard Boecher for their help and assistance in different areas which made daily work and life easier in Germany.

I also want to acknowledge the funding that contributed to my research, including International Max Planck Research School, Max Planck Society, Inter-and intracellular Transport and Communication Philipps Uni Graduate School, and CNRS in Marseille.

Most importantly, none of this would have been possible without the love and immense support from my parents, my sister, and my brother. They have been a constant source of love, strength and support, and I cannot express enough how grateful I am to them. This dissertation is dedicated to my loving parents.

Curriculum Vitae

Erklärung

Hiermit versichere ich, dass ich die vorliegende Dissertation mit dem Titel „The small G-protein MglA connects the motility machinery to the bacterial actin cytoskeleton“ selbstständig verfasst, keine anderen als die im Text angegebenen Hilfsmittel verwendet und sämtliche Stellen, die im Wortlaut oder dem Sinn nach anderen Werken entnommen sind, mit Quellenangaben kenntlich gemacht habe.

Die Dissertation wurde in der jetzigen oder einer ähnlichen Form noch bei keiner anderen Hochschule eingereicht und hat noch keinen sonstigen Prüfungszwecken gedient.

_____ _____

Edina Hot Ort, Datum